Controlled Degradation of Biodegradable Polymers for Use in Melt-Blown Nonwovens

by

Gillian Ryder Binley

A thesis

presented to the University of Waterloo

in fulfillment of the

thesis requirement for the degree of

Master of Applied Science

in

Chemical Engineering

Waterloo, Ontario, Canada, 2025

© Gillian Ryder Binley 2025

Author's Declaration

This thesis consists of material all of which I authored or co-authored: see Statement of Contributions included in the thesis. This is a true copy of the thesis, including any required final revisions, as accepted by my examiners.

I understand that my thesis may be made electronically available to the public.

Statement of Contributions

Chapters 3 and 4 of this thesis are adapted from published or submitted manuscripts in which I am the first author. For chapter 4 Professor Tizazu Mekonnen is the corresponding author and sole coauthor, while chapter 3 also includes contributions from Dr. Dylan Jubinville and Professor Elisabeth Prince. For chapter 4, contribution of conceptualization, methodology, and resources were shared. I contributed validation, formal analysis, investigation, data curation, writing, and visualization. Prof. Mekonnen supported writing and contributed supervision, project administration, and funding acquisition. The same is true for chapter 3, however Dr. Dylan Jubinville also contributed to procedure, research, formal investigation, writing, and review/editing while Prof. Elisabeth Prince provided additional contributions to procedure, review, editing.

Chapter 3 is adapted from the published manuscript "Hydrogen Peroxide-Induced Controlled Degradation of Poly(Lactic Acid) for Melt-Blown Nonwovens. *ACS Appl. Polym. Mater.* **2024**, *6* (21), 13427–13438."

Chapter 4 is adapted from the submitted manuscript "Controlled Degradation of PBAT for use in PBAT/PLA Blend Melt-Blown Nonwovens"

Abstract

Nonwovens have many applications; however, they are typically made from petroleum-based polymers that are unsustainable and release microplastics upon breakdown that pose a risk to the health of both us and the environment. As such, it is necessary to shift to more environmentally benign materials such as biodegradable polymers. Unfortunately, readily available biodegradable polymers do not have the properties required, namely high melt flow index (MFI), for use in melt blowing, a common method for producing nonwovens. Therefore, this thesis aims to modify biodegradable polymers through aqueous hydrogen peroxide-induced controlled degradation to make them compatible with the melt blowing process.

Two different biodegradable polymers are subjected to this treatment: poly(lactic acid) (PLA) and poly(butylene adipate-co-terephthalate) (PBAT). Both systems demonstrated clear evidence of molecular weight reduction due to random chain scission induced by the peroxide radicals with additional contributions from thermal degradation and hydrolysis. PLA was also shown to begin crosslinking once a critical processing time was reached, while processing time appeared to have little effect on PBAT. The degraded products were then melt-blown to produce nonwoven mats with much finer and more uniform fibers compared to their untreated counterparts. The degraded PBAT from the second study was then blended with untreated PLA to develop a final melt-blown nonwoven with more balanced tensile properties than either material alone. Finally, since PLA and PBAT are immiscible when both are present in large quantities, maleation was used as a compatibilization technique to successfully enhance the quality of the melt-blown blends. Overall, reactive batch mixing with aqueous hydrogen peroxide is demonstrated to be a sustainable method for the molecular weight reduction of low MFI biodegradable polymers, allowing them to be well suited for use in melt-blown nonwovens.

Acknowledgements

This may be my thesis, but it would not have been possible without the support of many other people in my life, both professionally and personally. First, thank you to my supervisor, Professor Tizazu Mekonnen, for being a hard-working, dedicated, and inspiring mentor. Thank you to Dylan Jubinville as well for being able to help with just about any process question I could possibly have. To all my other lab mates, thank you for creating a positive lab culture, it has been a pleasure working alongside all of you.

Thank you to my friends and family. Most of you have no idea what I'm talking about when I discuss my work, but you listen anyways, and I truly appreciate it. And to those of you that do understand my scientific rambling, first, I'm sorry, and second, I'm incredibly grateful for your input.

An immeasurable thank you to my partner as well. Your support and belief in me kept me going even when I was overwhelmed and feeling down. I appreciate you reading all my papers and hyping me up even though you are much more of a biotech ChemE person than a polymer ChemE person. I truly could not have done it without you and even if I could, I wouldn't have wanted to. Thank you.

Lastly, I would like to thank the Natural Sciences and Engineering Research Council of Canada (NSERC), the Canada Foundation for Innovation (CFI), and the Canada research Chairs Program for the financial support that made this thesis possible as well as TotalEnergies Corbion for the gracious donation of PLA resin.

Table of Contents

Author's Declaration ii

Statement of Contributions iii

Abstract iv

Acknowledgements v

List of Figures ix

List of Tables xi

List of Abbreviations/Nomenclature (Alphabetical) xii

Chapter 1 – Introduction 1

1.1 Overview and motivation 1

1.2 Objectives 2

1.3 Outline of thesis 3

Chapter 2 – Literature Review 5

2.1. Introduction 5

2.2 Controlled Degradation 10

2.2.1 Enzyme-induced degradation 10

2.2.2 Radical-induced degradation 14

2.3. Crystallinity Modification 21

2.3.1 Processing techniques 21

2.3.2 Nucleating Agents 23

2.3.2 Plasticizers 30
2.4. Polymer Blends 33
2.4.1 Starch Blends 33
2.4.2 PLA Blends 36
2.5. Conclusions 39
Chapter 3 – Hydrogen peroxide-induced controlled degradation of poly(lactic acid) for melt-blown nonwovens 44
3.1 Introduction 44
3.2 Experimental 46
3.2.1 Materials 46
3.2.2 Methods 46
3.3 Results and discussion 51
3.1 Chemical structure changes 51
3.2 Rheological properties 55
3.3 Crystallization 59
3.4. Application in Melt Blowing 64
3.4 Conclusions 69
4.1 Introduction 71
4.2 Experimental 73
4.2.1 Materials 73

4.2.2 Methods 73

4.3 Results and Discussion 78

4.3.1 Controlled Degradation of Poly(butylene adipate-co-terephthalate) (PBAT) 78

4.3.2 Blending with PLA 85

4.3.3 Melt blowing of PBAT/PLA Blends 90

4.4 Conclusions 93

Chapter 5 – Conclusions and Future Work 95

5.1 Conclusions 95

5.2 Future Work 96

References 98

Appendix A – Supporting Information from Chapter 3 110

List of Figures

Figure 1: Reaction mechanisms of enzyme driven polymer degradation using PLA as a representative polymer. 11

Figure 2: Competition between chain scission and crosslinking during radical-induced polymer degradation. 14

Figure 3: Summary of the sources of radicals commonly used in controlled polymer degradation. 21

Figure 4: Summary of crystallinity modification techniques. 22

Figure 5: Homogeneous and heterogeneous nucleation during polymer cooling. 24

Figure 6: Summary of compatibilization techniques used for PBAT/PLA blends. 37

Figure 7: SEC results for PLA and treated PLA samples. 52

Figure 8: (a) Possible reaction mechanisms during H_2O_2-induced degradation of PLA [84,91,135,136,153]; **(b)** full H-NMR spectra of samples; **(c)** changes in the methyl region; and **(d)** changes to the methylene peak. 55

Figure 9: (a) Melt flow index of PLA samples at 190 °C with a load of 2.16 kg; **(b)** Complex viscosity as a function of angular frequency at 200 °C; **(c)** Storage (G') and **(d)** Loss (G'') modulus of PLA samples at 200 °C. 57

Figure 10: (a) Storage and loss moduli cross-over for Ctrl 2, PLA-10-5, and PLA-7.5-7.5 and **(b)** Corrected shear viscosity as a function of shear rate at 190 °C. 58

Figure 11: (a) PLA crystallization upon cooling using POM; close up of the crystal structure of **(b)** raw PLA and **(c)** PLA-5-10 after cooling to 100 °C. 60

Figure 12: **(a)** DSC heating thermogram (2nd cycle); **(b)** Flory-Fox plot of PLA molar mass and glass transition temperature; **(b)** WAXD profiles; **(d)** %crystallinity for all samples. 62

Figure 13: Fiber mats produced from Raw PLA at 180–200 °C **(a-c)** and PLA-5-5 at 170–190 °C **(d-f).** 66

Figure 14: SEM images of Raw PLA at 50x **(a)** and 600x **(b)** as well as the fiber distribution of Raw PLA **(c).** 68

Figure 15: SEM images of PLA-5-5 at 50x **(a)** and 600x **(b)** as well as the fiber distribution of PLA-5-5 **(c).** 69

Figure 16: MFI (a), complex viscosity (b), storage modulus (c), and loss modulus (d) of hydrogen-peroxide treated PBAT. 80

Figure 17: DSC thermograms of H_2O_2 treated PBAT samples. 81

Figure 18: Proposed mechanism for reactions occuring during reactive batch mixing **(a)**; 1-H NMR spectrum **(b)** of treated PBAT samples with focus on the **(c)** terephphtalic acid region and **(d)** butylene region. 83

Figure 19: SEM images of melt-blown PBAT **(a)** and PBAT-10-5 **(b)** at 500X magnification. As well as fiber diameter distribution of PBAT **(c)** and PABT-10-5 **(d)**. 85

Figure 20: AFM images of 70_30 **(a)**, 50_50 **(b)**, 50_50_M **(c)**, 30_70 **(d)**, and PLA **(e);** POM images of the same blends in the same order **(f-j).** 86

Figure 21: DSC thermogram of PBAT/PLA blends (a) with emphasis on the glass transition regions of PBAT (b) and PLA (c) as well as the cold crystallization region of PLA (d) and melting region of PBAT (e). 89

Figure 22: SEM image of 50-50 with beading (a) and 50-50-M (b) as well as their associated fiber diameter distributions (c and d). 91

Figure 23: Tensile properties of PBAT/PLA nonwovens (**a-d**)..... 92

List of Tables

Table 1: Sample code and formulation. 46

Table 2: Sample identification and formulation of treated PBAT samples 74

Table 3: Sample code and formulation of PBAT/PLA melt-blown fibers 76

Table 4: Glass transition, melting temperatures, enthalpy of melting, and percent crystallinity of treated PBAT samples. 82

Table 5: Glass transition, melting, and cold crystallization temperatures of PBAT/PLA blends as well as their enthalpies of melting and cold crystallization with calculated crystallinity. 89

Table 6: Fiber distribution of PBAT/PLA blends 90

List of Abbreviations/Nomenclature (Alphabetical)

AFM	Atomic Force Microscopy
BCOE	Bicyclooctene
BHET	Bis(2-hydroxyethyl) terephthalate
CBI	Cyclobutene imide monomers
CSF	Cotton stalk fiber
DCP	Dicumyl peroxide
DHBP	2,5-dimethyl-2,5-di-tert-butylperoxyhexane
DSC	Dynamic Scanning Calorimetry
EBH	*N*,*N*-ethylenebis(12-hydroxystearamide)
ESO	Epoxidized soybean oil
FESEM	Field Emission
G'	Storage Modulus
G"	Loss Modulus
HDPE	High density polyethylene
H-NMR	Proton nuclear magnetic resonance
$\mathbf{H^0_m}$	Heat of fusion value for a 100% crystalline polymer
$\mathbf{H_{cc}}$	Enthalpy of cold crystallization
$\mathbf{H_m}$	Enthalpy of melting
K	Flory-fox constant
LDPE	Low density polyethylene
MA	Maleic anhydride
MFI	Melt flow index
Mn	Number average molecular weight
MS	Mean Square
MSA	Methanesulfonic acid
Mw	Weight average molecular weight
MW	Molar mass
n	Power law index
NHC	N-heterocyclic carbenes

PBAT	Poly(butylene adipate-co-terephthalate)
PBS	Polybutylene succinate
PCL	Poly(ε-caprolactone)
PE	Polyester
PEA	Poly(ethylene adipate)
PEG	Poly(ethylene glycol)
PEO	Poly(ethylene oxide)
PET	Polyethylene terephthalate
PHA	Polyhydroxyalkanoates
PHB	polyhydroxybutyrate
PHBV	Poly(3-hydroxybutyrate-co-3-hydroxyvalerate)
PHO	Poly-3-hydroxyoctanoate
PHV	Polyhydroxyvalerate
PLA	Poly(lactic acid)
POM	Polarized optical microscope
PP	Polypropylene
PS	Polystyrene
PU	Polyurethane
PVA	Polyvinyl alcohol
PVC	Poly(vinyl chloride)
SEC	Size exclusion chromatography
SS	Sum of squares
TBD	Triazabicyclodecene
T_c	Crystallization temperature
Tg	Glass transition temperature
T_{ginf}	Infinite glass transition temperature
T_m	Melting temperature
TEC	Triethyl citrate
THF	Tetrahydrofuran
TPS	Thermoplastic starch
WAXD	Wide angle x-ray diffraction

Đ	Dispersity
η	Viscosity
η*	Complex viscosity
η_0	Zero shear viscosity
η_∞	Infinite shear viscosity
ω	Angular frequency
ω_β	Critical angular frequency
%χ	Percent crystallinity

Chapter 1 – Introduction

1.1 Overview and motivation

Plastics are integrated deeply into society and, while they offer undeniable benefits, the majority of commonly used plastics pose many risks to the health of people and the environment. Therefore, to maintain the convenience of plastics while mitigating contributions to climate change and microplastics, scientists are turning to biodegradable plastics. Nonwoven fabrics are a major culprit of microplastic release as the incredibly fine fibers the fabric is comprised of are susceptible to fragmenting into even smaller pieces.[1] With so many applications of nonwoven fabrics being disposable (e.g. face masks, cleaning wipes, and diapers)[2] these fragments inevitably end up contaminating soil and water. As such, nonwoven fabrics are an obvious target for making the swap to biodegradable plastics.

One method for the production of nonwovens is melt blowing, an extrusion technique in which a custom die is used to subject the molten polymer to high velocity hot air which stretches the plastic into extremely fine fibers that meld together into a mat when they hit a rotating collector.[3] Unfortunately, readily available biodegradable polymers are not well suited for this process as it requires the molten polymer to achieve a near waterlike viscosity which most biodegradable polymers do not possess. Therefore, to be used in this process, biodegradable polymers must undergo modification. One option to decrease the melt viscosity, i.e. increase the melt flow index, is to purposely degrade the material to reduce the molecular weight and therefore decrease chain entanglement. This can be achieved through reactive batch mixing with peroxide. Many peroxides, however, release undesirable byproducts when they undergo this process.[4] Thus, to maintain the sustainability of the process, hydrogen peroxide can be used as the radical source since it releases environmentally neutral byproducts upon breakdown.[5]

This thesis examines aqueous hydrogen peroxide-induced degradation of two different biodegradable polymers. The first is poly(lactic acid) (PLA), one of the most widely available biopolymers on the market. In 2021, PLA held the largest market share for the production capacity of biodegradable bioplastics worldwide.[6] It is highly sustainable since it is biodegradable, biobased, and can be produced from renewable resources such as corn starch and sugarcane. PLA is semi-crystalline and typically has a high level of crystallinity, giving it good mechanical strength, but making it relatively brittle. The second polymer of interest is poly(butylene adipate-co-terephthalate) (PBAT). PBAT is also semi-crystalline, however, it typically has very low crystallinity levels resulting in a tougher more flexible material compared to PLA. While it is not bioderived, it is still biodegradable, therefore making it a more sustainable choice than traditional polymers. The two polymers studied are complementary to each other and therefore are frequently blended together to balance their properties and create a more versatile plastic.[7] Thus, for applications in melt blowing, blends of the two materials are examined in addition to both PLA and PBAT individually. Since they are not inherently miscible, compatibilization techniques are also explored.

1.2 Objectives

This thesis aims to investigate the modification of biodegradable polymers through controlled degradation to adapt them to the melt blowing process and produce compostable nonwoven fabrics. This was done using two separate biodegradable polymers. While both systems include characterization of the modified materials, the first focuses extensively on the characterization of the degraded material, while the second emphasizes blending materials to improve the characteristics of the melt-blown nonwovens.

First, hydrogen peroxide is investigated as a radical source for controlled degradation through reactive extrusion. The first system examined the effectiveness of this method for PLA while the second system examined the same process for PBAT. Therefore, the first objective is to determine the reaction mechanisms involved in the degradation process through analysis of properties such as molecular weight, melt flow index, and crystallinity.

The second objective was then to use these modified polymers in melt-blown nonwovens. The PLA system was used to demonstrate the impact to processing temperature and overall fiber size and quality. The PBAT system examined the fibers and the benefits and requirements for blending with PLA to establish a more versatile product. Overall, the objective of this work is to expand the applications of biodegradable polymers through controlled degradation with exploration of degradation mechanisms, rheological behavior, thermal behavior, and crystalline properties and how these characteristics come into play for applications in melt-blown nonwovens.

1.3 Outline of thesis

Chapters of this thesis beyond this introduction are comprised of the following: Chapter 2 presents a literature review that examines the current state of rheology and crystallinity modification of biodegradable polymers. This chapter discusses controlled degradation and crystallinity modification techniques that can be applied to expand the potential applications of biodegradable polymers. Chapter 3 demonstrates a completed experimental research work on the controlled degradation of PLA using hydrogen peroxide with application in melt-blown nonwovens. Characterization of the degraded material is examined as well as its performance in the melt blowing process. Chapter 4 consists of a separate experimental work applying the controlled degradation method to PBAT. It examines the use of this degraded material both alone and blended

with PLA for applications in melt-blown nonwovens. Finally, Chapter 5 provides overall conclusions and recommendations based on findings from both literature and experiments.

Chapter 2 – Literature Review

2.1. Introduction

Plastics are an undeniable part of day-to-day life from takeout containers to trash bags, car parts to coffee cups, even musical instruments; however, the majority of commercially available plastics are derived from petrochemicals, fill landfills, and release microplastics into the environment making them unsustainable.[1] Since completely ridding society of plastics is an unrealistic expectation, efforts are being made to instead make plastics from sustainable sources that allow them to completely degrade naturally in the environment rather than accumulating. Unfortunately, these sustainable plastics have much more limited applications compared to traditional plastics. As such, research focusing on the modification of sustainable plastics to expand their use is of high interest.

One application for sustainable plastics currently limited by their properties is nonwoven fabrics. Fabrics are generally classified into three types: wovens, knits, and nonwovens. Wovens and knits are identifiable by their distinct patterns, with wovens being made by interlacing two sets of strings at ninety-degree angles while knits are made from a looped pattern using one continuous string.[2] Nonwovens, on the other hand, are characterized instead by their lack of pattern and organization, being created by randomly placed fibers melded together into a sheet.[3] Of the three, nonwovens are the cheapest and easiest to manufacture as they do not require an elaborate process for interlocking individual fibers. This allows for a continuous process with simpler machinery. There are many applications for nonwoven fabrics including medical products (e.g. face masks, surgical gowns, and wound dressings), automotive filters, and geotextiles.[4–7] Nonwovens, however, are not only for industrial applications; many examples of nonwoven fabrics can be found throughout the average home with air filters in the HVAC system, tea bags in the pantry,

disinfectant wipes under the sink, and even diapers in the nursery if there is a baby in the family.[8–11] With such a wide variety of applications, advancing nonwoven technologies to improve sustainability is a necessity.

Currently nonwovens can be made from an ever-expanding wide variety of materials using various techniques. The top methods for producing nonwovens are spun bonding, needle punching, and melt-blowing. Spun bonding is a single-stage method involving fiber spinning, web formation, and bonding.[5,12,13] Processes that fall under this method include melt spinning, wet spinning, and electrospinning. [5,12,13] Spun bond fabrics are typically made from polymers like polypropylene (PP) and polyester (PET). They are known for having excellent strength-to-weight ratios, high tear resistance, and good liquid retention.[5,12,13] These properties make them suitable for applications in medical textiles, packaging, and other various disposable products. Needle punching is a mechanical process in which barbed needles are repeatedly inserted into a fibrous web.[14] This causes the fibers to entangle and interlock resulting in a coherent structure. This technique is used with a variety of fiber types, both natural like cotton and wool as well as synthetic like PP, PET, and even glass. Needle-punched nonwovens are frequently used as reinforcements in polymer composites as they effectively absorb resin and readily conform to different shapes.[14] Finally, melt-blowing is an extrusion technique in which a specialized die is used to apply high-speed hot air to the molten polymer as it exits the extruder.[15–17] This results in ultra-fine fibers which land on a rotating collector and solidify into a web. These webs are characterized by high porosity and small pore sizes making them perfect for applications in filtration and insulation.[15–17] These ultra-fine fibers, unfortunately, are frequently made from conventional polymers like PP and PET, which release microplastics into the environment as they break down. As such, it would be beneficial to

melt blow biodegradable polymers, however commercially available biopolymers do not have the properties required to produce high-quality melt-blown nonwovens without modification.

The most important property requirement for melt-blowing is a high melt flow index (MFI). MFI is a measure of how easily a polymer flows in the melt state and is inversely related to viscosity.[18] It is defined as the mass of polymer that flows through a standardized die at a specific temperature and load over the course of 10 minutes. Factors that influence MFI include molecular weight, temperature, and polymer composition including additives and fillers.[19,20] Since extremely high temperatures are hazardous and result in increased operational costs, molecular weight and polymer composition are the typical targets for modification. Molecular weight can be modified to improve melt flow through controlled degradation. This is an effective technique because shorter chain length (i.e. lower molecular weight) polymers exhibit reduced entanglement allowing them to flow more readily. There are several established methods for controlled degradation including introduction of enzymes, thermal treatment, and radical induced chain scission that will be explored further in this review.[21–23]

Another factor influencing the processability and resulting fiber quality is the crystallinity of the material. Crystallinity primarily affects fiber length and uniformity. Lower crystallinity allows for better elongation and stretching producing finer, more uniform fibers whereas high crystallinity can cause fiber breakage due to reduced molecular mobility.[24,25] Too low of a degree of crystallinity, however, can also cause reduced fiber uniformity and breakage due to lack of control as a result of excessive polymer chain mobility.[24,25] Additionally, slow crystallization kinetics, either inherent to the polymer or caused by excessively reduced crystallinity, can completely prevent the successful production of nonwoven mats as slower cooling can cause the fibers to stick together, melding into a flat sheet rather than a uniform, airy structure.[24] As such,

managing processability requires carefully regulating the degree of crystallinity. This control is also required to fine-tune the properties of the resulting fibers. High crystallinity offers better durability at the cost of flexibility while the opposite is true for low crystallinity. Thus, in order to have a more versatile product, it is necessary to balance the crystallinity.

As with MFI, crystallinity can be influenced by a variety of factors including processing conditions and molecular weight. Processing temperature and cooling rate both influence crystallinity with high melting temperatures and slow cooling rates promoting crystallinity.[26,27] As mentioned before, however, processing temperature is limited by operational costs and safety and if cooling rate is too slow, melt-blown fibers meld together and fail to form an airy porous structure. Therefore, once again, molecular weight is a focus area for modification. The greater mobility of shorter polymer chains allows them to pack more efficiently into an ordered crystalline structure resulting in higher crystallinity. It is not just the average molecular weight that matters, however, as dispersity can also impact crystallinity. Narrow molecular weight distribution yields a more uniform crystallization since all the chains are nearly the same length leading them to behave very similarly.[27,28] Broad dispersity, on the other hand, hinders crystallization as the wide variety of chain lengths can get in the way of each other and disrupt ordered packing. [27,28] Thus, the methods of degradation explored in this review also allow for potential crystallinity regulation.

Additives such as nucleating agents, plasticizers, and even other polymers can also be used to control crystallinity and its associated properties. Nucleating agents are fine particles that promote crystallization by providing sites for crystal growth.[29,30] This speeds up the crystallization process in addition to increasing the overall crystallinity. Some commonly used nucleating agents include talc, calcium carbonate, and silica.[29,30] Plasticizers are used to move in the opposite direction, reducing crystallinity and increasing flexibility.[31] They achieve this by reducing

intermolecular forces between polymer chains. Many traditional plasticizers are phthalate-based such as di(2-ethylhexyl) phthalate which is used in poly(vinyl chloride) (PVC) for medical tubing, cables, and flooring.[32] Some phthalate-based options, however, are being phased out due to health concerns and replaced with non-phthalate plasticizers such as epoxidized soybean oil which is also used in PVC.[33] Finally, rather than adding non-polymeric materials to control crystallinity and its associated properties, the starting polymer is often combined with another polymer creating a blend with the desired properties. When it comes to biodegradable polymers, one of the most common blends is poly(lactic acid) (PLA) and poly(butylene adipate terephthalate) (PBAT).[34–36] PLA is known for being highly crystalline making it strong but brittle, while PBAT is primarily amorphous making it weak but flexible. Combining the two in various ratios depending on the desired final properties allows one to find a balanced degree of crystallinity. The various additives capable of promoting or limiting crystallization will be further explored throughout this review.

Overall, non-woven fabrics are found throughout all parts of daily life. Thus, for the sake of our health, as well as that of the planet, efforts should be made to make these materials from sustainable sources. Unfortunately, readily available biodegradable polymers are not well suited to the processes, like melt blowing, that produce nonwovens. Melt blowing requires a specific rheological profile characterized by high MFI as well as a balanced degree of crystallinity. Both of these properties are impacted by the processing parameters as well as the molecular weight of the polymer. Since processing parameters are limited by operating costs and safety, this review will focus primarily on methods of controlled degradation for molecular weight reduction. Crystallinity can be further controlled by incorporating additional materials such as nucleating agents and plasticizers. Finally, polymer blends will be explored as an option for obtaining the desired properties.

2.2 Controlled Degradation

There are many reasons one would want to control the degradation behavior of plastics whether it is to change their flow behavior for expanding applications, control drug release in the body, or simply ensure they break down more rapidly when discarded. Various factors impact the degradation mechanism of polymers including temperature, moisture, and the presence of radicals from various sources such as oxygen and UV exposure. These factors can be manipulated to purposely speed up degradation in a way that suits the desired outcome such as creating a controlled rheology grade product. Therefore, controlled polymer degradation is a highly studied topic, and many approaches have been taken to achieve it.

2.2.1 Enzyme-induced degradation

One method of controlling polymer degradation that is typically used for end-of-life breakdown of plastics is the introduction of enzymes. Enzyme-driven polymer degradation is often referred to as biodegradation and is primarily relevant for natural and biodegradable plastics, however it can also be applied to polyurethane (PU) and polyesters as ester, amide, and glycosidic bonds are more prone to enzymatic attack.[37,38] Other factors impacting biodegradation include crystallinity, with amorphous regions allowing for easier enzyme penetration, and surface properties, with roughness and hydrophilicity improving enzyme adsorption.[39] Environmental conditions such as temperature, pH, and moisture also play an essential role in this degradation method. There are a variety of enzymes that can help break down plastics such as cutinases, peroxidases, cellulases, and laccases.[40] Many of the enzymes used are sourced from fungi, however they may also be derived from various other sourcing including microalgae, bacteria, and even dietary supplements.[41–44]

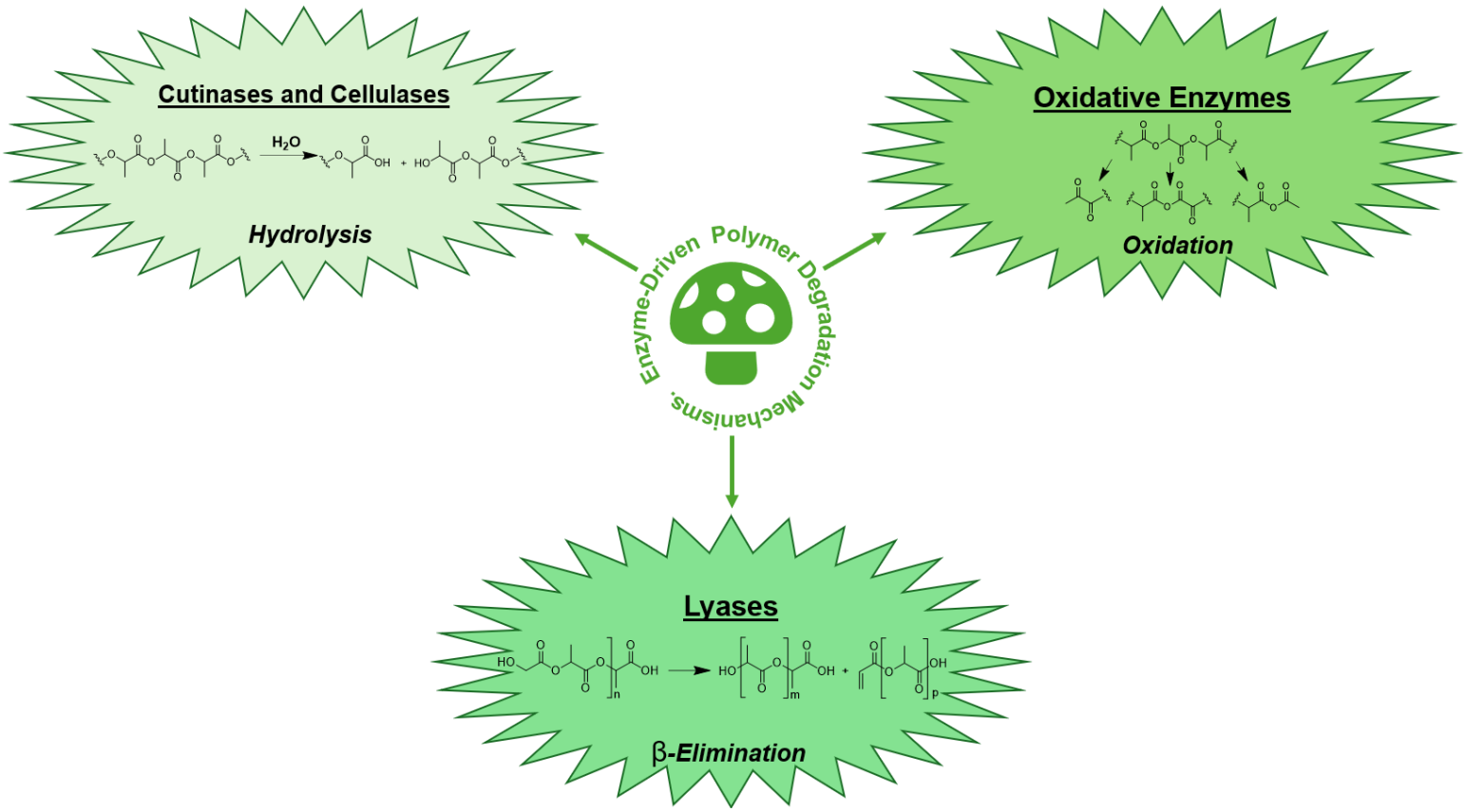


Figure 1: Reaction mechanisms of enzyme driven polymer degradation using PLA as a representative polymer.

Cutinases get their name from their function which is to break down cutin, a natural polyester found in plant cuticles.[45] By extension, these enzymes are also able to breakdown synthetic polyesters like polyethylene terephthalate (PET) and polybutylene succinate (PBS). Cutinases are a promising option as they work at low and moderate temperatures and are produced by a variety of different fungi like *Cladosporium* species and *Aspergillus nidulans*, commonly known as black and green molds respectively.[46] Álvarez-Barragán et al studied the use of these black molds for degradation of PU, both polyester and polyether variants.[46] It was found that the specific strain, *C. pseudocladosporioides,* was capable of degrading the polyester PU 87% in 14 days; the same strain also achieved 65% weight loss for polyether PU foams.[46] Di Bisceglie et al investigated the use of fungal based cutinases for PU degradation as well.[47] Polyurethane-polyester copolymers were

incubated with *Humicola insolens* cutinase for 168 h resulting in number average molecular weight (Mn) and weight average moleucular weight (Mw) reductions of 84% and 42% respectively.[47] PU, however, is not the only polymer of interest for cutinases as Alvarado et al also used cutinases to induce degradation, sourcing their enzymes from *Aspergillus nidulans* for use with PLA.[48] The cutinases were shown to be effective for both poly L lactic acid and poly D lactic acid and a decrease in weight of 46% was reported.[48] The results were compared to the PLA-hydrolyzing enzyme proteinase K and released 483% more lactic acid which can be recovered and used to produce more PLA.[48] Another biodegradable polymer susceptible to degradation by cutinases is PBS as demonstrated by Lin et al who used *P. chrysanthemicola* cutinase to reduce the mass of PBS by over 50% with just 60 h of treatment.[49] Overall, cutinases show a lot of promise for use in controlled degradation of various polymers.

Oxidative enzymes such as peroxidases and laccases are also frequently used for polymer degradation. These enzymes oxidize lignin-like and aromatic structures in plastics and are effective for complex, highly crystalline polymers.[50] Chaudhary and Vijayakumar, for example, used the laccase from *Cochliobolus* to degrade polystyrene (PS).[51] After an eight-week incubation period, the PS showed a weight loss of approximately 2%.[51] Gowthami et al. also targeted PS, observing a 23% weight loss after only a 45 day incubation period with laccase producing microalgae. In addition to PS, PE has been subjected to degradation using oxidative enzymes. Zhang et al.[52] used *Aspergillus flavus* to degrade high density polyethylene (HDPE) while Gómez-Méndez[53] et al. used *Pleurotus ostreatus* on low density polyethylene (LDPE). Zhang et al demonstrated a nearly 4% mass loss for treated HDPE over a 28-day period.[52] Gómez-Méndez was unable to accurately detect mass loss, however, after a 150-day incubation period, a 27% reduction in mechanical properties (Young's modulus and yield strength) was observed therefore supporting the idea of

degradation occurring.[53] All in all, oxidative enzymes demonstrate a promising ability to break down plastics.

Lyases and cellulases are most commonly used for biopolymers. Cellulases use hydrolysis to cleave glycosidic bonds[54] while lyases use β-elimination or similar non-hydrolytic mechanisms to break bonds.[55] As such cellulases are mainly used to target cellulose such as in biomass degradation.[54] Karimi-Avargani et al., however, used it to rapidly degrade PLA, reducing M_n by 85% in just four months.[56] Most of the research surrounding lyase induced degradation surrounds natural substances, often focusing on alginate. Spiridonov et al investigated the reaction of four different polymers when subjected to an alginate lyase and hyaluronidase: sodium alginate, carboxymethylcellulose, artificially modified sodium carboxymethylcellulose, and synthetic sodium polyacrylate.[57] The alginate lyase was only able to cleave a specific alginate substrate while the hyaluronidase successfully degraded all but the synthetic polymer.[57] Thus, while their applications are more limited than cutinases and oxidative enzymes, lyases and cellulases maintain their places in discussion of enzyme induced polymer degradation.

Overall, a wide variety of enzymes can be utilized for end-of-life treatment of plastics. There are a wide variety of sources for these enzymes, but fungi are the most commonly used. The enzymes can be broken down into their mechanisms for degradation. Cutinases are good for breaking down polyesters however polystyrene requires oxidative enzymes like peroxidases. Finally, lyases and cellulases are almost exclusively used on biomaterials. While enzymes are not compatible with controlled degradation for rheology modification purposes, they are an essential degradation mechanism for biodegradable polymer products. Thus, as scientists continue to study these enzyme-based controlled degradation systems, the world gets one step closer to sustainable plastic disposal.

2.2.2 Radical-induced degradation

Just as radicals can cause polymer growth, they can also be used to break them down. Radicals can be formed from a variety of sources including heat, light, mechanical stress, or chemical agents.[58] When radicals are introduced to a polymer system, there are a few different paths they can take. First, chain scission may occur where the polymer backbone is attacked and broken resulting in reduced molecular weight.[59] Additional degradation can occur when the radicals instead react with oxygen forming additional peroxyl radicals.[60] This is the desired reaction for controlled degradation, thus making radical induced chain scission a common method for crafting a rheology grade polymer. Another possible route for the radical to take, however, is crosslinking. When this process occurs the radicals recombine to form bonds between polymer chains and create a three-dimensional network.[61] Crosslinking typically enhances strength, elasticity, and thermal stability which is the opposite of what is desired for increased MFI rheology grade polymers. As such, when radicals are introduced to a polymer system, chain scission and crosslinking are in competition[62]; therefore processing conditions must be finetuned to ensure a chain scission dominated mechanism for controlled degradation.

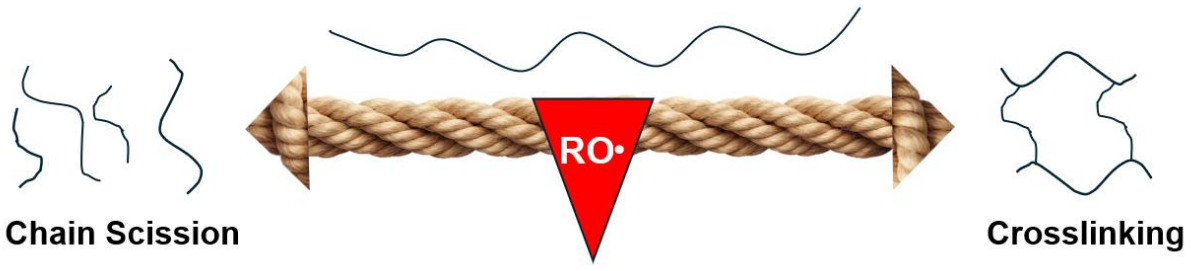


Figure 2: Competition between chain scission and crosslinking during radical-induced polymer degradation.

Thermo-oxidative Degradation

One of the simplest kinds of radical induced degradation is thermo-oxidative degradation. In this case, heat and oxygen alone are the sources of the radicals that break down the polymer. Research on controlling this type of degradation typically focuses on minimizing its effect as heat is generally unavoidable during polymer processing rather than inducing it for rheology purposes. As such, modelling thermo-oxidative degradation is of great interest. Models for a wide variety of polymer types have been established. Li et al., for example, modelled the thermal and thermos-oxidative degradation of PLA using reactive force field molecular dynamics.[63] The model successfully replicated experimentally observed degradation products and revealed that thermal degradation begins with homolytic cleavage of C-O bonds near the ester group, resulting in the formation of carbon monoxide, carbon dioxide, and acetaldehyde.[63] Bahrololoumi et al established a physically-based model for thermos-oxidative, as well as hydrolytic, aging of elastomers which takes into account both crosslinking and chain scission.[64] This relatively simple model included only six material parameters, yet showed good agreement with experimental data.[64] Thermo-oxidative degradation has even been modeled for epoxy by Jewell et al.[65] Overall, models aid greatly in controlling degradation as they aid in the understanding of how the process is occurring.

Many seek to reduce this type of degradation by polymer modification of composition or structure. Since this mechanism is driven by oxidative degradation, the obvious solution is to impede the oxidation which can be achieved with antioxidants. Dintcheva et al. incorporated clay with built in antioxidant activity into PLA.[66] This PLA-based nanocomposite proved to have higher thermal stability than those prepared using commercial clay.[66] Antunes et al. examined HDPE containing pro-degradant and antioxidants to manage degradation during processing and end of life dispoal.[67] The antioxidants were not shown to reduce the overall extent of degradation, however the

induction time of HDPE oxidative degradation was significantly increased improving the lifetime of the material.[67] Antioxidants, however, are not the only solution for retarding thermos-oxidative degradation. Fan et al. aimed to improve the thermos-oxidative stability of carbon fiber polymer-matrix composites by braiding the carbon fibers to reinforce the structure.[68] These three-dimensional and four-directional braided carbon fiber/epoxy composites demonstrated improved thermo-oxidative stability evidenced by higher mass and strength after isothermal aging compared to laminated plain woven carbon fiber/epoxy composites.[68] Further methods for reduction of this type of degradation continue to be studied.

Some, however, aim to use this degradation to their advantage to reduce the environmental impact of discarded plastics. Karlsson et al., for example, lessened the ability of PE to spread throughout temperate coastal waters by predegrading the films and therefore accelerating the oxidation process.[69] These pretreated films fragmented more rapidly than untreated films causing them to sink earlier and making them less likely to travel further and accumulate the open ocean.[69] Dümichen et al. also examined plastic contaminated water by developing a thermal degradation method for rapid identification and quantification of microplastics in water sources.[70] Overall, whether it is for preventing or accelerating plastic break down, understanding of thermo-oxidative degradation is critical for controlling it since it is an inextricable factor in polymer processing.

Mechanochemical Degradation

Mechanical force can be used to breakdown polymers, like in traditional recycling, but when those mechanical forces exceed the bond dissociation energy of the polymer back bone, it may break via homolytic cleavage, producing two free radicals in a process referred to as mechanochemical degradation.[71] Scientists utilize this type of degradation to modify the polymer backbone and create sites that are prone to other types of degradation. Liu et al., for example, co-polymerized

traditional polymers, including styrene, methyl acrylate, methyl methacrylate, with cyclobutene imide monomers (CBI).[72] These CBI underwent a mechanically triggered ring-opening reaction which rearranged the polymer chains and placed the imide groups into the polymer backbone, creating sites where hydrolysis could occur and transforming the material into one that can undergo biodegradation.[72] Li et al performed a similar study, introducing cyclobutene-fused succinimide along the backbone of polymethylacrylate which, when subjected to mechanical force through sonication, caused the ring-opening reaction to occur, once again placing imide groups in the polymer backbone.[73] Lin et al. took a different approach for mechanochemical controlled degradation, using bicyclooctene (BCOE) mechanophores, specialized molecules that undergo a chemical transformation in response to mechanical force, instead of a butene based cyclic monomer.[74] When BCOE was put under mechanical stress, a ring-opening reaction occurred, the product of which was capable of spontaneous, intramolecular lactonization setting it up for greater extents of mechanical degradation.[74] Considering these studies, it is clear that degradation can be controlled and accelerated by introducing mechanically activated materials into polymers that are traditionally difficult to degrade.

Chemical Agents

Adding certain chemicals to the polymer melt can also introduce radicals that promote and control degradation. Depending on the level of these radical sources, polymers may proceed towards crosslinking, chain scission, or a combination of the two. As such, to control the degradation, understanding of how these additives function is essential.

Peroxides are a common source of radicals for controlled degradation during reactive melt blending because they decompose easily under heat or light.[75] The weak O-O bond breaks easily when heated, forming reactive alkoxy (RO•) and hydroxyl (HO•) radicals.[76] In oxygen-rich

environments, peroxide-derived radicals also promote thermo-oxidative degradation.[77] Therefore, peroxides are a powerful tool for degradation. They are frequently used for developing controlled-rheology polypropylenes via reactive extrusion for use in melt spinning and melt-blowing as these processes benefit from reduced molecular weight. Ji et al used small quantities of 2.5-dimethyl 2.5-di(tert-butylperoxy) hexane for this purpose, producing staple PP fibers via melt spinning.[78] Azizi and Ghasemi investigated dicumyl peroxide (DCP) as the radical source for rheology grade PP.[79] They found that peroxide levels below 0.1% had no effect, however once that threshold is met, MFI increased with peroxide concentration.[79] Peroxides, however, typically produce undesirable byproducts such as acetophenone and α-methylstyrene from DCP. Thus, to improve the sustainability and safety of the process, Moad et al. used hydrogen peroxide (H_2O_2) to degrade PP.[80] H_2O_2 proved equally effective as organic peroxides while releasing only water and oxygen, environmentally benign byproducts.[80] As such, peroxides prove to be a great source of radicals for developing rheology grade polymers through controlled degradation.

Metal-based catalysts can also be used to induce radicals and promote polymer degradation. One metal frequently used for this application is tin. Xu et al., for example, developed rapidly degradable PLA by melt blending with stannous octoate ($Sn(Oct)_2$).[81] The Sn atom in $Sn(Oct)_2$ interacts with the ester group of PLA, resulting in the breakdown of the polymer chain and doubling the degradation rate in alkali solution compared to pure PLA.[81] Hofmann et al. also examined $Sn(Oct)_2$ for end of life treatment of PLA.[82] Using this method, they were able to break down PLA and obtain high yields of methyl lactate, a valuable product, within 5-20 min.[82] Zinc-based catalysts have also been used in polymer degradation. Song et al used zinc acetate to accelerate the degradation of PLA[83] while Roy et al used cobalt stearate to achieve the same for LDPE.[84] While metal-based catalysts show a lot of promise for depolymerization and degradation,

they do not come without their own environmental risks. Many metal-based catalysts leave behind toxic residues; tin ions can be toxic to aquatic organisms and accumulate in biological systems, cobalt ions can leach into soil and water resulting in long-term environmental toxicity, and zinc can inhibit microbial activity in compost and bioaccumulate in plants.[85] As such, while depolymerization and rapid polymer degradation is a step towards sustainability, metal-based catalysts can also cause environmental harm while trying to prevent it.

Organocatalysts are often viewed as a more environmentally sustainable alternative to metal-based catalysts as they are non-toxic and biodegradable. Organocatalysts can be designed to match specific polymer degradation pathways. As such, different ones are typically used for different polymers. For example, 4-dimethylaminopyridine is commonly used for PLA degradation by activating ester bonds and facilitating hydrolysis under mild conditions[86–88] whereas N-heterocyclic carbenes (NHC) are commonly used for PET[89–91] by acting as nucleophiles and directly attacking carbonyl groups in the polymer backbone. Ionic liquids are also used for PET degradation by dissolving the polymer chains, allowing for selective bond cleavage. Jehanno et al. combined equimolar quantities triazabicyclodecene (TBD) and methanesulfonic acid (MSA) to form a thermally stable protic ionic salt capable of depolymerizing PET into 91% pure bis(2-hydroxyethyl) terephthalate (BHET) monomer in less than 2 h.[92] Overall, organocatalysts show promise as a relatively environmentally friendly option for depolymerization and controlled degradation.

Photooxidation and radiation

An unavoidable contributor to polymer degradation that can be purposefully applied to accelerate and control degradation is radiation, most commonly in the form of UV radiation from light. Photooxidation occurs when polymers absorb energy from UV radiation leading to the formation

of free radicals within the polymer matrix.[93] Purposeful photooxidation is usually performed with additional assistance from photocatalysts. One common target of degradation by photooxidation is polystyrene.[94] Nikitas et al. used anthraquinone as a photocatalyst to upcycle polystyrene into benzoic acid when exposed to an LED irradiation source.[95] Oh and Stache instead used ferric chloride ($FeCl_3$) to convert PS to benzoic acid.[96] PS is not the only target for these methods, photo-degradation in conjunction with ferric stearate powders as a thermo-oxidant promoters to increase the rate of degradation of polyethylene in the natural environment.[97] An alternative approach for promoting radiation based degradation was taken by Bäckström et al who used microwave irradiation and nitric acid to convert LDPE to dicarboxylic acids with a yield of 71%.[98] Radiation, from various sources, has proven to be an effective tool for controlled complete degradation down to functional molecules, otherwise known as upcycling.

Overall, degradation is an essential part of polymer processing. Whether the goal is preventing it or controlling the speed and the extent to which it occurs, understanding degradation mechanisms is critical. The major ways that polymer degradation occur are through microbial breakdown (e.g. enzymes) and radical-induced chain scission. There are several types of enzymes that may be used depending on the polymer which follow different mechanisms including cutinases, oxidative enzymes, lyases, and cellulases. Radicals can be sourced from many places as well including sources inextricably linked to processing such as heat and mechanical degradation. Radicals can also be introduced purposely with the addition of chemicals such as peroxides, metal-catalysts, and organocatalysts as well as exposure to radiation. By utilizing these degradative tools, it is possible to modify the MFI of more sustainable polymers through molecular weight reduction and expand their applications.

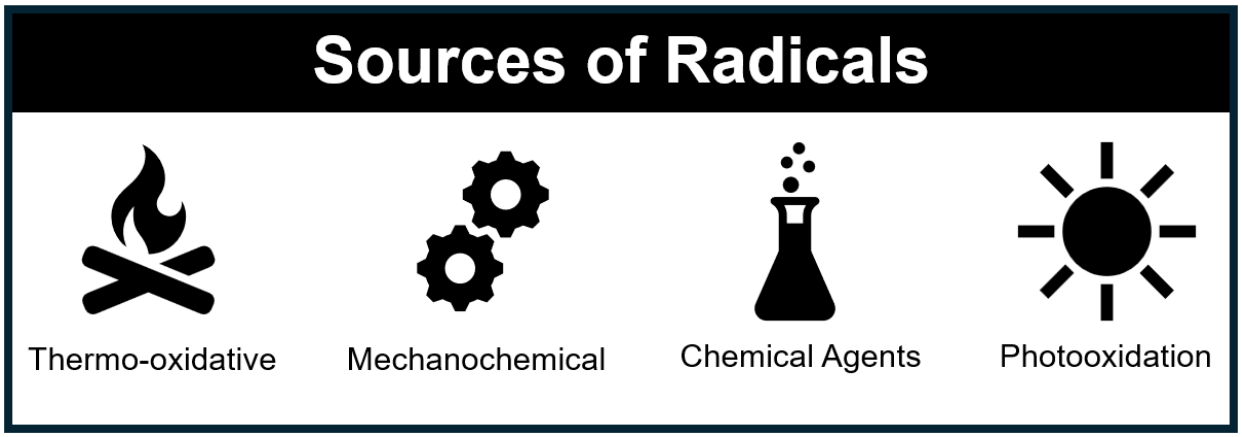


Figure 3: Summary of the sources of radicals commonly used in controlled polymer degradation.

2.3. Crystallinity Modification

In addition to molecular weight, crystallinity is also an essential aspect of polymer processing. Crystallinity can determine which processes a polymer can be used for; therefore, modifying the crystallinity can expand the applications of polymers. While processing parameters such as temperature, cooling rate, and annealing time can be adjusted to maximize the desired crystallization effect, the extent to which crystallization can be controlled is limited by what is intrinsically possible for the polymer. As such, additives of various kinds are typically used to modify crystalline properties.

2.3.1 Processing techniques

There are several processing decisions that impact the final degree of crystallinity of the polymer including temperature, annealing rate, and polymer orientation. For example, selecting a processing temperature just above the melting point ensures the polymer melts completely. This allows the polymer to flow smoothly while eliminating residual crystalline structures that could serve as nucleation sites leading to inconsistent crystallization.[99] Temperature remains important post processing as well with slow controlled cooling (i.e. annealing) producing more uniform

crystals. When a polymer is held just below its melting point and allowed to cool slowly, the crystals have more time to grow and arrange themselves thus creating a more uniform crystalline structure.[100] Finally, the direction in which the polymer is stretched also plays a role in crystallinity. Orienting the polymer chains in a specific direction during processing, such as in uniaxial or biaxial stretching, facilitates ordered packing resulting in improved crystallinity.[101] A similar effect can also be achieved through cold drawing, a technique in which a polymer is stretched while below its melting point. The stress of this method forces molecular chains to align and form new crystalline regions.[102] Overall, processing parameters can be fine-tuned to maximize crystallization, but the polymer's fundamental properties set the ultimate limits. Thus, to exceed the crystallinity limitations of biodegradable polymers, additives are required.

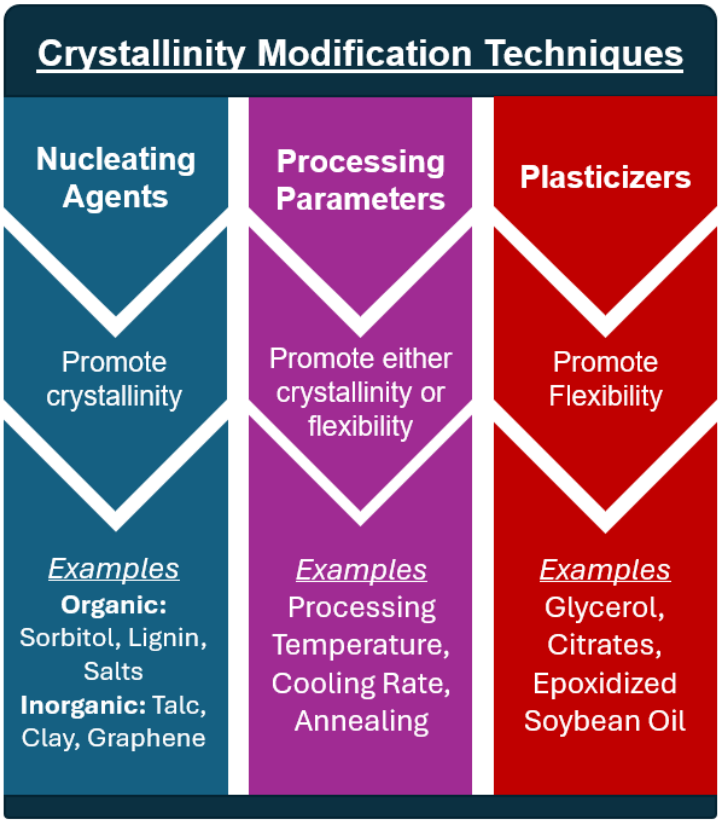


Figure 4: Summary of crystallinity modification techniques.

2.3.2 Nucleating Agents

One of the most well-known limitations of many biopolymers is incredibly slow crystallization kinetics. When crystallization kinetics are slow, polymers require extended cooling times during which the polymer may deform. This limits applications where the material produced is required to maintain a precise shape and size such as injection molding and blow molding. To mitigate these issues and speed up crystallization, scientists turn to nucleating agents. Nucleating agents can be homogeneous, where nucleation is promoted by lowering the energy barrier for the formation of a crystalline nucleus, or heterogeneous, in which foreign particles are dispersed within the polymer matrix to provide a surface on which the polymer chains can align and crystallize.[103] Homogeneous nucleating agents are generally the less efficient of the two, and as such are less common; however, they lead to much more uniform nucleation and therefore are used in applications where that is the priority.[104] Additionally, since they do not rely on external particles or surfaces, they are frequently used in systems where it is necessary to avoid physical particles or when the polymer matrix needs to undergo a specific chemical transformation.[105] Heterogeneous nucleating agents, on the other hand, provide much faster nucleation at the cost of crystal uniformity, making them useful in systems where rapid crystallization is critical.[104] Overall, both types of nucleating agents can be used to accelerate crystallization processes.

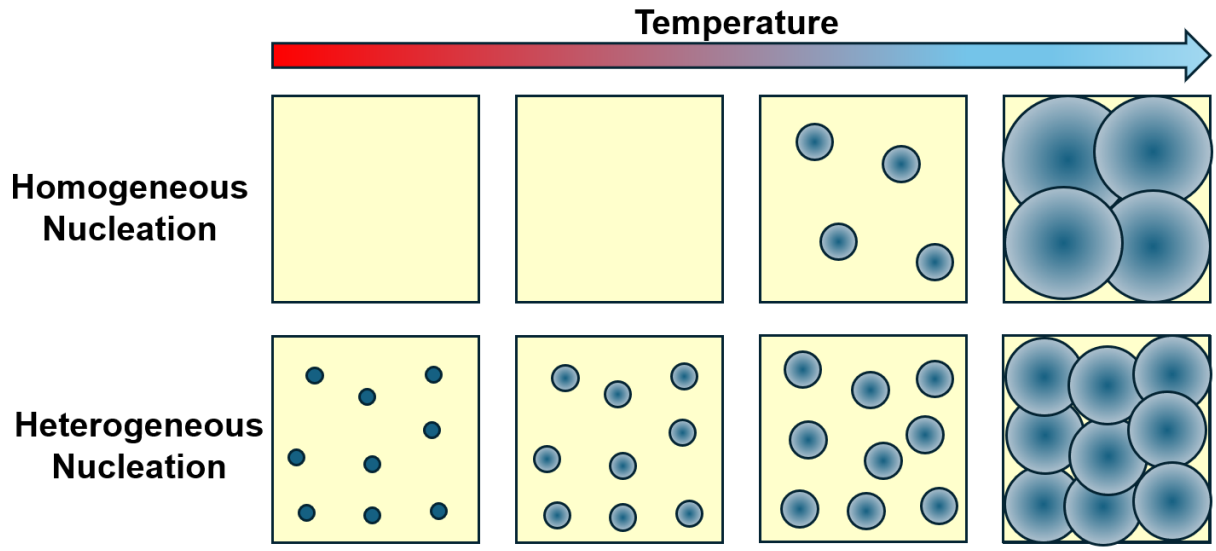


Figure 5: Homogeneous and heterogeneous nucleation during polymer cooling.

Organic Nucleating Agents

Organic materials can be used as both homogeneous and heterogeneous nucleating agents and are typically the preferred choice for improved sustainability. One organic option is sorbitol-based nucleating agents which are commonly used for promoting homogeneous nucleation. When the polymer is melted, these agents dissolve in the matrix. As the polymer cools, the sorbitol molecules start to self-assemble into a nanofibrillar network which provides a high-density distribution of nucleation sites where polymer chains begin to crystallize.[106] This results in small, uniform spherulites which can improve the transparency, stiffness, and strength of the polymer.[106] Sorbitol-type nucleating agents are used most notably for PP. Schawe et al., for example, added various amounts of 1,3:2,4-bis(3,4-dimethylbenzylidene)sorbitol and 1,2,3-tridesoxy-4,6:5,7-bis-O-[(4-propylphenyl)methylene]nonitol to PP to improve the optical properties and examine the connection to cooling rate.[107] It was determined that the haze of the injection molded samples produced correlated linearly to the peak temperature of the main crystallization event.[107] It was also found that the sorbitol content influenced the crystallization temperature and likely changed

the crystallization mechanism.[107] Iwasaki used a similar sorbitol compound, 1,3:2,4-bis-*o*-(4-methylbenzylidene)-D-sorbitol, as a nucleating agent for injection-molded isotactic PP that greatly enhanced the molecular orientation of the PP.[108] These additives are not only used for injection molding, however, as Wang et al. explored the impact of adding 1,3:2,4-bis(*p*-methylbenzylidene) sorbitol on PP foams.[109] When sufficient quantity was added, the system exhibited improved foaming performance characterized by uniform cells with well-defined structures and higher cell density compared to neat PP.[109] The use of sorbitol based nucleating agents can be extended to PLA as well, such as by Zhang et al. who melt blended PLA with D-sorbitol to enhance crystallization and heat resistance[110] and Sebek et al. who did the same with 1,2,3-tridesoxy-4,6:5,7-bis-O-[(4-propylphenyl) methylene]-nonitol.[111] Considering their successes, sorbitol-based nucleating agents show great promise for use as homogeneous nucleating agents in nonbiodegradable and biodegradable polymers alike.

Various promising organic heterogeneous nucleating agents can be obtained from biomass including cellulose, lignin, amino acids, starch, and wood flour.[112] Shazleen et al. used cellulose nanofibers to function as both a nucleating agent and reinforcement material in PLA.[113] The resulting PLA nanocomposites demonstrated a 65-fold increase in crystallization rate as well as a 10% increase in tensile strength.[113] Banpean et al., instead selected softwood lignin nanoparticles as their bio-based nucleating agent for PLA.[114] The total spherulite number of these 1 wt% nanocomposites increased 29-fold while crystallization rate and overall crystallinity increased 240% and 8.3% respectively.[114] Dartora et al. took yet another approach to modifying PLA, using a polysaccharide derived from cashew gum as a nucleating agent which also served to increase crystallization rate and degree of crystallinity.[115] As previously mentioned, nucleating agents also improve foaming performance. As such Chauvet et al. used starch to enhance PLA foams,

producing foams with an expansion ratio greater than 20 and a porosity over 95%.[116] Overall, biomass proves to be a sustainable and effective source of nucleating agents especially for use in PLA.

Amide-based nucleating agents are also frequently used to modify crystallization behavior. These heterogeneous nucleating agents function by promoting hydrogen bonding upon cooling which leads to the formation of fibrillar or platelet-like structures that serve as nucleation sites for the polymer.[117] Like with biomass derived nucleating agents, amide-based nucleating agents are often paired with PLA. Kong et al.[118], Chen et al.[119], and Leoné et al.[120] each examined the impact of a different amide-based compounds (*N,N′,N″*-tricyclohexyl-1,3,5-benzenetricarboxylamide, *N*,*N*-ethylenebis(12-hydroxystearamide) (EBH), and *N*,*N*′-bis(2-hydroxyethyl)terephthalamide respectively) on PLA. Kong et al. determined the effect of the amide additive was enhanced at increased cooling rates while Chen et al. focused on the enhanced heat resistance and transparency obtained.[118,119] Leoné et al., on the other hand, demonstrated that the function of the amide-based agent could transition from a nucleating agent to a plasticizer depending on the conditions.[120] When allowed to crystallize during processing the nucleating effect is observed, however this can be bypassed for a plasticizing effect with rapid cooling to temperatures below the glass-transition, preventing crystallization from having time to occur.[120] PLA is not the only biopolymer of interest for this type of nucleating agent, however. Like Chen et al., Tang et al., used EBH, however they did so with poly(ethylene adipate) (PEA), successfully increasing crystallization rate and thermal stability.[121] As such, amide-based nucleating agents show promise for improving the crystallization rates of biodegradable polymers.

Organic salts provide another source of heterogeneous nucleating agents. These salts function due to their ionic nature which helps them to interact with polymer molecules and promote ordered

crystallization and are used with synthetic and organic polymers alike.[122] Some of the most common types of salts used are benzoates such as by Wang et al. who used sodium benzoate in recycled PET to improve crystallization behavior[123] and Cao et al. who used clay-supported sodium benzoate to promote crystallization and foaming of long chain branched PP.[124] Zhang et al. also worked with PP, promoting nucleation using various hexahrydophthalic acid metal salts including sodium, calcium, lithium, magnesium, and barium.[125] Yang et al. turned to PLA, using zinc phenylphosphonate as a nucleating agent to reduce the isothermal crystallization half time from 28.1 min for amorphous PLA to less than 1 min.[126] PLA was also studied by Nagarajan et al who used an aromatic sulfonate derivate (Lak-301) which increased crystallization rate and nucleation density. A few years later, Jongpnaya-Ngam and Masato synthesized sodium dimethyl 5-sulfoisophthalate to use as a nucleating agent.[127] This synthesized sulfonate derivative outperformed the commercial sulfonate salt, Lak-301, in overall crystallinity and crystallization half time.[127] Overall, a wide variety of acid salts can be used to improve the crystallization rate of polymers.

For crystallization control of biodegradable polymers, it is beneficial for the nucleating agent to also be organic. Various sources of organic nucleating agents exist including sorbital compounds, biomass derived materials, amide-based agents, and acid salts. Sorbital compounds function as homogeneous nucleating agents while the others serve as heterogeneous nucleating agents. While not all polymers studied using the nucleating agents discussed were for biodegradable polymers, the mechanisms can be extended to them to expand their applications.

Inorganic Nucleating Agents

Inorganic compounds can also be used as nucleating agents. These compounds typically serve as heterogeneous nucleating agents as they do not dissolve in the system but rather become dispersed

throughout the polymer matrix to create nucleation sites. Some common inorganic nucleating agents include minerals, nanoparticles, and zeolites. While the inorganic nature of these materials may reduce sustainability, the risk can be mitigated by using materials that maintain their function over multiple recycling cycles or ensuring the nucleators are non-toxic and ideally biodegradable. Overall, these materials maintain their place in the world crystallinity modification of biodegradable polymers.

Minerals, especially talc and clay, are commonly used as heterogeneous nucleating agents. While these materials do not degrade in the environment, they can still be paired with biodegradable polymers relatively sustainably since they are naturally occurring materials and therefore have less of a negative environmental impact than synthetic additives. With this in mind, it is still necessary to consider the sustainability risks associated with mining processes required to obtain these additives. As such these additives are typically used in small quantities like by Huang et al who combined polyvinyl alcohol (PVA) with <10% talc powder to increase crystallinity and improve thickness uniformity of thin films.[128] Talc has also been incorporated into blends of other biodegradable polymers such as PLA/PBAT blends by Phetwarotai and Aht-Ong[129] and PLA/PBS blends by Petchwattana et al.[130] Talc, however, has poor compatibility when blended with polymers; thus, to combat this, Zhu et al. grafted talc to PLA during a ring-opening polymerization of lactide.[131] This modified talcum powder (Talc-g-pla) served as a bridge between PLA and talc, improving dispersion and enhancing nucleating efficiency at lower loadings.[131] An alternative approach to improving efficiency at lower talc loading levels is to combine talc with a biodegradable nucleating agent. Kovalcik et al. for example utilized a combination of lignin and talc to enhance PLA crystallinity and shorten crystallization half time for isothermal crystallization without affecting the thermal processing window of PLA.[132] The same concerns and mitigation

strategies for talc also apply to clay. Ouchiar et al. actually compared the effectiveness of a talc agent against a clay agent, specifically kaolin, demonstrating that for PLA, talc is the much more efficient choice.[133] Thus, while talc is inorganic, it can still be used sustainably to enhance crystallinity of biodegradable polymers.

Graphene is another commonly used nucleating agent in biodegradable polymers. Like minerals, these inorganic compounds come with their own sustainability concerns since they do not biodegrade. Graphene has the benefit of being synthesized rather than mined like talc and clay, reducing that specific environmental impact, however the method of synthesis can greatly impact the sustainability depending on the energy requirements.[134] Processes like chemical vapor deposition, for example, produce high-quality graphene, but require significant energy while graphite exfoliation and synthesis from biomass are more sustainable at the cost of quality.[134] Kashi et al. examined the influence of graphene nanoplatelets in both PLA and PBAT, finding that PLA's crystallinity was significantly increased while PBAT responded with a decrease in crystallinity.[135] Despite the opposite effect of the graphene on PBAT observed by Kashi et al., Ye et al. found that graphene nanoplatelets enhanced the performance of PLA/PBAT blends.[136] This success is likely attributed to the enhanced dispersion of the nanoplatelets achieved by incorporating small amounts of poly(ethylene oxide) (PEO).[136] Liu et al took a similar approach to enhance graphene dispersion in PLA, but with poly(ethylene glycol) (PEG) in place of PEO.[137] This difference did not change the effectiveness and PLA crystallinity and crystallization rates were greatly improved.[137] Overall, when properly dispersed, graphene nanoparticles demonstrate strong nucleating agent capabilities in biodegradable polymers.

In conclusion there are various materials that can be used as nucleating agents to enhance the crystallinity and crystallization rate of biodegradable polymers, both organic and inorganic.

Organic materials are ideal since they are capable of biodegrading alongside the polymers of interest. These materials include sorbitol-type materials capable of promoting homogeneous nucleation in addition to bioderived materials like lignin, starch, and wood flour for heterogeneous nucleation. Additional organic materials that have proven effective for heterogeneous nucleation include amide-based compounds and organic salts. Inorganic materials such as talc, clay, and graphene may be used as heterogeneous nucleating agents, however special measures must be taken to ensure sustainable use of these materials and limit negative environmental impacts.

2.3.2 Plasticizers

Some materials may be overly crystalline, making them too brittle for applications like melt-blown nonwovens that require a minimum level of flexibility. To overcome brittleness, scientists turn to plasticizers. These additives reduce the intermolecular forces between polymer chains, allowing them to more easily slide past each other and therefore increasing elasticity.[33] Plasticizers also lower the glass transition temperature, allowing the polymer to become rubbery and flexible at lower temperatures.[33] Historically, phthalates such as di(2-ethylhexyl) phthalate and diisononyl phthalate were commonly used however use of these materials has decreased in recent years due to health concerns such as endocrine disruptions and reproductive toxicity.[33] As such, this review will focus on non-phthalate options.

Glycerol

Glycerol is a commonly used sustainable plasticizer in biodegradable polymers as it is also biodegradable as well as bioderived and nontoxic. Tarique et al., for example, used glycerol as a plasticizer to develop polymer films from arrowroot starch for food packaging.[138] Glycerol, however, does not always give the desired effect when used alone and therefore is frequently paired

with additional plasticizers like by Harussani et al who combined sorbitol and glycerol to enhance the tensile properties of cornstarch-based biopolymers.[139] While sorbitol was discussed as a nucleating agent for semicrystalline polymers earlier in this review, it can also be used as a plasticizer in amorphous or hydrophilic polymers like starch-based bioplastics. This is because of the many hydroxyl groups contained within this small, hydrophilic molecule which can disrupt hydrogen bonding or Van der Waals interactions between polymer chains and therefor increase chain mobility.[140] Abotbina et al. paired glycerol with a different sugar, fructose, for their cornstarch-based films.[141] The combination of glycerol and fructose outperformed both substances when used independently.[141] Starches are not the only biopolymers treated with glycerol, however; Jost and Langowski examined the performance of glycerol as a plasticizer for PHBV.[142] While it was not the most effective of the plasticizers used, there was still a demonstrable increase in elongation at break and decrease in melting temperature.[142] As such, glycerol can be considered a sustainable option for biodegradable polymer plasticization.

Citrates

Citrates are another option for the plasticization of biopolymers. The most commonly used citrate is triethyl citrate (TEC), a bio-based, nontoxic and biodegradable compound derived from citric acid. Teixeira et al. even compared the effect of TEC against glycerol for use in cellulose acetate films.[143] While both plasticizing agents achieved the same primary effect, secondary properties were distinctly different with glycerol plasticized films excelling in light protection and citrate plasticized films excelling in mechanical properties.[143] Therefore, the choice of plasticizer comes down to the desired final application. Jost and Langowski also looked at TEC along with glycerol, as previously discussed, and other options such as PEG and castor oil for use with PHBV.[142] In their study, TEC was the most effective plasticizer which was attributed to the high amount of

hydrophilic groups.[142] Slongo et al. observed the effect of TEC on PHBV as well, corroborating the results obtained by Jost and Langowski.[144] TEC was also shown to be effective for plasticizing PLA as demonstrated by Maiza et al.[145] As such, citrates prove to be a highly effective sustainable plasticizer for use in biodegradable polymers.

Epoxidized Soybean Oil

Epoxidized soybean oil (ESO) and its ester derivatives can also be used as plasticizers in biodegradable polymers. As the name implies, ESO is derived from soybeans making it bio-based, renewable, and nontoxic. ESO was used as a plasticizer in cellulose-based films by Rebelo et al.[146] It was found the ESO can enhance the flexibility and hydrophilicity of cellulose films, expanding their potential applications.[146] The effects of ESO can be further enhanced through modification or in combination with other materials. For example, starch-based films modified by ESO and citric acid oligomers were produced by Yang et al.[147] Hydrogen bonding interactions were observed between the starch and the oligomers indicating that the addition of citric acid improved the compatibility of ESO with the starch.[147] This also resulted in enhanced tensile strength and thermal stability compared to ESO alone.[147] Li et al. took another approach, adding ESO to PLA and cotton stalk fiber (CSF) composites.[148] The ESO reacted with PLA and CSF to form branched polymers and microgels with increased impact strength and elongation at break.[148] Other groups modified ESO by further processing it into epoxidized isobutyl esters such as Nájera et al.[149] These esters were then used in PLA to increase elongation at break from 8.8% to up to 32%.[150] Overall ESO and its derivatives demonstrate great success as plasticizers for biodegradable polymers.

While phasing out phthalate-based plasticizers is an ongoing project, many nontoxic and sustainable options have demonstrated promising results in biopolymers. Glycerol, citrates, and epoxidized soy oil have all been shown to successfully act as plasticizers. Since these materials

are all biodegradable, they can be trusted to safely break down alongside the biodegradable polymer matrix in which they are dispersed, making them valuable tools for plasticization.

2.4. Polymer Blends

Instead of introducing new types of materials, crystallinity and other polymer properties can be modified by blending polymers with complementary strengths. Poly(3-hydroxybutyrate-co-3-hydroxyvalerate) (PHBV), for example, is a well-known biopolymer that was developed to combat the brittleness of polyhydroxybutyrate (PHB) and the high cost associated with the difficult production of polyhydroxyvalerate (PHV).[151] Alone each of these polymers demonstrate poor processability, but by combining them into a copolymer, PHBV, their weaknesses are overcome resulting in a flexible polymer with good processability and tunable crystallinity.[151] Copolymerization, however, is not a requirement to obtain the benefits of combining polymers as balanced properties can be obtained during processing such as melt-blending. While not all biodegradable polymers are inherently miscible, compatibilization techniques such as malleation, the grafting of maleic anhydride to the polymer backbone using peroxide, can be used to overcome issues of phase separation. As such, many biodegradable polymers are blended with each other, often in the presence of compatibilizers, to establish a material with balanced properties while maintaining biodegradability.

2.4.1 Starch Blends

Starch has been blended with nearly all biodegradable polymers because it is abundant, cheap, and biodegradable. Blending with starch has many functions including accelerating biodegradability and enhancing hydrophilicity. It can also serve as either a nucleating agent if used unmodified or a plasticizer in the case of thermoplastic starch (TPS).[152] Since starch can be obtained from many

crops (e.g. corn, potato, cassava, and rice) it is incredibly sustainable and low cost, making it a great tool for lowering production costs.

Starch/PHA Blends

When TPS is combined with polyhydroxyalkanoates (PHAs) (e.g. PHBV and PHB) it can be used for reinforcement as demonstrated by Eslami et al.[153] Trilayer films were prepared with PHBV as the outer layers and a TPS or TPS/PHBV blend as the core material.[153] The films produced in this manner demonstrated excellent barrier properties making them a great option for sustainable food packaging.[153] Food packaging was also the desired use for starch/PHBV blends prepared by Drummond et al. from cassava root waste.[154] El-Taweel and Al-Hamdi used starch as a nucleating agent in PHBV/ Poly-3-hydroxyoctanoate (PHO) blends.[155] The starch was shown to reduce the activation energy of PHBV and shorten its half-crystallization time enhancing the strength of the material.[155] Similarly, starch was used to enhance the thermal stability of PHB by Lai et al.[156] who grafted corn starch to PVA to improve the compatibility and then blended with PHB to produce a biodegradable and thermally stable blend.[156] As such, PHB and PHBV can be blended with starch, thermoplastic or otherwise, to enhance desired properties while maintaining biodegradability.

Starch/PLA Blends

Starch can also be blended with PLA to serve as a nucleating agent and increase biodegradation rates. PLA, while biodegradable, is only biodegradable under specific conditions such as those found in industrial composting facilities. Even in those conditions, the degradation rate is rather slow. Since starch readily biodegrades, combining it with PLA accelerates the degradation rate compared to pure PLA. Yu et al demonstrated just this, blending TPS with PLA to increase crystallinity and promote degradation in soil.[157] Like with PHBV, combining starch and PLA can

for food packaging can be achieved using the trilayer sandwich method like by Zhou et al.[158] The starch/PLA films consisted of a layer of pea starch and a layer of PLA held together by octenyl succinic anhydride-modified pea starch as a core to improve compatiblity.[158] Applications, however, are not limited to films for food packaging. Starch can be used in PLA foams as well to lower production costs; Chauvet et al. found that an 80/20 blend of PLA/TPS behaved the same way as pure PLA, thus producing a high porosity foam at a reduced cost.[159] Modification of PLA with TPS has even already been used to produce melt-blown nonwovens by Ávila-Orta et al.[160] TPS, like many other biodegradable polymers, has a low MFI and therefore was modified through oxidation and maleation using reactive extrusion. This reduced the molecular weight, increasing the MFI, as well as improving the compatibility between the materials. With the increased MFI, it was possible to melt-blow the blend and achieve a reasonable fiber diameter, albeit larger than that of pure PLA. Overall, PLA/starch blends have a wide variety of applications including melt-blowing.

Other Starch Blends

Starch blends have also been prepared with many other biodegradable polymers for a variety of applications. Da Silva et al., for example, developed physically cross-linked aerogels for use as water absorbers for food packaging from wheat starch and PEO.[161] PBAT has been blended with starch for strengthened films[162] and anti-shrinkage foams with high compression resilience.[163] Starch has also been blended with PVA for foams with higher expansion ratios, cell densities, and melt strengths.[152,164] As society moves towards more sustainable materials, starch blends will inevitably continue to be a part of current research and discussion.

2.4.2 PLA Blends

In addition to starch, PLA has been paired with a wide variety of biodegradable polymers since it the most readily available commercial biopolymer with the global PLA market reaching over 1 billion USD.[165] This biodegradable aliphatic polyester is produced from lactic acid which can be obtained from similar sustainable sources to starch including corn, sugarcane, and cassava.[166] PLA is quite versatile and used in many applications including packaging, 3D printing, textiles, and medical supplies.[166] On its own, it has decent strength, transparency, and barrier properties, however when combined with other biopolymers, these properties can be further enhanced.

PLA/PBAT Blends

PLA is frequently blended with PBAT, a synthetic yet biodegradable polymer that is not yet quite as readily available as PLA. These two biodegradable polymers are commonly combined because they have complementary properties with the high crystallinity of PLA bringing strength and the low crystallinity of PBAT bringing elasticity. Additionally, PLA is less expensive than PBAT and therefore may be used to reduce material cost. Since they are so different, however, they are not entirely miscible and tend to separate if large quantities of both materials are present.[167] When no compatibilizers are present, DSC reveals that the materials behave separately as indicated by the two distinct glass transition and melting temperatures, however there are still tensile benefits when small amounts (<10%) of one are added to the other.[167] Su et al. established that the miscibility of the two can be raised to partially miscible without a compatibilization agent if low molecular weight PLA and PBAT are used,[168] however, to achieve near complete miscibility compatibilization agents are required. Compatibilizing the blends further enhances the benefits of combining them. For example, Zhou et al. used a phosphorus-based ionic liquid compatibilizer which increased elongation at break of the blend by 330% relative to pristine PBAT/PLA.[169] Sui

et al. instead used a random poly(methyl methacrylate) and glycidyl methacrylate random copolymer as a compatibilizer.[170] The addition of this copolymer nearly doubled the maximum strain and quadrupled the tensile strength compared to the pure PBAT/PLA sample.[170] Qiu et al. turned to an epoxy to chemically bind PBAT and PLA at the boundary phase via an epoxide ring opening reaction.[171] These films not only outperformed neat PBAT/PLA films, but also proved superior to PE films in food storage tests.[171] Numerous other methods exists to improve the miscibility of PLA/PBAT including maleation and nanofillers such as graphene oxide and nanocellulose.[172] All of these methods lead to multifunctional versatile polymers, greatly expanding the possible applications of biodegradable polymers.

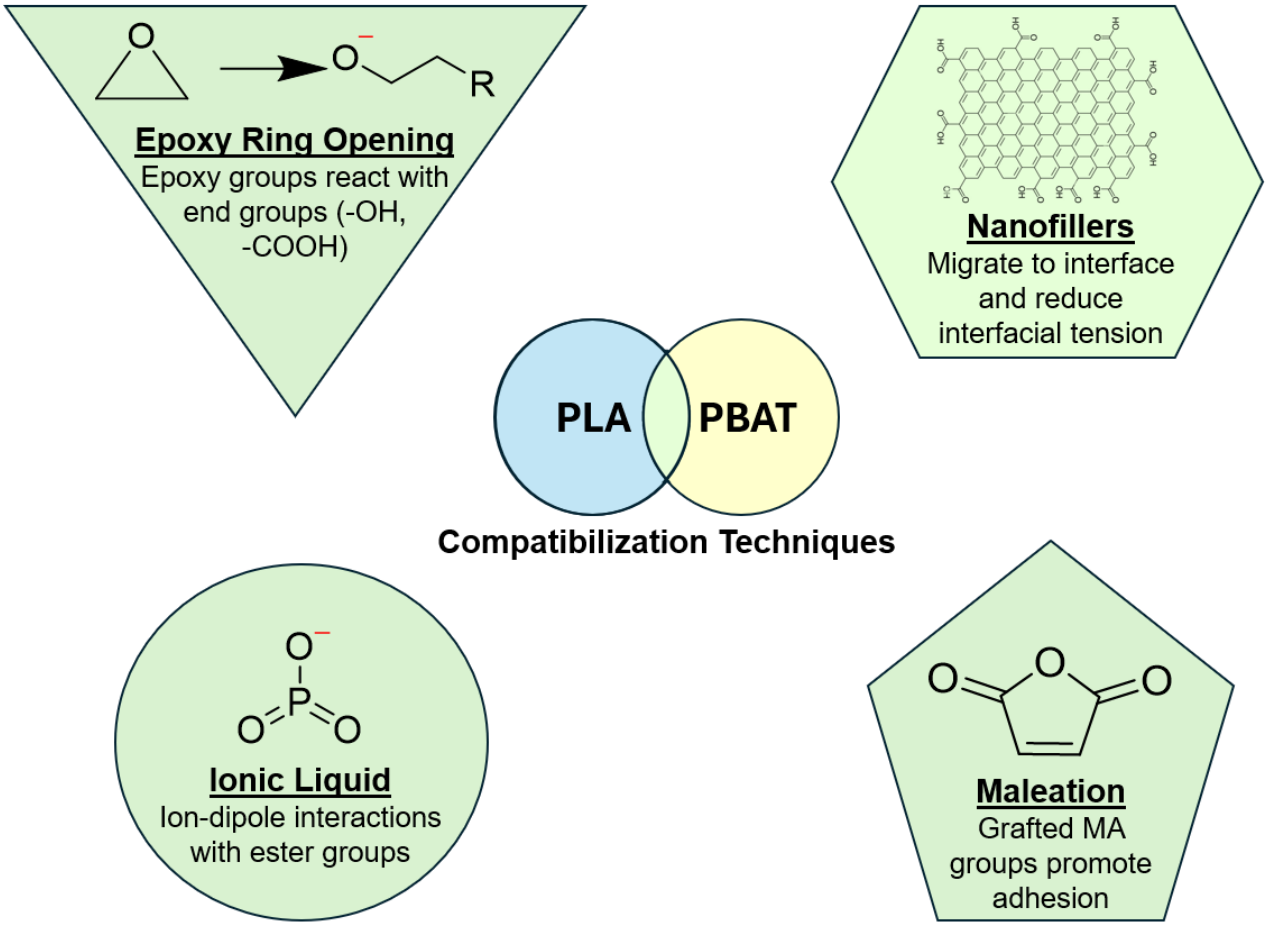


Figure 6: Summary of compatibilization techniques used for PBAT/PLA blends.

PLA/PHA Blends

PLA is also commonly blended with PHAs to accelerate biodegradation and increase toughness. Like with PLA/PBAT blends, compatibilization may be required to obtain the full benefits of the blends depending on various factors such as blend ratio, molecular weight, and crystallinity.[173] Burzic et al., for example, used small amounts of amorphous copolymer PHAs, thus bypassing the need for compatibilization, to improve the impact toughness of PLA.[174] Ecker et al. also used PHAs to improve the impact toughness of PLA but with a focus on processing method.[175] It was found that blends prepared by the 3D printing method known as fused layer modelling outperformed injection molded samples in notched impact properties.[175] Torğut and Gürler, on the other hand, reinforced their PHA/PLA composites with montmorillonite, a mineral compatibilizer, improving thermal stability at the cost of transparency.[176] Szuman et al even produced melt-blown nonwovens from PLA/PHA blends.[177] It was determined that, as expected, phase separation occurred when the two biopolymers were combined in even amounts, however when a majority PLA was melt-blown, finer fibers were produced at lower processing temperatures.[177] Overall, PLA/PHA blends demonstrate properties that expand their applications beyond what each is capable of individually.

Other PLA Blends

PLA has also been blended with a variety of other biopolymers for similar purposes. PLA has been blended with PVA to accelerate biodegradation like by Meng et al who showed that a 20/80 blends of PLA/PVA lost over 85% of its weight in 20 days in soil while pure PLA lost <1% of its weight under the same conditions.[178] These blends also demonstrated increased tensile and flexural strengths.[178] PLA has been blended with poly(ε-caprolactone) (PCL) as well to enhance toughness.[179] PLA has even been blended with additional biopolymers such as chitosan and

collagen for use in medical applications such as scaffolds for cartilage tissue engineering.[180] Overall, blending PLA with other biopolymers allows for additional applications and enhanced properties without sacrificing sustainability.

Various combinations of biodegradable polymers continue to be examined every day as blends can achieve combinations of properties that are rarely found in a single material. While many blends require compatibilization when blended in large amounts, small amounts of one dispersed evenly throughout the other can often achieve the desired effect. If a more equal blend is desired, many compatibilization techniques exist to enhance miscibility and prevent the negative consequences of phase separation. Starch and PLA are both readily available and relatively low-cost biodegradable polymers and as such are frequently blended with other biopolymers to reduce costs or finetune specific properties. While certain blend combinations are more common, new blends are explored every day and continue to expand potential applications for sustainable materials.

2.5. Conclusions

Modern society is dependent on plastics; however, this dependence is putting a strain on the planet that needs to be reduced. The majority of commodity plastics are unsustainable on multiple fronts including synthesis from petrochemicals, accumulation in the environment due to the lack of biodegradability, and contamination of food and water supplies through microplastic release. The ease of processability and convenience of single use plastic materials ensures that no other material can currently replace them despite these sustainability concerns. As such, the solution is to instead develop polymers from renewable sources with structures that promote biodegradability, ensuring they break down completely into harmless byproducts. Many of these polymers have been developed, however, their properties are lacking relative to traditional synthetic plastics and as a result require further development and modification. These biodegradable polymers also suffer

from high production costs which must be reduced in order to make the swap economically feasible.

One method of modification to expand applications and enhance the sustainability of biodegradable polymers is controlled degradation. Many biodegradable polymers are known for having low MFI making them unsuitable for processes requiring high flow speed such as melt-blowing, a simple processing technique for producing melt-blown nonwovens. By purposely reducing molecular weight, it is possible to increase the MFI as shorter chain lengths exhibit less entanglement and therefore flow more readily. Some biodegradable polymers, such as PLA, also suffer from relatively slow biodegradation that requires specific conditions to occur. Thus, to further enhance sustainability, purposely induced degradation can also be used to accelerate end of life breakdown. Overall, understanding and controlling degradation is a critical step towards environmentally friendly polymers.

Enzymes are often utilized for accelerated degradation of polymer waste. These biological catalysts can be sustainably farmed from fungi and other microbes. There are various types of enzymes that break down biodegradable polymers (as well as some that are not typically biodegradable) via different reaction mechanisms. Cutinases, for example, promote hydrolysis while oxidative enzymes such as peroxidases and laccases lead to oxidation. Lyases, on the other hand, lead to β-elimination. Enzymes can be encapsulated and dispersed throughout the polymer matrix to allow for activated degradation or simply introduced to soil or other degradation environments. Either way, enzymes are essential workers in the polymer degradation world.

Radicals are another key to controlling polymer degradation. Radical-induced chain scission can be achieved by radicals obtained from a variety of sources including heat, additives, and radiation. Since heat is a generally unavoidable part of polymer processing, studies revolving around this

type of degradation are often trying to mitigate it rather than accelerate it. Additives, however, like peroxides, are a common choice for controlled degradation in rheology modification. Other additives like metal catalysts and the more environmentally friendly organocatalysts can also be added to the polymer matrix to induce degradation. Finally, radiation, from sun exposure or otherwise, can also contribute to degradation via radical-induced chain scission. No matter what the source, when there are radicals there is chain scission, however it is important to note that crosslinking also occurs in the presence of radicals. As such, in any study utilizing radicals for controlled degradation, it is essential to adjust processing parameters to ensure a chain-scission dominated reaction.

Beyond molecular weight, crystallinity is also an essential parameter requiring modification to expand biodegradable polymer applications. Crystallinity can be altered by a variety of means including processing parameter adjustments and additives such as nucleating agents and plasticizers. Process related changes like operating just above melting temperature and incorporating annealing time and slow cooling rates can help promote crystallization by removing thermal history and allowing time for crystals to align into an ordered structure. Processing parameters, however, can only maximize the crystallization potential inherent to the polymer and thus additives are required to overcome limitations.

Many biodegradable polymers have either low crystallinity overall or slow crystallization kinetics and require assistance from nucleating agents to reach their full potential. Nucleating agents can promote crystallization either by lowering the activation energy such as in homogeneous nucleation or providing surfaces on which the crystals can grow such as in heterogeneous nucleation. Nucleating agents can be either organic like cellulose and lignin obtained from biomass or inorganic like clay or talc. When using inorganic options, it is important to consider the

environmental impacts of both sourcing and disposing of the materials since they do not biodegrade alongside the polymers. To mitigate these impacts, processes are generally optimized to use minimal amounts. As such, both organic and inorganic nucleating agents show promise for use in expanding the applications of biodegradable polymers.

Overly crystalline polymers, however, are extremely brittle and as such are limited in their applications. Plasticizers can be used to overcome this brittleness and enhance elasticity by reducing the intermolecular forces between polymer chains and allowing them to more easily slide past each other. Traditional plasticizers are phthalate based, however due to health concerns, there has been a shift towards organic alternatives such as glycerol and epoxidized soybean oil. These materials are frequently paired with biodegradable polymers since they also degrade naturally in the environment. Thus, organic plasticizers are a sustainable option for modifying biopolymers to allow for expanded applications.

Finally, biopolymers can be modified to achieve all sorts of specific property combinations by combining materials with complementary properties. Starch has been incorporated into nearly every biodegradable polymer as it is low cost and easily obtainable but generally does not perform well independently. By adding starch into other more expensive polymers it can reduce cost and also potentially enhance strength. PLA, while not as inexpensive as starch, is the most widely available biodegradable polymer and as such has been blended with the majority of biopolymers. PLA is most commonly blended with PBAT, however they are immiscible in large amounts and therefore require compatibilization techniques to prevent phase separation. Despite this extra step, PLA/PBAT remains a versatile and relatively accessible biodegradable polymer blend. Overall, blending biodegradable polymers allows them to be used in applications where a single material does not provide the necessary properties.

As research continues, even more modifications of biopolymers will be proposed bringing the world one step closer to sustainable plastic usage. From controlled degradation for viscosity reduction to novel nucleating agents and plasticizers the possibilities are endless. Thus, with all these modification options, it will be possible to expand the number of biopolymers capable of producing melt-blown nonwovens, a major culprit of microplastic contamination. Overall, by utilizing the techniques described to produce sustainable nonwovens, all sorts of disposable items can be used as intended and discarded with a clear conscience.

Chapter 3 – Hydrogen peroxide-induced controlled degradation of poly(lactic acid) for melt-blown nonwovens

3.1 Introduction

Polylactic acid (PLA) is a material of interest to increase sustainability in the realm of polymers since it is both bioderived and biodegradable, under the appropriate conditions (e.g. industrial composting). This versatile thermoplastic can be entirely disintegrated within weeks to months while most traditional petroleum-based plastics may take hundreds of years to decompose and leave behind microplastics in the process, if they even decompose [127]. Currently, about 36% of PLA is used in single use packaging through the use of plasticizers and blown film technology as a replacement for polyolefins, since disposal of these materials has a well-known environmental concern [128]. Additional applications of PLA include agriculture, textiles, electronics, 3D printing, and construction [128,129]. Furthermore, PLA's biodegradability and biocompatibility have led to many biomedical applications where breakdown and/or assimilation of the PLA is required including 3D printed scaffolds, skin regeneration, and drug delivery [128,130].

While PLA is biodegradable, the natural degradation is slow and requires specific conditions to occur, thus PLA degradation techniques have often been studied with the intent to increase composting efficiency or develop sustainable chemical recycling techniques. For example, Xu et al.[84] melt blended PLA with stannous octoate to produce a more rapidly degrading product where the biodegradation rate of the modified samples was increased by 74% under controlled composting conditions. While, Iñiguez-Franco et al.[131,132] successfully degraded PLA samples in a water-ethanol solution for chemical recycling using a sustainable solvent. Modification through intentional and regulated degradation, however, can also be applied for the purpose of creating a controlled rheology grade product. Such controlled rheology polymers could have appealing

processibility and a wider range of applications, including melt spinning, melt blowing, and injection molding. Unlike the previously mentioned applications, in this case, it is necessary to control the extent of degradation to maintain a processable product. This concept has previously been applied to traditional plastics such as polypropylene (PP) by using peroxides to perform radical-induced chain-scission through reactive extrusion [4]. Peroxides, more specifically organic peroxides, are typically used as the source of radical formation along the polymer's backbone; however, they are objectionable as they release undesirable organic volatiles as by-products (e.g. acetone and tert-butanol from 2,5-dimethyl-2,5-di-tert-butylperoxyhexane (DHBP)) [4]. An alternative is to use hydrogen peroxide (H_2O_2) which would instead generate water and oxygen, environmentally benign by-products, and reduce the overall hazard level of the process[133]. Hydrogen peroxide-induced degradation has been applied by Moad et al.[5] to reduce PP's molar mass (MW) through reactive extrusion, successfully mimicking the outcome of using organic peroxides. Thus, it should be possible to extend this theory to PLA and use hydrogen peroxide for controlled MW reduction to develop a product that has high flow ability while remaining processable in desired applications. The introduction of peroxides to PLA has previously been used to improve the strength of PLA by inducing crosslinking [134–139], however it is hypothesized that fine-tuning the reaction conditions (temperature, process time, and H_2O_2 concentration) could promote chain scission while restricting the development of crosslinks.

This study examines the use of hydrogen peroxide for controlled degradation of PLA through reactive batch mixing where both H_2O_2 concentration and processing time are examined. The resulting materials are characterized to determine the impact of the process on molar mass, rheological properties, chemical structure, crystallinity, and other physicochemical properties to gain insight into the ideal reaction conditions and degradation mechanism.

3.2 Experimental

3.2.1 Materials

The PLA used was Luminy L105 (MFI at 210 °C 70g//10 min, T_{melt} 180 – 220 °C) from Total Corbion. Aqueous hydrogen peroxide (H_2O_2) (30 wt. %) was purchased from Sigma Aldrich. Tetrahydrofuran (THF, Acros, 99.9 %), chloroform-D (Cambridge Isotope Laboratories, 99.8%), and chloroform (Sigma Aldrich, ≥99.8%) were used as solvents in this study.

3.2.2 Methods

2.2.1. Reactive batch mixing

Approximately 200 g of PLA was spray coated with varied amounts of aqueous H_2O_2 at room temperature. The mixture was then processed in a HAAKE Polylab QC torque batch mixer at 250 °C and 60 rpm for 0, 5, 7.5, and 10 min trials, after which, the samples were allowed to stabilize at room temperature for at least 24 h prior to characterization. H_2O_2 concentration and processing times are summarized in **Table 1**. Control sample parameters were selected to account for the effects of water and heat introduced by the aqueous solution and melt blending process, respectively.

Table 1: Sample code and formulation.

Sample ID	**H_2O_2** ***Concentration (phr)***	***Processing Time (min)***
Raw PLA	0	0
Ctrl 1	0	10
Ctrl 2	0 (10 phr Water)	10
PLA-5-5	5	5
PLA-5-10	5	10
PLA-7.5-7.5	7.5	7.5
PLA-10-5	10	5
PLA-10-10	10	10

2.2.2. Compression molding

PLA samples were compression molded into flat sheets using a Carver hydraulic press. Sheets of (L x W x T) 76 x 75 x 2.5 mm^3 and 76 x 75 x 0.2 mm^3 were molded between two compressed hot plates that were heated to 190 °C and subjected, incrementally, to six metric tons for 5 min. The sheets were cooled at ambient temperature prior to use in parallel plate rheology and polarized optical microscopy (POM).

2.2.3. Size exclusion chromatography (SEC)

Approximately 2.5 g of sample was dissolved using a condenser set up (130 °C, 1 h) in 50 mL of chloroform to produce a 5 wt.% solution. The dissolved sample was then diluted in THF to reach a concentration of ~ 3 mg/mL and filtered through a 20 µm syringe filter. The samples were analyzed using a Viscotek TDA 302 Gel Permeation Chromatograph equipped with three PLgel columns using THF as the mobile phase and a refractive index detector. A conventional calibration was performed using narrow polystyrene standards (dispersity ≤ 1.1) ranging from 1 to 1000 kDa. Dispersity (*Đ*) was subsequently determined with MATLAB per the procedure described in Mage et al [140].

2.2.4 Proton nuclear magnetic resonance (H-NMR) spectroscopy

Proton (^{1}H) spectra were obtained on a Bruker 300 MHz high-resolution nuclear magnetic resonance spectrometer at room temperature using a total of 64 scans with a relaxation delay of 10 s. Deuterated chloroform was used as a solvent and the sample concentration was ~5 mg/mL.

2.2.5. Melt flow index (MFI)

The MFI, following ASTM D1238, was evaluated using a Kayeness D4002 melt flow indexer. Testing was performed at 190 °C with a load of 2.16 kg and a quarter size bore of 0.45 mm for the die in order to increase control over the flow of the treated samples. Measurements were performed three times per sample and results are reported in units of g/10 min.

2.2.6. Parallel plate rheology

All samples were compression molded at 190 °C into a 2.5 mm sheet as previously described. Disks were cut from the sheets using a heated 25 mm diameter circular punch. Measurements were conducted using a HAAKE MARS rheometer. The linear viscoelastic region was determined using a strain sweep test from 0.001 to 10 at a frequency of 1 Hz and a shear strain of 0.01 was selected for testing. The dynamic measurements were conducted in the range of 0.1 to 100 Hz at 200 °C and a gap of 1 mm. Samples were held at 200 °C for 5 minutes before the frequency sweep test was initiated.

2.2.7. Capillary rheology

Additional rheological studies were performed using a NETZSCH twin-bore Rosand RH2000 capillary rheometer. Two different dies with a 1 mm inner diameter opening, a capillary die with an L/D (length/diameter (inner)) of 16 and an orifice die with an L/D of 0.25, were used at the same time to compensate for the pressure drop and conduct the Bagley end correction. Testing was performed at 190 °C with shear rates of 50 to 3000 s^{-1}.

2.2.8. Polarized optical microscopy (POM)

The crystal structure of the PLA samples (before and after treatment) was investigated using an Olympus BX53M POM optical microscope equipped with a 20x objective lens and a polarized light filter equipped with a Linkam heat stage accessory. Samples were prepared from the 20 μm thick compression molded films. Samples were heated to 200 °C at a rate of 10 °C/min and held at the respective temperature for five minutes. Images were captured at 10 °C intervals as the samples cooled.

POM was also used to determine fiber distribution of melt-blown fiber mats. Fiber mats were placed between glass slides and images were captured at 10x magnification. The diameters of approximately 90-120 fibers per sample were individually measured using the Olympus Stream Basic software measuring tool.

2.2.9. Differential scanning calorimetry (DSC)

Thermal analysis was performed using a DSC Q2000 (TA Instruments). Approximately 6 mg per sample was placed in a separate aluminum T_{zero} pan. Samples were heated up to 200 °C at a rate of 10 °C/min, held at temperature for 3 min and then cooled at 10 °C/min to 0 °C before once again being raised to 200 °C at the same rate. All experiments were conducted under a nitrogen flow rate of 50 mL/min. To avoid any thermal histories found within the systems, the glass transition temperature (T_g), melting temperature (T_m), crystallization temperature (T_c), and melting enthalpy (H_{mPLA}) were all taken during the second heating cycle. Equation 1 was used to calculate percent crystallinity of PLA ($\%\chi_{CrPLA}$) where H_{ccPLA} is the enthalpy of cold crystallization and H^0_{mPLA}, the heat of fusion value if PLA was 100% crystalline, is 93.7 J/g [132].

$$\%\chi_{CrPLA} = \left(\frac{H_{mPLA} - H_{ccPLA}}{H^0_{mPLA}}\right) * 100\% \quad \textbf{(1)}$$

2.2.10 Wide angle x-ray diffraction (WAXD)

Wide angle X-Ray diffraction was performed on a Rigaku Miniflex II with a Cu radiation source and a fixed voltage and current of 30 kV and 15 mA, respectively. Samples were scanned in the 2θ region from 5 to 40° at a rate of 2 °/min with a step size of 0.05°. Percent crystallinity was calculated using **Equation 2** where A_C is the area under the crystalline peaks and A is the total area under the curve.

$$\%\chi_{Cr} = \left(\frac{A_C}{A}\right) * 100\% \quad \textbf{(2)}$$

2.2.11 Melt Blowing

Non-woven mats were prepared using a horizontal twin-screw extruder (Process 11 Parallel Twin-Screw Extruder, Thermofisher Inc) equipped with a custom die for melt-blowing. The die configuration included a jet angle cap, a melt feed nozzle, and a gas feed. The gas flow direction and custom die were reminiscent of Exxon slot dies that are often used in commercial melt-blown fiber production [3,141,142]. The outer cap contained a single outer hole 2.5 mm in diameter and a 128° impinging air jet angle to generate blown fibers with heated nitrogen gas. The extruder temperature was set to 170 – 200 °C while the nitrogen air jet was controlled to ~350 °C using a transformer (Powerstat® Variable Transformer) connected to a 750W heating torch (Laramy Products, Lyndonville, VT, USA). The screw speed was set to 100 rpm and the gas volumetric flow rate (0.5 L/min) was adjusted using the nitrogen gas gage pressure. Fibers were collected from ~40 cm away from the die opening using a parchment paper-covered conveyor belt rotating at 60 rpm. Further details and depiction of the experimental set up is found in Lee et al [143,144].

2.2.12 Scanning electron microscopy (SEM)

Field emission scanning electron microscopy (FESEM) (FEI Quanta Feg 250, Oxford Instrument) was used to examine the surface morphology of the fiber mat samples at a 20kV voltage. Observations were conducted at 50x and 600x magnification levels.

3.3 Results and discussion

3.1 Chemical structure changes

3.1.1. Size exclusion chromatography (SEC)

The dispersity of the treated PLA samples was evaluated using SEC as a function of the processing conditions, as molecular size is a critical polymer property that affects physico-mechanical properties, including rheology, solubility, processibility, thermal, and tensile properties. It is important to note that SEC was performed using a polystyrene standard, as such, the results can only be considered semiquantitatively. This is because SEC separates on the basis of hydrodynamic volume of polymer coils in solution and PLA and PS behave differently in THF so a direct comparison cannot be made. For the purpose and scope of this study, semiquantitative results are sufficient as the focus lies on the relative values between treated and untreated samples, thus absolute values are not required for this distinction. The refractive index data obtained through this method in **Figure 7** shows a clear shift in retention volume for the treated samples, indicating that a decrease in MW has occurred as a result of chain scission.

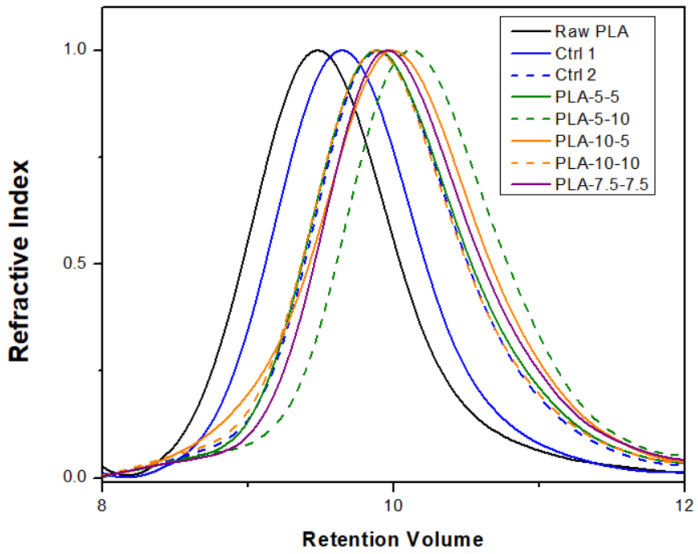


Figure 7: SEC results for PLA and treated PLA samples.

The samples with the greatest decrease in molar mass, PLA-5-10, PLA-7.5-7.5, and PLA-10-5, show a reduction in their weight average molar masses (M_W) of 70, 61, and 57%, respectively. This suggests that lower concentrations of H_2O_2 along with high processing times work synergistically towards reducing the M_W of the samples. However, at higher H_2O_2 concentrations it was found that processing time has the opposite effect meaning that long processing time allowed the system to repair itself (i.e. crosslinking) and maintain more of its original M_W. It is well known that PLA begins to crosslink with itself in the presence of peroxides as a result of the chain radicalization [134–139,145].

Peroxide-induced polymer crosslinking is believed to follow three key steps. First, primary radicals are generated by the thermal decomposition of peroxides. These primary radicals then generate polymer radicals through abstraction of tertiary hydrogen atoms found weakly bonded along the polymer's chain structures. Finally, the polymer radicals recombine to form carbon-carbon cross-links [134]. This technique is often used to increase the strength of PLA, all the while increasing the PLA's viscosity. Therefore, it can be assumed that a critical processing time exists

where the primary mechanism transitions from chain scission to crosslinking. SEC data suggests that this shift would occur more quickly as peroxide concentration increases. The shift has likely already occurred within PLA-7.5-7.5 and PLA-10-5 in addition to PLA-10-10 as the MW of these samples is significantly higher than that of PLA-5-10.

This transition to crosslinking is further supported by the Đ increase seen in PLA-10-10. All the samples exhibit some level of Đ increase, as can be seen by the broadening of the peaks. This implies random chain scission as there is no preference for where in the chain the break will occur, thus resulting in a wider Đ. PLA-10-10, however, shows the greatest increase by far. This can be explained by the impact of branching or crosslinking combining multiple smaller adjacent polymer chains together to create a subset of chains much larger than the rest. This is reflected by the nearly 20% increase in weight average molar mass (M_W) from PLA-10-5 to PLA-10-10 accompanied by only about a 2% increase in number average molar mass (M_n) leading to a wider dispersity overall.

In addition to the random chain scission and crosslinking reactions, heat and water are also contributors to the changes in MW as demonstrated by the Ctrl 1 and Ctrl 2 samples. Ctrl 1 shows that heat alone causes significant degradation to PLA, reducing the M_W by 25% after being subjected to 10 mins of heating. Thermal decomposition of PLA is known to begin at 200 °C, therefore it is unsurprising that processing at 250 °C would result in a noticeable decrease in MW [146]. The addition of water in Ctrl 2 also introduces hydrolysis, a known contributor to PLA and many other polyester degradations, causing the M_W to decrease by more than half. While this decrease in MW is not as substantial as that experienced by the peroxide treated samples, it is far from negligible. Since the H_2O_2 solution is aqueous and water is introduced as a byproduct, a significant portion of the degradation exhibited by the peroxide treated samples can be attributed to hydrolysis, however additional degradation cannot be explained by water alone.

3.1.2. Proton nuclear magnetic resonance (^{1}H-NMR)

To determine the exact structural changes occurring during the peroxide-induced degradation, proton NMR was performed. As seen in **Figure 8 (b)** to **(d)**, NMR revealed the introduction of a new peak at 1.69 ppm and the reduction of the peak at 3.73 ppm. The new peak at 1.69 ppm is within the methyl (CH_3) region [147–149]. This could represent an increase in D-isomer causing a change in stereo-tacticity [150]. This change, along with the likely methylene group change at 3.73 ppm, could be occurring due to a combination of chain scission and potentially trans-esterification reactions through alcoholysis [151]. Smaller molecules have shown to initiate alcoholysis in PLA more easily and therefore the OH radicals produced by the decomposition of hydrogen peroxide would likely be capable of executing this process [152]. Alcoholysis is typically studied for chemical recycling of PLA, however H_2O_2 would not be a good candidate for that since, if alcoholysis is occurring, it is only a minor contributor to the overall process and is quickly overtaken by crosslinking which has the opposite effect. Thus, overall, there are several reactions that may be occurring during the processing of PLA with aqueous H_2O_2 including hydrolysis, chain scission, crosslinking, and potentially alcoholysis; a summary of the possible reaction mechanism can be found in **Figure 8 (a)**.

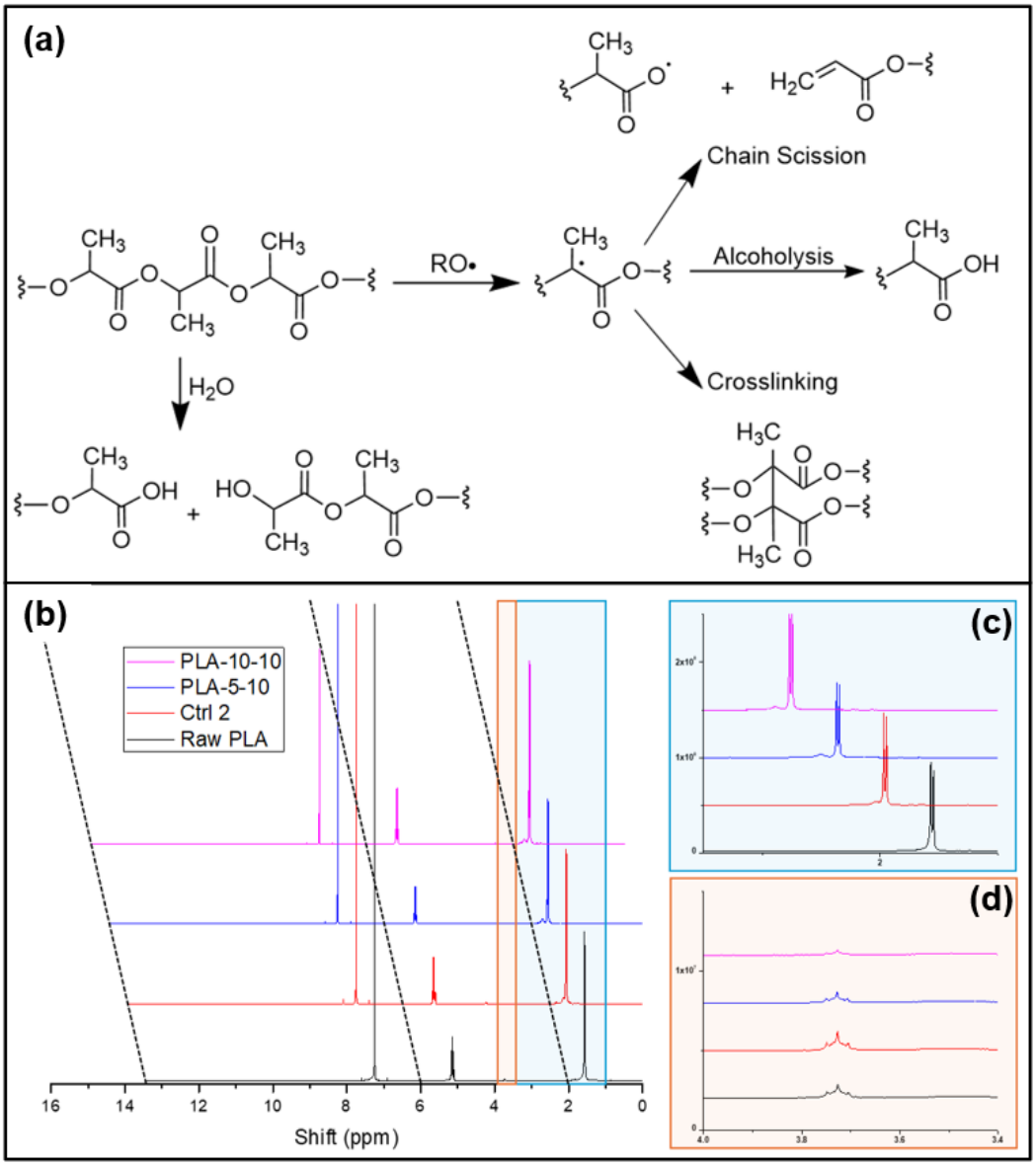


Figure 8: (a) Possible reaction mechanisms during H_2O_2-induced degradation of PLA [84,91,135,136,153]; **(b)** full H-NMR spectra of samples; **(c)** changes in the methyl region; and **(d)** changes to the methylene peak.

3.2 Rheological properties

3.2.1. Melt flow index (MFI)

The calculated MFI for each sample is shown in **Figure 9 (a)**. The control samples (temperature and moisture effect) exhibited a slight rise in MFI, while the magnitude of the change in MFI for all peroxide treated samples was much greater. Of the treated samples, PLA-5-10 had the greatest

increase in MFI (15,000 %). This aligns well with the SEC results where PLA-5-10 was shown to have the greatest decrease in MW. The overall increase in MFI makes the treated PLA suitable for processes that require low viscosity, such as melt blowing operations. However, the trend among the other treated samples is not as clear in this test. This is likely due to the increased error of measuring a high flow material using a manual testing method. Further rheological studies using more precise methods were performed to bring greater insight into which treatment combinations were most effective.

3.2.2. Parallel plate rheology

Viscoelastic behaviour is an essential part of polymer rheology and characterization, requiring extensive testing beyond that of only MFI. To determine the impact of the hydrogen peroxide and prolonged heat exposure treatment(s) on the viscoelastic behaviour of PLA (shown in **Figure 9 (b)** to **(d)**), isothermal frequency sweeps were performed on all samples at 200 °C using a parallel plate rotational rheometer at a constant shear strain of 0.01% (in the linear viscoelastic region). **Figure 9 (b)** shows the complex viscosity (η*) of the samples as a function of angular frequency (ω). All samples exhibit shear thinning behaviour that closely follows a simplistic Carreau model (**Equation 3**).

$$\eta = \eta_\infty + (\eta_0 - \eta_\infty) / \left(1 + \left(\frac{\omega}{\omega_\beta}\right)^2\right)^n \quad \textbf{(3)}$$

Where η is viscosity, η_∞ is the infinite-shear viscosity, η_0 is zero shear viscosity, ω is angular frequency, ω_β is the critical angular frequency, and n is the power law index.

The overall fit of the model does not appear to change with hydrogen peroxide treatment conditions; however, the zero-shear viscosity is reduced for the treated samples. PLA-5-10, PLA-10-5, and PLA-7.5-7.5 show the most significant drop in viscosity. This aligns well with the SEC

results where the same samples show the greatest decrease in MW. This provides further evidence that lower concentrations of hydrogen peroxide have an increased effect when treated with heat for longer periods of time while higher concentrations benefit from shorter processing times, suggesting a shift from chain scission to crosslinking that occurs more quickly at higher peroxide concentrations.

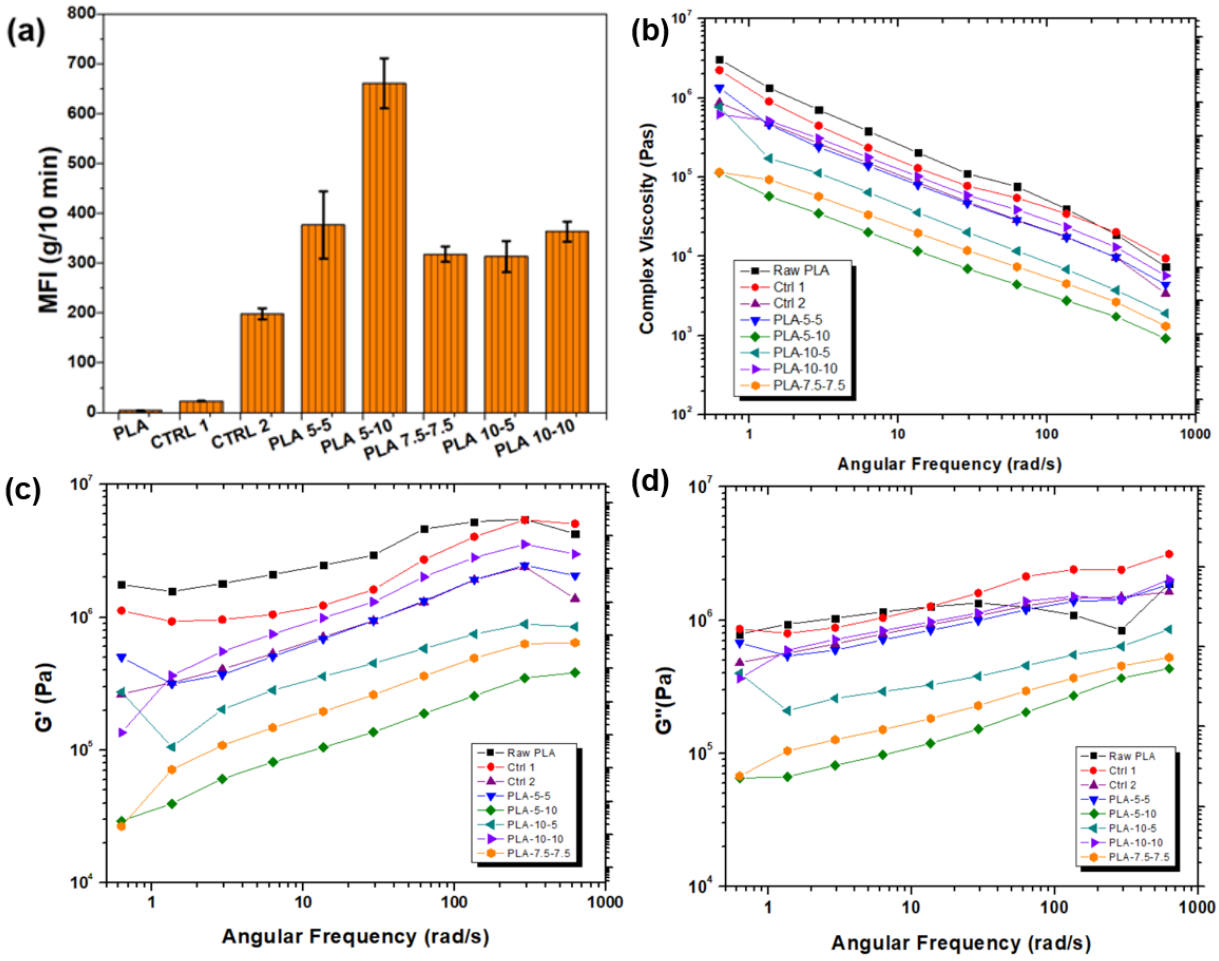


Figure 9: (a) Melt flow index of PLA samples at 190 °C with a load of 2.16 kg; **(b)** Complex viscosity as a function of angular frequency at 200 °C; **(c)** Storage (G') and **(d)** Loss (G") modulus of PLA samples at 200 °C.

Storage and loss modulus of the samples as a function of angular frequency at 200 °C can be seen in **Figure 9 (c)** and **(d)**. As with the viscosity results, there is no apparent change to the behaviour

of these parameters other than a decrease in magnitude which is expected as smaller chains found in lower MW samples exhibit less entanglement and thus have a lower capacity for deformation. The cross-over point of the storage and loss modulus can also be evaluated to gain insight into the system's MW and, in this case, also shows the decrease in MW trend among the treated samples. As seen in **Figure 10 (a)**, the cross-over point among PLA-10-5 and PLA-7.5-7.5 occurs at a much lower angular frequency than that of the control sample shown. The cross-over, or gel point, occurs when the material switches from liquid-like to solid-like behaviour and is related to the structure of the material [154]. A decrease in MW would alter the structure by reducing chain length and explain the shift towards lower MW seen in the treated samples.

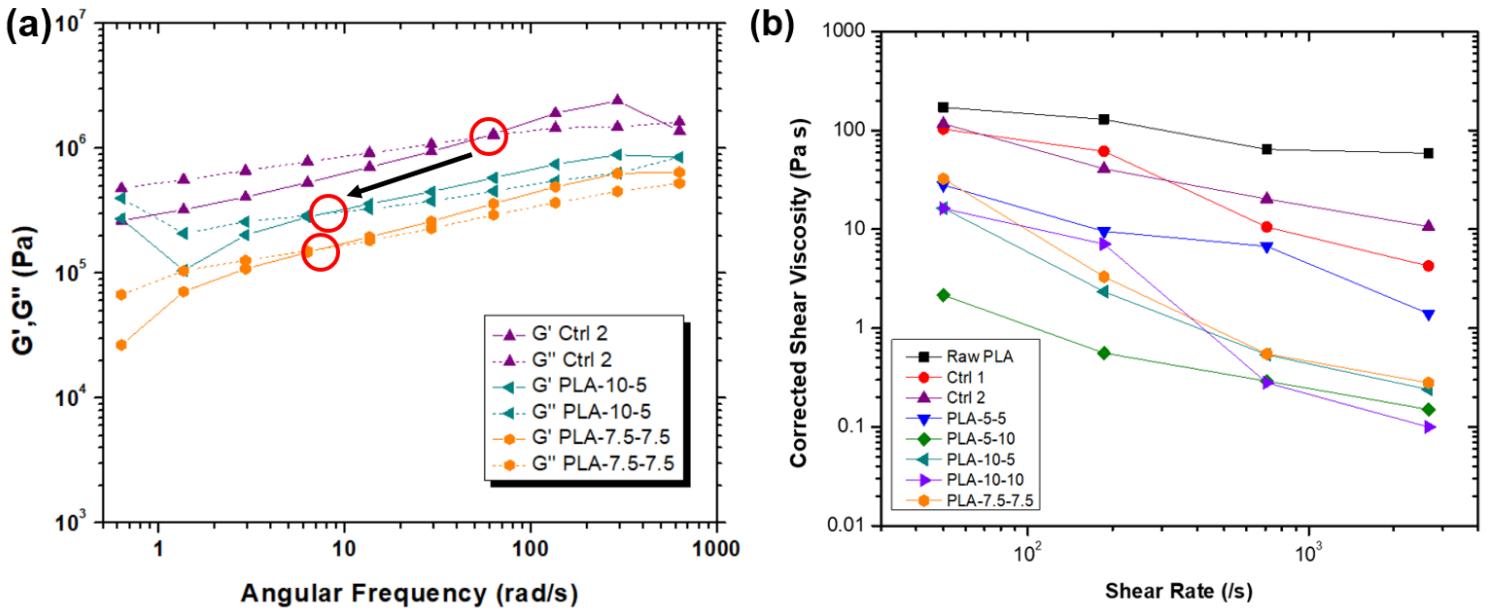


Figure 10: (a) Storage and loss moduli cross-over for Ctrl 2, PLA-10-5, and PLA-7.5-7.5 at 200 °C and **(b)** Corrected shear viscosity as a function of shear rate at 190 °C.

3.2.3 Capillary rheology

Rheological measurements were also performed using a capillary rheometer to better imitate extrusion applications. Corrected shear viscosity as a function of shear rate can be found in **Figure**

10 (b) where a clear decrease in viscosity is seen for the peroxide treated samples. As with the parallel plate rheometer, the samples that experienced the greatest decrease in viscosity were PLA-5-10, PLA-10-5, and PLA-7.5-7.5, indicating again that longer processing times increase the effect of low hydrogen peroxide concentrations while longer processing times decrease the effectiveness of high peroxide concentrations on viscosity. As previously stated, there is likely a transition from chain scission to crosslinking that occurs as the higher concentration sample is processed resulting in the increased viscosity. Overall, this trend suggests that using lower peroxide concentrations would give greater control over the extent of degradation as the reaction transitions to crosslinking much later, allowing for more flexibility in processing time and the ability to achieve lower MWs.

3.3 Crystallization

3.3.1 Polarized optical microscopy (POM)

Crystal formation and structure was studied using a POM where the samples were heated to 200 °C and, upon cooling, the crystal formation was observed until the samples returned to ambient temperature. Pictures were captured to track crystallite growth as a function of cooling temperature and can be seen in **Figure 11 (a)**. Compared to the raw PLA, the treated samples formed fewer crystallites upon cooling with peroxide concentration appearing to have the greatest effect on the number of crystals formed. The lower concentration samples formed the fewest crystallites, therefore experiencing the greatest decrease in crystallinity, while the higher concentration samples exhibited no obvious change. The onset of crystallite formation, however, was reduced among all the treated samples; crystallization occurs at a lower temperature for the treated samples and the overall growth was slower. Interestingly, this shift in crystallization temperature, rather than the decrease in overall crystallinity, is what aligns with the degradation trend seen in previous tests where PLA-5-10, PLA-7.5-7.5, and PLA-10-5 experience the greatest effect.

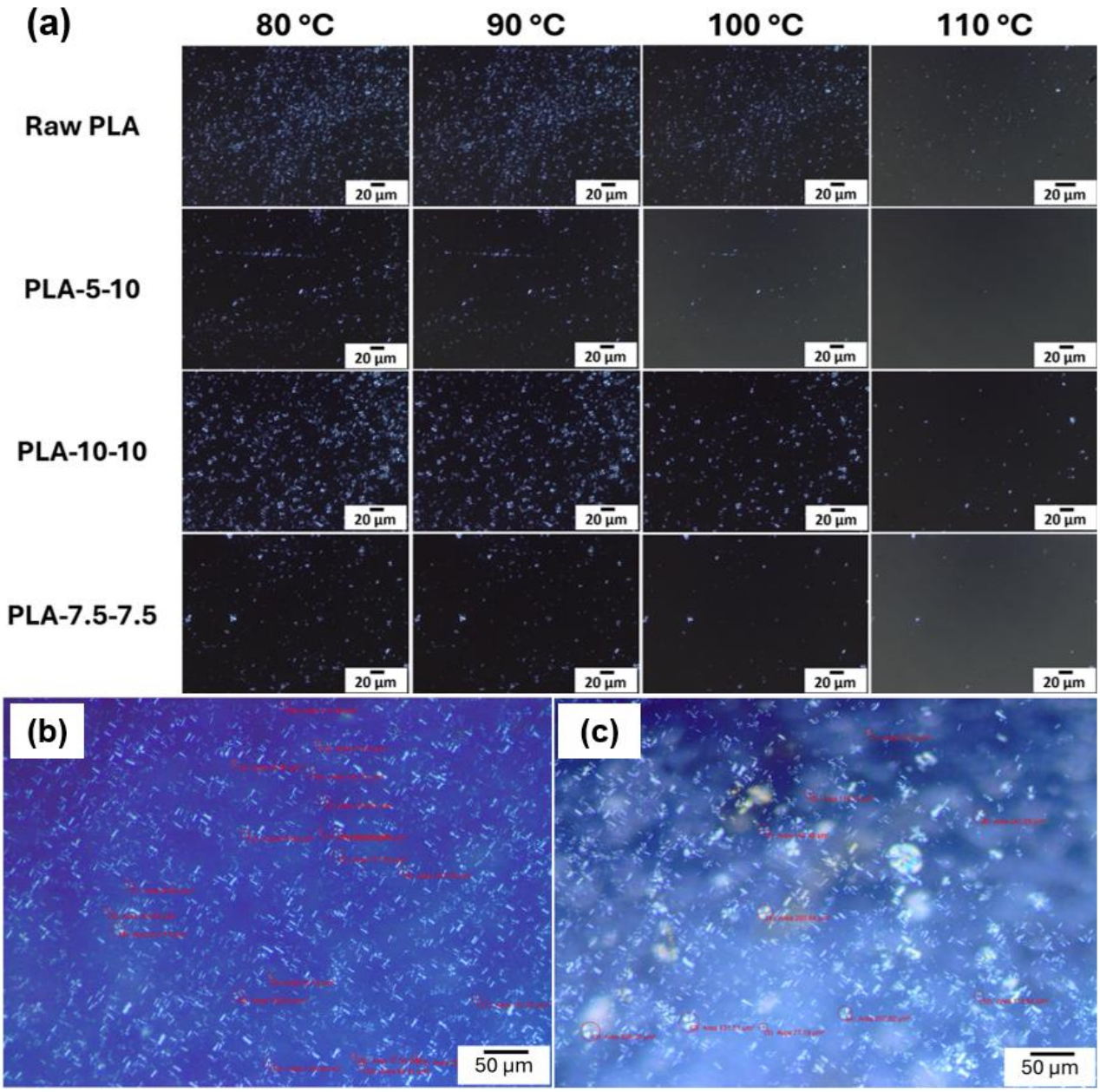


Figure 11: (a) PLA crystallization upon cooling using POM; close up of the crystal structure of **(b)** raw PLA and **(c)** PLA-5-10 after cooling to 100 °C.

Looking more closely at crystallite size and structure (**Figure 11 (b)** and **(c)**) it can be seen that a large quantity of small crystallites formed uniformly in the raw PLA sample as it cooled while the peroxide degraded sample developed fewer, but larger crystallites, many of which failed to form a complete Maltese cross. When treated as a circle, the average area of the crystallites in the degraded sample was 204.2 μm^2 (n = 10), approximately twice that of the raw PLA whose average

was 101.7 μm^2 (n = 20). Additionally, the standard deviation among the degraded samples crystallites was 129.0 μm^2 and while it was only 51.0 μm^2 in the untreated sample showing a greater crystallite size distribution among the degraded samples. This is likely due to the reduction in chain length increasing the mobility of the chains and therefore making it difficult to form stable crystal nuclei [155].

3.3.2. Differential scanning calorimetry (DSC)

DSC can give further insight into quantifying crystallization behaviour. The DSC thermogram and calculated percent crystallinity for the samples are shown in **Figure 12 (a)** and **(d)** while additional parameters including T_g, T_{cc}, and T_m can be found in **Table A1.**

. The treated samples display a lower degree of crystallinity than the raw PLA, however the control samples showed a reduction as well. The reduction in the control samples, especially Ctrl 1, is due to the heat as thermal degradation has shown to decrease crystallinity [156]. The increase in crystallinity between Ctrl 1 and Ctrl 2 can be explained by chemi-crystallization. In semi-crystalline polymers, the chain scission process occurs only in the amorphous phase by freeing new chain segments which, if they have sufficient mobility, can then integrate into the crystalline phase [157]. This is known to occur for the hydrolytic degradation of PLA as water can more readily penetrate amorphous regions due to their larger free volumes relative to crystalline regions, thus reducing the amorphous regions and increasing crystallinity [132]. For the peroxide treated samples it can be seen that the lower peroxide concentration had a much greater impact on crystallinity than the higher concentration, however the most significant reduction in crystallinity was seen at the midpoint of PLA-7.5-7.5.

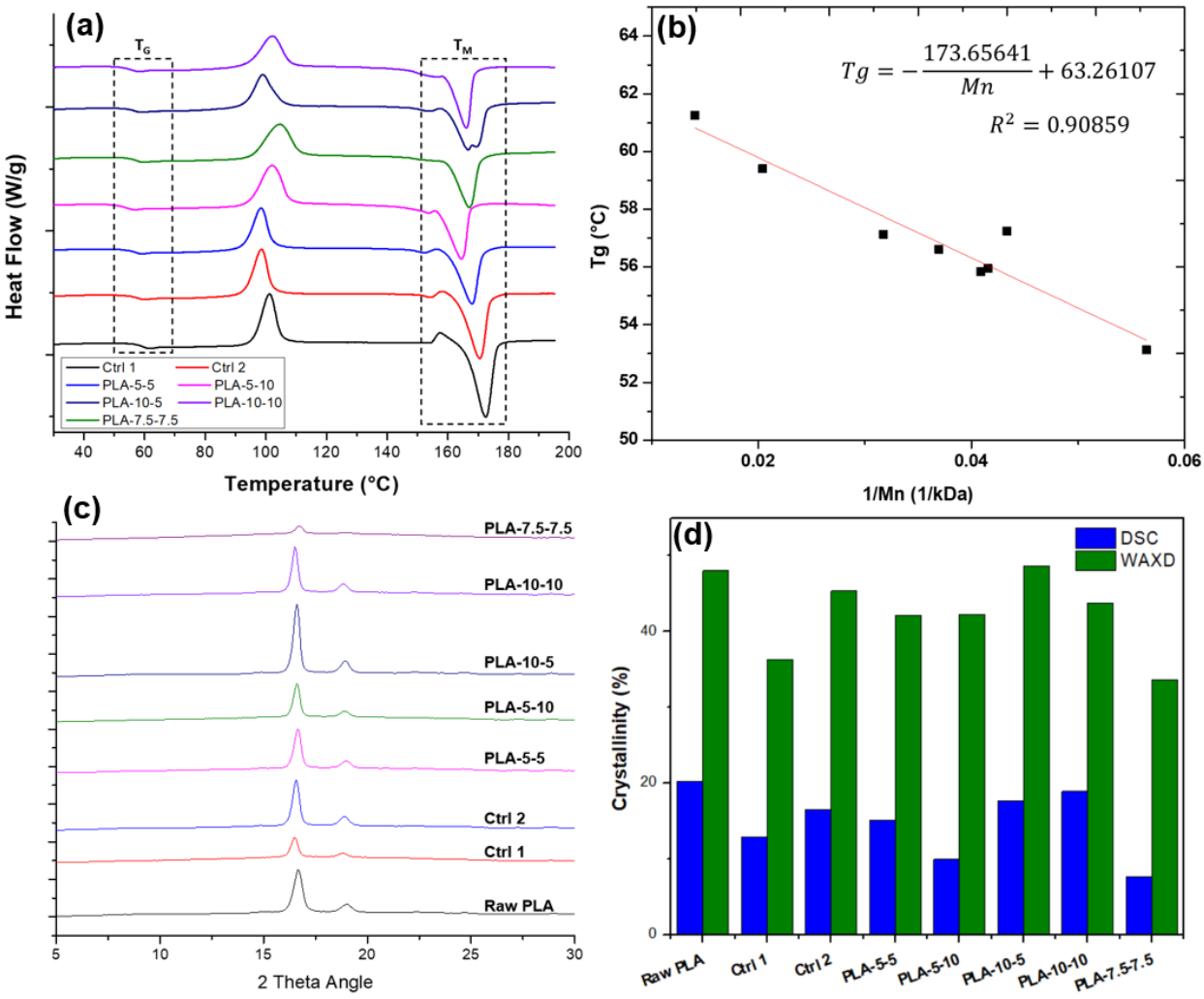


Figure 12: **(a)** DSC heating thermogram (2nd cycle); **(b)** Flory-Fox plot of PLA molar mass and glass transition temperature; **(b)** WAXD profiles; **(d)** %crystallinity for all samples.

Additionally, the higher concentration showed greater levels of crystallinity than the control samples, suggesting the formation of additional new crystals beyond the water induced chemi-crystallization. Notably PLA-10-5 exhibits two different melting peaks which is indicative of the formation of both alpha and beta crystals with the less ordered beta crystals melting first [158]. These less ordered crystals may be responsible for the increase in overall crystallinity exhibited by the higher peroxide concentration samples.

Treated samples also showed a clear decrease in T_g and T_m which can be linked to crystallinity. Amorphous PLA has lower T_g and T_m values than crystalline PLA, therefore the decreased values among the peroxide treated samples further confirm a decrease in crystallinity [159]. The decreased T_g can also be related back to MW. This relationship is described by the Flory-Fox equation (**Equation 4**) where $T_{g,\infty}$ is the glass transition temperature at infinite molar mass and K is a constant [160].

$$T_g = T_{g,\infty} - \frac{K}{M_n} \quad \textbf{(4)}$$

Plotting the T_g of the treated samples against $1/M_n$ as in **Figure 12 (b)** reveals that the samples follow this relationship quite well producing a K value of 173.7 and a $T_{g,\infty}$ of 63.3 °C. K values reported in literature vary, ranging from 80-160, so the obtained value, while on the higher end, can be considered reasonable [161–163]. The value for $T_{g,\infty}$ aligns with values reported in literature [161–163]. The sample that deviates most from the trend is the midpoint samples, PLA-7.5-7.5, which experienced a much greater decrease in crystallinity than any other sample, thus the shift in T_g may be more greatly influenced by crystallinity than molar mass in the case of this sample. Removing this sample improves the fit, increasing the R^2 value to 0.988 and slightly increasing K and $T_{g,\infty}$ to 184.7 and 63.4 °C respectively.

Additionally, the treated samples exhibit broadening of the melting peak which can be attributed to degradation via random chain scission as it is a sign of a wider dispersity. Further indication of a change in crystal structure is the decrease or disappearance of the second cold crystallization peak among degraded samples.

3.3.3. Wide angle x-ray diffraction (WAXD)

For further confirmation of crystallinity, WAXD was performed, and the crystalline fraction was calculated from the results (Error! Reference source not found. **Figure 12 (c) and (d)**). Among all s amples, the same two peaks were identified at 16.8 and 19.1° which correspond to the formation of alpha crystals [164]. Despite indication of additional crystal structures from DSC of treated samples, no additional peaks were observed. This, however, may be due to relatively low sensitivity of the WAXD testing parameters. While there were no noticeable changes to the number of peaks, there were clear changes to peak intensities indicating an effect on overall crystallinity. Calculating crystallinity from WAXD produced absolute values for crystallinity two to three times greater than those calculated using DSC, however the trend among samples remains unchanged. The lower peroxide concentration had a greater impact on crystallinity than the higher peroxide concentration, however the midpoint had the greatest reduction overall.

3.4. Application in Melt Blowing

3.4.1 Processing

PLA-5-5 was selected as the optimum candidate for melt blowing since it achieved a significant melt flow increase while using minimal hydrogen peroxide and processing time and exhibiting only a moderate degree of degradation. Raw PLA was processed as well for comparison. The initial processing temperature for each sample was selected to be just above the melting point after which the temperature was increased twice by 10 °C giving a range of 170-190 °C for PLA-5-5 and 180-200 °C for Raw PLA. Fiber mats produced in this manner can be seen in **Figure 13**. While PLA-5-5 produced smooth fibers across all temperatures, the Raw PLA did not begin to do the same until 200 °C with lower temperatures resulting in loosely packed rough strands dotted with hard beads. Considering the melting point of PLA-5-5 was determined to be 168 °C, this suggests that

the treated samples exhibit high flow behavior immediately upon melting while the Raw PLA (T_M = 174 °C) requires processing temperatures >25 °C above melting point to achieve sufficient flow. This increased flow behaviour of the treated material is further exhibited by the wider angular distribution compared to the untreated PLA. Additionally, melting occurred much more rapidly with the treated samples, producing usable final material within minutes of loading whereas, even at 200 °C, the raw PLA required 10-15 min to begin producing material representative of the final product. This is significant as the treated sample greatly reduced the amount of scrapped product during initialization. Together, the lower temperature requirements, wider angular distribution, and reduced scrap associated with the treated PLA suggest a strong potential compatibility with industrial scale melt blow processing.

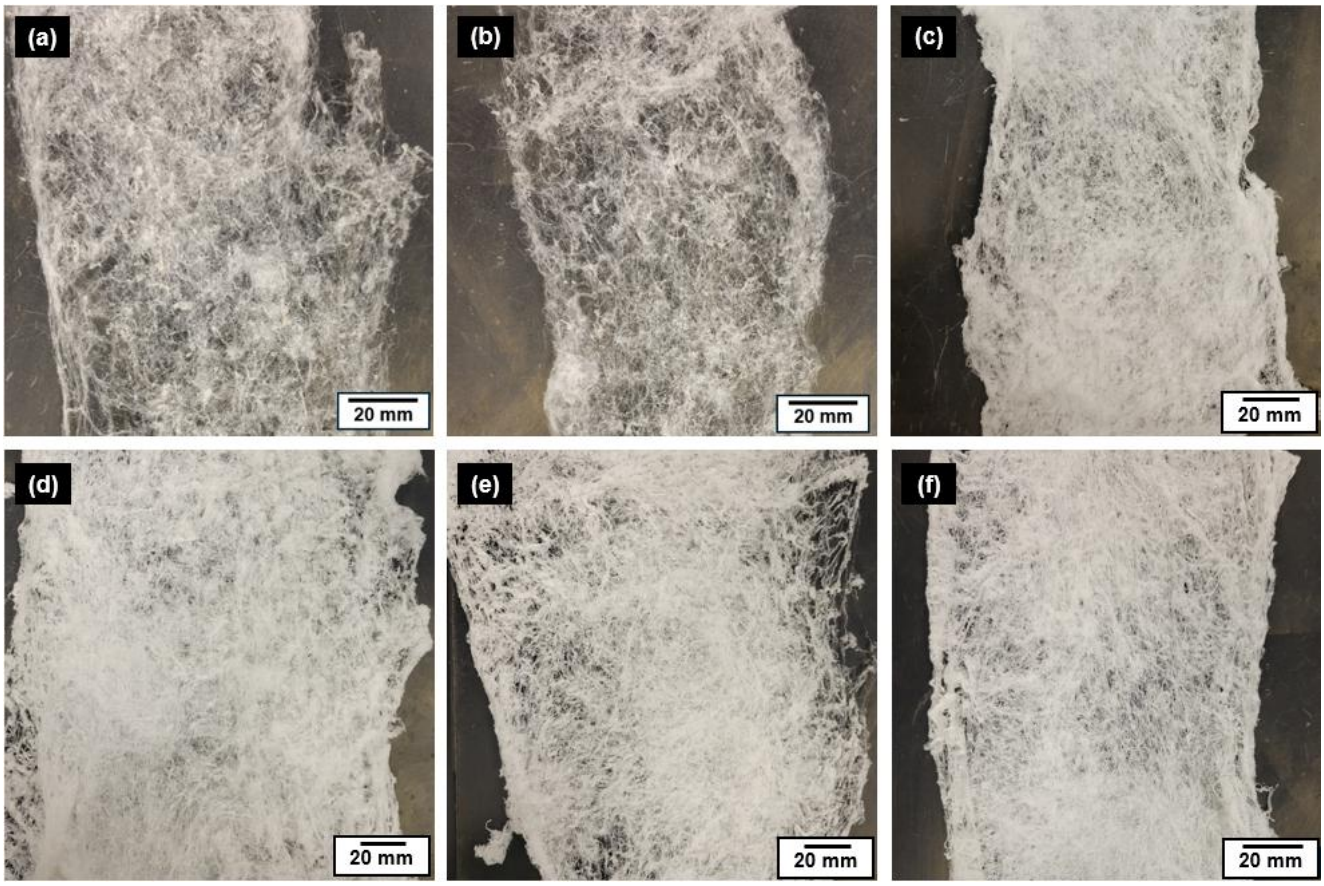


Figure 13: Fiber mats produced from Raw PLA at 180–200 °C **(a-c)** and PLA-5-5 at 170–190 °C **(d-f).**

3.4.2 Fiber Characterization

Looking more closely at the fiber mats using POM and SEM provides further insight into the fiber quality. **Figures 14 and 15** show the morphology and fiber size distribution of Raw PLA and PLA-5-5, respectively. Average fiber size decreases as temperature increases across both Raw PLA and PLA-5-5, however the change is much more drastic for Raw PLA. From 180 °C to 190 °C the average fiber size of Raw PLA dropped by 52%. An additional 63% drop was seen from 190 °C to 200 °C, resulting in an overall decrease of 82% and indicating a strong dependence of fiber size on processing temperature. PLA-5-5 showed a similar initial drop of 47% from 170 °C to 180 °C, however no significant changes were observed from 180 °C to 190 °C. This suggests that, beyond

180 °C, increasing temperature provides no benefit in terms of fiber size reduction. As such, higher temperatures should be avoided to reduce the risk of further degradation and fiber breakage as well as to minimize operating cost.

With the help of high temperatures, Raw PLA was able to achieve an average fiber diameter of 12.5 µm. On the other hand, PLA-5-5 was able to achieve an even smaller average diameter of 9.0 µm at only 180 °C. Smaller fiber sizes are generally preferable for melt-blown fabrics as they increase surface area allowing for greater contact with materials that pass through them improving filtration and absorption abilities [20]. It is possible that at even higher temperatures, Raw PLA may be able to achieve similar fiber size, however at 200 °C there is already evidence of degradation in the form of "flies", excessively thin frizzy fibers caused by fiber breakage [20]. Flies are typically caused by extreme operating conditions, therefore raising the temperature further would likely exacerbate the issue. Interestingly, flies are also present in PLA-5-5 at 170 °C, the lowest operating temperature, but are significantly reduced at the higher operating temperatures. Flies are mainly caused by an extreme difference between air and fiber speed [20], therefore it is possible that the PLA flow at 170 °C was too slow relative to the airflow causing the force of the air to snap the fibers prematurely. Considering the fiber size is comparable between PLA-5-5 at 170 °C and Raw PLA at 200 °C, the ratio between flow speed and air speed was also likely similar, resulting in the same issue. Increasing the temperature to 180 °C to achieve optimum flow of the PLA may have reduced the inconsistency between the two streams, thus resolving the issue. Finally, in addition to fiber size, fiber uniformity is of interest. PLA-5-5 at 180 °C has the lowest fiber size variability of all samples with a CV of 39% suggesting a more uniform fiber distribution and further solidifying 180 °C as the preferred operating temperature. Overall, PLA-5-5 shows great promise for use in the melt blowing process since it produces thinner, more uniform fibers at lower

temperatures compared to the untreated PLA. Optimization of the processing conditions, such as air flow speed and distance from die to collector, may allow for even higher quality material to be produced using the treated PLA.

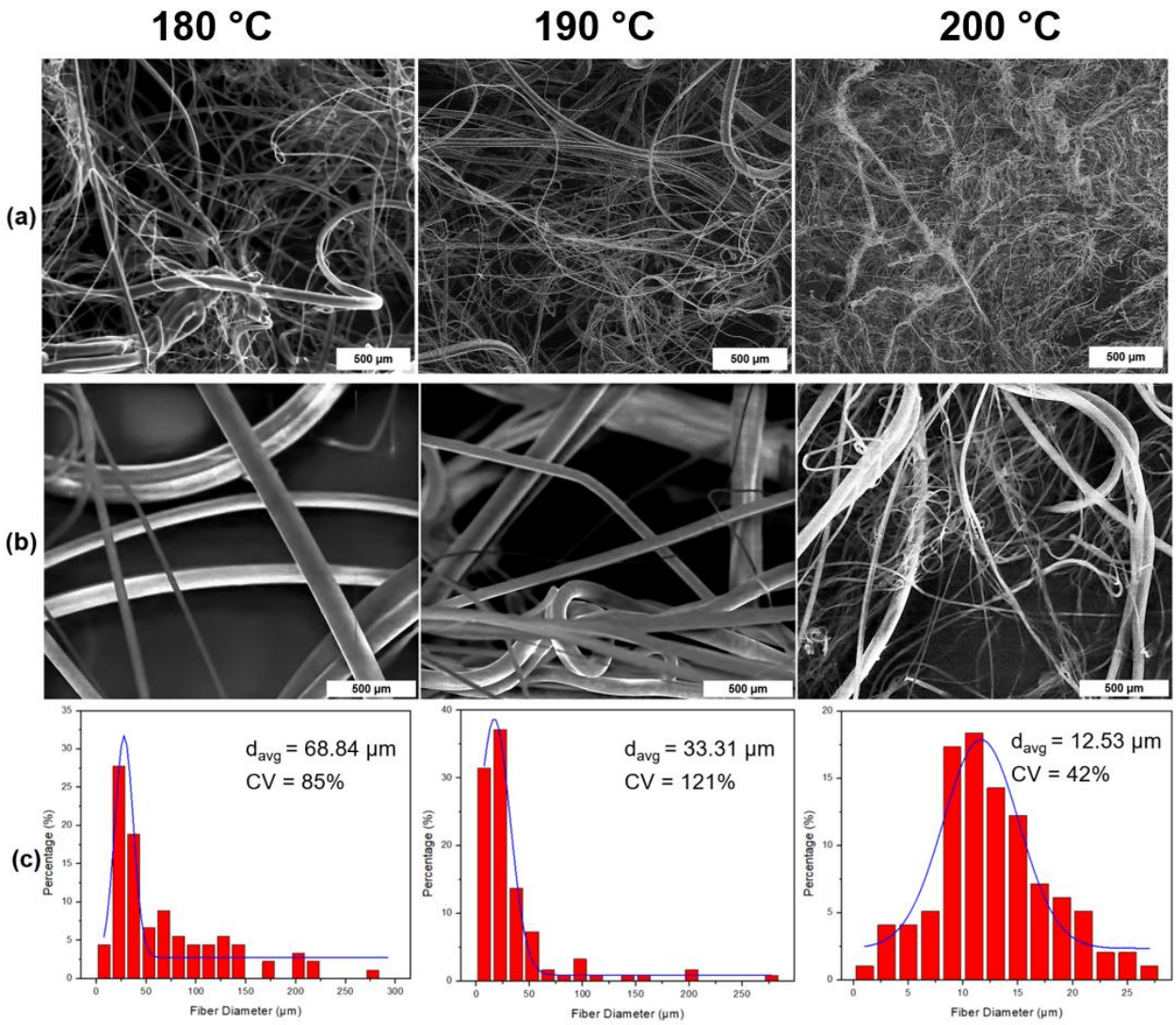


Figure 14: SEM images of Raw PLA at 50x **(a)** and 600x **(b)** as well as the fiber distribution of Raw PLA **(c).**

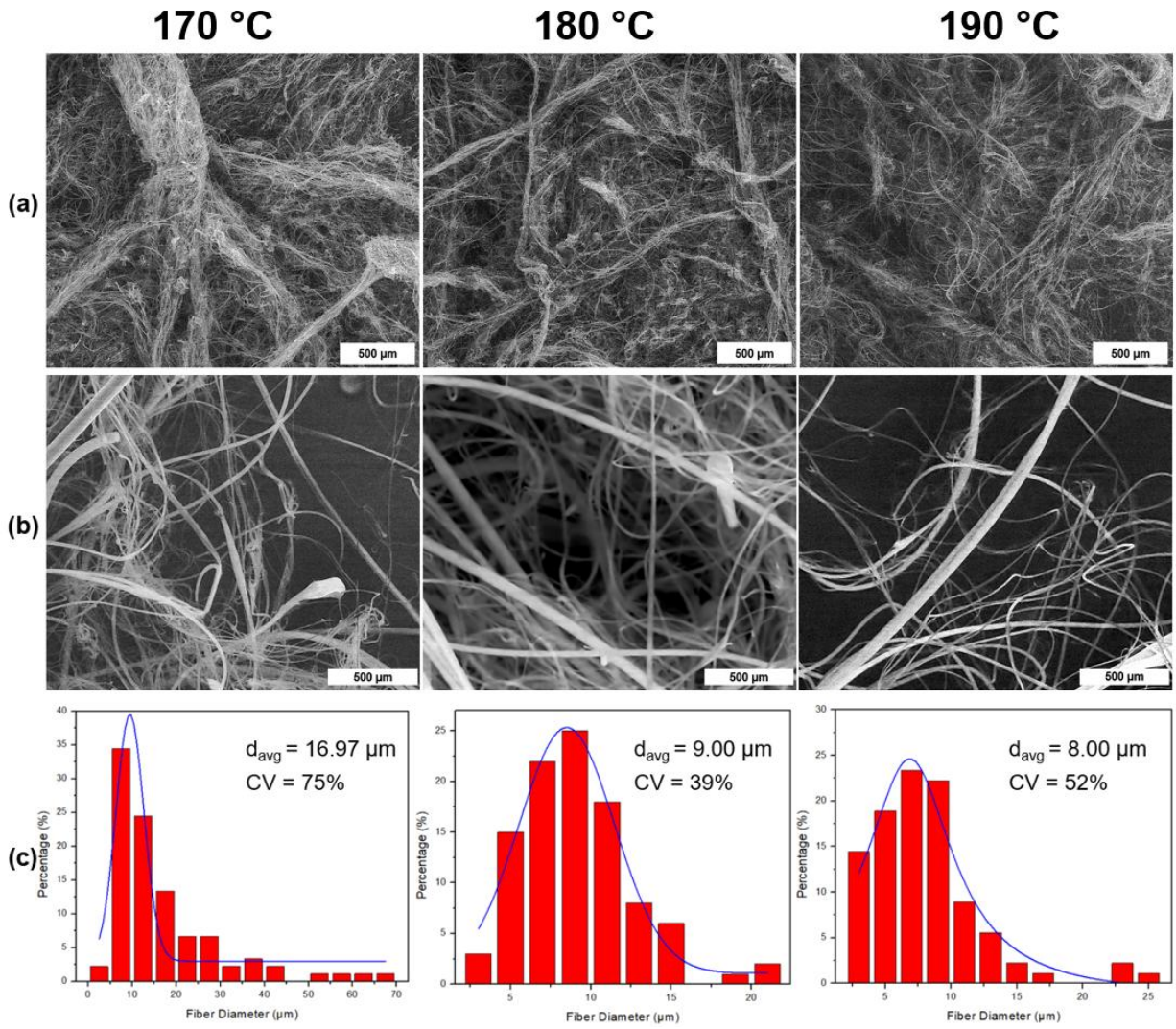


Figure 15: SEM images of PLA-5-5 at 50x **(a)** and 600x **(b)** as well as the fiber distribution of PLA-5-5 **(c).**

3.4 Conclusions

Hydrogen peroxide has proven to be an effective tool for controlled degradation of PLA. Structural analysis showed a decrease in the MW for samples treated with hydrogen peroxide. The decrease in MW appears to be greatest when low H_2O_2 concentrations are subjected to extended processing times. Increasing processing time for higher peroxide concentrations reverses the MW reduction, as a result of increasing the degree of crosslinking. Spectroscopic analysis provided insight into the structural changes responsible for the decrease in MW and substantiated the occurrence of

chain scission and hydrolysis as well as potential alcoholysis-type reactions. Rheological studies aligned well with structural investigation and demonstrated changes in viscosity following the same trend as the MW. Changes to crystal structure and order further support the theory of degradation where lower peroxide concentrations significantly decreased overall crystallinity while higher peroxide concentrations showed minimal change potentially due to the formation of lower ordered crystals. In light of these effects, lower H_2O_2 concentrations are preferred for fine control over the extent of degradation as high levels of degradation can be achieved within a feasible timeframe. Overall, the study demonstrates the successful reduction of PLA viscosity and molar mass using hydrogen peroxide thus expanding the applications of PLA by introducing it as an option for low viscosity polymer processes, such as melt blowing where the degraded sample was shown to produce thinner, more evenly distributed fibers at economical operating temperatures compared to the Raw PLA.

Chapter 4 – Controlled Degradation of PBAT for PBAT/PLA Melt-Blown Nonwovens

4.1 Introduction

Plastic is deeply enmeshed in our day-to-day lives from car parts to coffee cups to clothing that have limited life span. Regrettably, the majority of such plastics are nonbiodegradable, and stay hundreds of years in the ecosystems, while slowly shedding micro-plastics to the air we breathe in, drinking water and arable land with serious safety concerns.[165] In an attempt to maintain the convenience and reliability of plastic while reducing the environmental impact, researches have turned to studying biodegradable plastics, such as poly(butylene adipate-co-terephthalate) (PBAT) and poly(lactic acid) (PLA).[127] Unfortunately, these substitutes are relatively new and have limitations that are not present in the conventional polymers used today. One such limitation is the low melt flow index (MFI) of the available biodegradable options[7]. Low MFI can make plastics unsuitable for processing techniques requiring low melt viscosity including melt spinning, melt blowing, and blow molding. Implementation of biodegradable polymers in these applications necessitates engineering improved compatibility with these processes.

One method to modify the viscosity and MFI of polymers is through controlled degradation. Reducing the molecular weight of the polymer increases the flow by decreasing the chain entanglement.[26] There are several techniques that can be applied during polymer processing to induce controlled degradation such as the introduction of enzymes, thermal treatment, and reactive extrusion. [26–28] Reactive extrusion frequently utilizes the chain scission capability of peroxides to promote degradation.[4,83] Typically, organic peroxides are chosen, however, they are known to release undesirable volatile compounds (e.g. acetone and tert-butanol in the case of 2,5-dimethyl-2,5-di-tert-butylperoxyhexane (DHBP)).[4] Hydrogen peroxide (H_2O_2), on the other hand, generates only water and oxygen as byproducts, making it a suitable option for a more environmentally

friendly approach. H_2O_2 has proven effective for use in controlled degradation of several polymers including polypropylene and chitosan.[5,166]

In our previous work, this technique was applied to PLA where the molecular weight was successfully reduced by up to 70% and the MFI increased by 150x.[167] In this work, we instead focus on the controlled degradation of PBAT, a biodegradable polymer with an even lower MFI than PLA.[168] While unmodified PLA had been previously melt-blown[143,169,170], there are currently no studies focusing on melt-blown PBAT as it is generally considered incompatible with the process. Therefore, this work aims to modify PBAT through aqueous H_2O_2 induced controlled degradation to produce melt-blown nonwovens.

The modified PBAT can then be blended with PLA to reduce costs and improve the final material. PBAT and PLA are known for having opposite weaknesses; while PLA is strong and brittle, PBAT is elastic and relatively weak.[40] There are many studies that blend the two polymers in order to get the best of both worlds.[171–173] A study by Yu et al. added modest amounts of PBAT (2-10%) to PLA-based nonwovens to improve elongation at break and enhance hydrophobicity, creating a material with an oil water separation efficiency of 96%.[174] In this study, along with several others, it was noted that phase separation occurs when the two polymers are combined in larger quantities (>10% of one with the other). [171–175] To combat the immiscibility and poor compatibility, compatibilization techniques like the use of epoxy oligomers, isocyanates, ionic liquids, and combinations of anhydrides and peroxides have been employed.[40]

This study, therefore, examines the degradation effect of reactive batch mixing with aqueous H_2O_2 at different processing times and concentrations on PBAT. The study further looks at how this degradation impacts the compatibility of PBAT with the melt-blowing process, both as an independent material and blended with various levels of PLA. Finally, maleation, grafting of

maleic anhydride using peroxide, is examined as a compatibilization technique to improve blend miscibility.

4.2 Experimental

4.2.1 Materials

The Poly(butylene adipate-co-terephthalate) (PBAT) was provided by T&T Industry Group Ltd. (Shenzhen, China) and the Poly(lactic acid) (PLA), Luminy L105 [melt flow index (MFI) at 210 °C, 70 g/10 min, T_{melt} 180-220 °C], was obtained from TotalEnergies Corbion. Aqueous hydrogen peroxide (H_2O_2) (30 wt %) was purchased from Sigma-Aldrich. Chloroform-D (99.8%) was used as a solvent and purchased from Cambridge Isotope Laboratories.

4.2.2 Methods

2.2.1 Reactive Batch Mixing

PBAT (~150 g) was spray coated at room temperature with varied amounts of aqueous H_2O_2 and melt-blended at 200 °C in a HAAKE Polylab QC torque batch mixer at 60 rpm for 5-10 min. The processed samples were allowed to stabilize for at least 24 h at room temperature before characterization commenced. The concentration of H_2O_2 and processing times are described in **Table 2**. The degradation effects of heat and water were accounted for by Controls 1 and 2 respectively. Additional sample parameters were chosen to align with previous study by Binley et al.[167]

Table 2: Sample identification and formulation of treated PBAT samples

Sample ID	H_2O_2 *Concentration (phr)*	*Processing Time (min)*
PBAT	0	0
Control 1	0	10
Control 2	0 (10 phr Water)	10
PBAT_5_5	5	5
PBAT_5_10	5	10
PBAT_7.5_7.5	7.5	7.5
PBAT_10_5	10	5
PBAT_10_10	10	10

2.2.2 Proton Nuclear Magnetic Resonance (H NMR) Spectroscopy

PBAT samples were dissolved at room temperature in deuterated chloroform to ~5 mg/mL. A Bruker 300 MHz high-resolution nuclear magnetic resonance spectrometer was then used to obtain Proton (^{1}H) spectra with 64 scans and a relaxation delay of 10 s.

2.2.3 Melt Flow Index (MFI)

Using a Kayeness D4002 melt flow indexer, the MFI was measured in accordance with ASTM D1238 at 190 °C with a load of 2.16 kg and a standard 1 mm bore. A total of three measurements were taken per sample.

2.2.4 Compression Molding

A Carver hydraulic press was used to compression mold samples into compatible shapes for testing. H_2O_2 treated PBAT samples were molded between two compressed hot plates at 180 °C under six metric tons of pressure for 3 min to produce rheology disks of 1 mm in thickness and 25 mm in diameter. PBAT – PLA blend samples were also compression molded under the same conditions to produce flat sheets (76 x 75 x 0.2 mm^3) for use in atomic force microscopy (AFM) and polarized optical microscopy (POM).

2.2.5 Parallel-Plate Rheology

Disks were prepared as previously described and measurements were conducted using a HAAKE MARS rheometer. A shear strain of 1% was selected based on the linear viscoelastic region of PBAT. The rheological properties were evaluated using a frequency sweep from 0.1 to 100 Hz at 200 °C with a 1 mm gap.

2.2.6 Differential Scanning Calorimetry

A DSC Q2000 (TA Instruments) was used to perform thermal analysis. Peroxide treated samples of approximately 6 mg were placed in separate aluminum T_{zero} pans. Testing was then conducted under a nitrogen flow rate of 50 mL/min. The samples were heated at a rate of 10 °C/min to 200 °C and held isothermal for 3 min after which they were cooled to -60 °C at the same rate. Finally, the temperature was raised once again to 200 °C at 10 °C/min. The second heating cycle was used to determine glass transition temperature (T_g), melting temperature (T_m), crystallization temperature (T_c), and melting enthalpy (H_{mPBAT}) to avoid any thermal histories within the systems. Percent crystallinity ($\%\chi_{CrPBAT}$) was calculated using **Equation 3** where H^0_{mPBAT}, the heat of fusion value if PBAT was 100% crystalline, is 114 J/g.[176]

$$\%\chi_{CrPBAT} = \left(\frac{H_{mPBAT}}{H^0_{mPBAT}}\right) * 100\% \quad \textbf{(3)}$$

PBAT/PLA blends were also evaluated in the same manner except at a rate of 20 °C/min to improve the detection of T_g. Once again the reported values including melting enthalpy of PLA (H_{mPLA}) and cold crystallization enthalpy (H_{ccPLA}) were taken from the second heating cycle and percent crystallinity of the blends ($\%\chi_{CrBlend}$) was calculated using **Equation 4** where X_{PBAT} and X_{PLA} are the mass fractions of PBAT and PLA, respectively and H^0_{mPLA}, the heat of fusion if PLA was 100% crystalline, is 93.7 J/g.[132]

$$\%\chi_{CrBlend} = (X_{PBAT}\left(\frac{H_{mPBAT}}{H^0_{mPBAT}}\right) + X_{PLA}\left(\frac{H_{mPLA}-H_{ccPLA}}{H^0_{mPLA}}\right)) * 100\% \quad \textbf{(4)}$$

2.2.7 Melt Blowing

Finely ground PBAT_10_5 and PLA were combined in various ratios (**Table 3**) prior to processing in a twin screw extruder (Process 11 Parallel Twin-Screw Extruder, Thermofisher Inc). The compatibilized sample mixture (50-50-M) included 0.2 wt% dicumyl peroxide and 4 wt.% maleic anhydride (MA) in addition to the two polymers. The extruder was equipped with a custom die for melt-blowing comprised of a jet angle cap, melt feed nozzle, and gas feed resembling Exxon slot dies commonly used in commercial melt-blown fiber production.[3,141,142] The outer cap featured a single 2.5 mm diameter outer hole and a 128° impinging air jet angle to create blown fibers with heated nitrogen gas. The temperature of the nitrogen air jet was controlled using a transformer (Powerstat® Variable Transformer) connected to a 750W heating torch (Laramy Products, Lyndonville, VT, USA) and set to ~350 °C and the gas volumetric flow rate was adjusted to 0.5 L/min using the nitrogen gas gage pressure. The extruder temperature and screw speed were set to 220 °C and 100 rpm, respectively. A parchment paper-covered conveyor belt rotating at 60 rpm was placed ~40 cm away from the die opening to collect the fibers and produce nonwoven mats. Additional description of the experimental set up is found in Lee et al [143,144,167].

Table 3: Sample code and formulation of PBAT/PLA melt-blown fibers

Sample ID	*PBAT Content (wt%)*	*PLA Content (wt%)*
70_30	70	30
50_50	50	50
50_50_M	50	50
30_70	30	70
PLA	0	100

2.2.8 Polarized Optical Microscopy (POM)

The fiber distributions and crystal structures of the melt-blown fabrics were investigated using an Olympus BX53M POM optical microscope equipped with a Linkam heat stage accessory and a polarized light filter. Fiber mat samples remained at ambient temperature and were placed between glass slides to capture images at 10x magnification. Using the Olympus Stream Basic software measuring tool, 95-105 fibers per sample were individually measured to determine fiber uniformity. Crystal structure was observed using thin film samples that were heated to 200 °C at a rate of 10 °C. Upon cooling, images were captured using a 20x objective lens.

2.2.9 Scanning Electron Microscopy (SEM)

A Phenom Desktop SEM (Thermofisher Scientific USA) was used to examine the surface morphology of the fiber mat samples at 500x magnification.

2.2.10 Atomic Force Microscopy (AFM)

The homogeneity and surface morphology of PBAT and PLA blends were examined using AFM (Veeco Digital Instrument, Dimension 3100) with a NanoScope IV controller. Images were captured at a size of 10 × 10 μm^2 using a scan rate of 1 Hz. To detect differences in stiffness of the two polymers in the blends, tapping phase mode was used.

2.2.10 Tensile

Tensile testing was conducted using a Shimadzu- AGS-X (Shimadzu Corp, Kyoto, Japan) tensile testing instrument equipped with a 2 kN load cell at 100 mm/min. Rectangular samples were cut from the center of the nonwoven mats and measured on average 25 mm in width, 100 mm in length, and 1 mm in thickness. A total of 5 samples were tested per processing condition.

4.3 Results and Discussion

4.3.1 Controlled Degradation of Poly(butylene adipate-co-terephthalate) (PBAT)

3.1.1 Rheology and MFI

To get the complete picture of the changes to the melt flow behavior of the H_2O_2 treated PBAT samples, both MFI testing and parallel plate rheology were performed (**Figure 16**). Both tests revealed the same pattern among samples with MFI increasing (i.e. viscosity decreasing) with both processing time and peroxide concentration. While the control samples show that the presence of heat and water are contributing to the overall effect, they are only contributing a small amount with all treated samples having MFI's at least 36% greater than that of Control 2. This increase in MFI and decrease in viscosity is indicative of molecular weight reduction. While both processing parameters appear to enhance the degradative effect, H_2O_2 concentration demonstrates a much greater impact than processing time. MFI results were statistically analyzed using a 2-factor ANOVA **(Table 3)** to confirm the significance of each process parameter. As anticipated, H_2O_2 concentration has an incredibly low P-value, while processing time and the interaction between the two have high values deeming them statistically insignificant. As such, it can be stated that H_2O_2 concentration is the driving force behind the increase.

Table 3: Two factor ANOVA analysis of hydrogen peroxide concentration and processing time during reactive batch mixing of PBAT.

Source	DF	Sum of Square (SS)	Mean Square (MS)	F Statistic (df_1,df_2)	P-value
H_2O_2 Concentration	1	898269.1	898269.1	593.8012	1.68E-05
Processing Time	1	3228.061	3228.061	2.1339	0.2179
Interaction	1	120.9012	120.9012	0.07992	0.7914
Error	4	6050.975	1512.744		
Total	7	907669	129667		

Interestingly, unlike with PLA[11], no crosslinking appears to be taking place despite the well-established crosslinking effect of peroxides.[28–31] PBAT has been shown to crosslink in the presence of peroxides like benzoyl peroxide[32] and di(tert-butylperoxyisopropyl) benzene, with increased effect if a co-agent, such as triallyl isocyanurate, is included in the reaction.[31] Considering the relatively high concentrations of peroxide used, it is possible that this crosslinking has begun to occur during the longer processing times if the maximum MFI was achieved between the points captured. This would cause the MFI values of the different processing times to be similar as the crosslinking would reverse the molecular weight reduction, restoring the original level of entanglement. If MFI were to decrease at much longer processing times, then it would be possible to confirm, however, at this time there is insufficient data to declare that crosslinking is occurring.

In addition to MFI measurement, parallel plate rheology analysis was used to observe the impact of the peroxide concentration and processing time to the complex viscosity, storage and loss moduli of the treated samples. Like with the complex viscosity, no change to the overall behaviour was shown, only a reduction among the treated samples. Once again, the greatest reduction was associated with the increase in the H_2O_2 concentration, while processing time had little impact. The decrease in these parameters further indicates molecular weight reduction as entanglement would be reduced resulting in a lower capacity for deformation. Further indication would be a shift in the crossover of storage and loss moduli; however, this did not occur within the testing range for neither treated nor untreated samples.

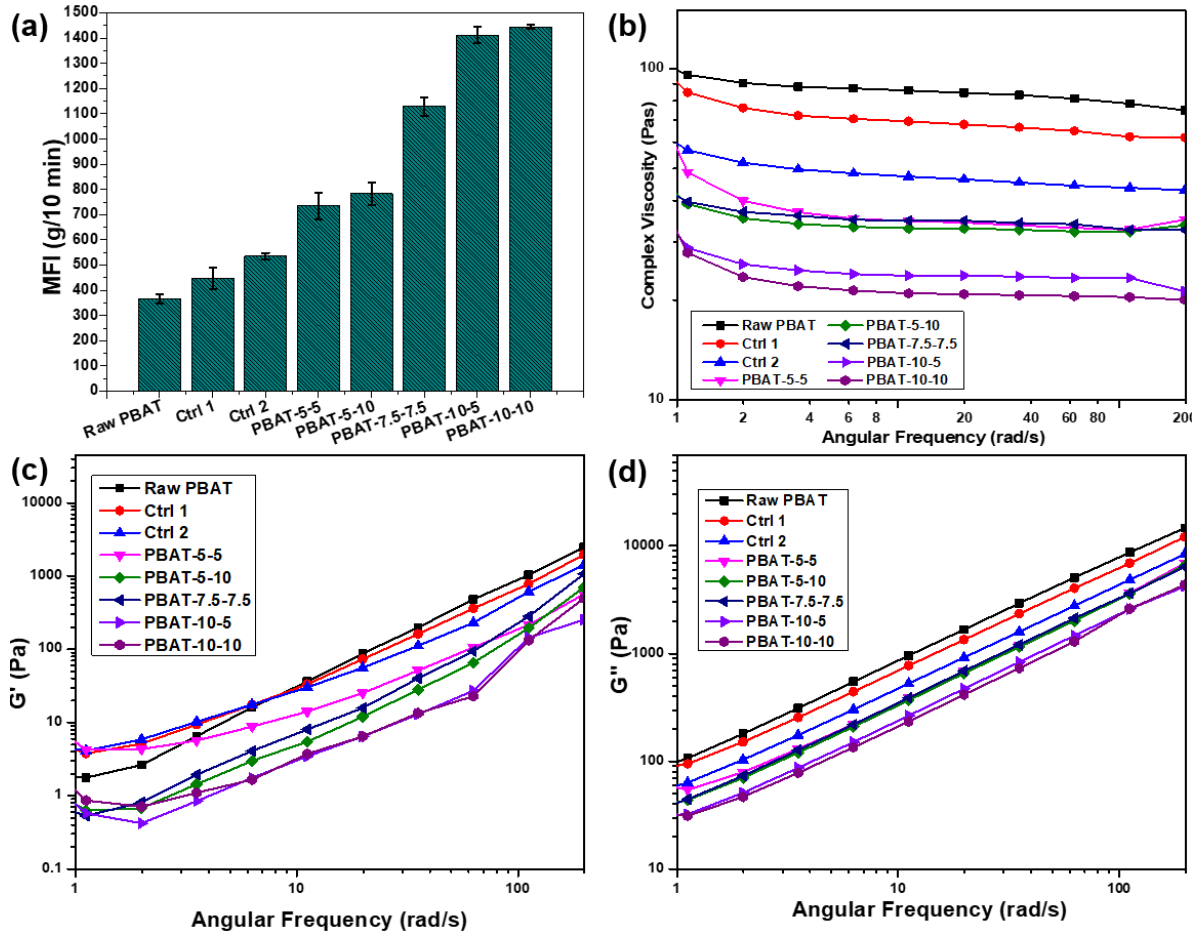


Figure 16: MFI (a), complex viscosity (b), storage modulus (c), and loss modulus (d) of hydrogen-peroxide treated PBAT.

3.1.2 Differential Scanning Calorimetry (DSC)

Thermal analysis was performed using DSC to gain insight into changes to glass transition temperature (T_g) and melting point (T_m) as well as crystallinity (**Figure 17**) of the samples. H_2O_2 treatment appears to have had little impact on the thermal behavior of PBAT. While there is a slight decrease in T_g and increase in T_m, these changes are also present in the control samples and therefore can be attributed primarily to the heat and moisture impacts during the treatment. Crystallinity, however, does appear to be minimally impacted at higher peroxide concentrations and processing times, with the highest concentration processed for the longest time demonstrating

a notable decrease in crystallinity. Interestingly, the highest crystallinity value, nearly equivalent to the untreated PBAT, is achieved in the PBAT_10_5 sample. This may suggest the possibility of chemi-crystallization, an increase in crystallinity as a result of chain scission to the amorphous regions of a semicrystalline polymer, which was occurring prior to the 29% reduction during the additional processing time..[162] As indicated by the rheology data, the higher peroxide concentration experiences significantly more molecular weight reduction (i.e. more chain scission) thus it is more likely for chemi-crystallinity to occur as chain scission occurs more readily in amorphous regions.[179] Overall, however, all changes observed during DSC testing were quite minimal, suggesting the impact of the treatment is insignificant.

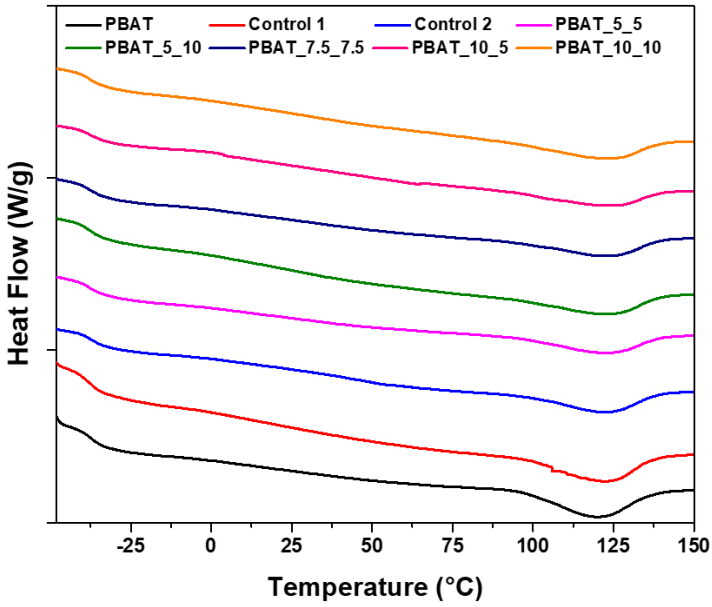


Figure 17: DSC thermograms of H_2O_2 treated PBAT samples.

Table 4: Glass transition, melting temperatures, enthalpy of melting, and percent crystallinity of treated PBAT samples.

Sample ID	Tg (°C)	*Tm (°C)*	ΔHm (J/g)	Crystallinity (%)
PBAT	-36.75	119.86	12.45	10.9%
Control 1	-38.54	121.52	10.34	9.1%
Control 2	-37.80	122.57	10.57	9.3%
PBAT_5_5	-38.26	122.32	10.36	9.1%
PBAT_5_10	-37.85	122.69	9.79	8.6%
PBAT_7.5_7.5	-37.62	122.60	11.07	9.7%
PBAT_10_5	-37.66	121.78	12.68	11.1%
PBAT_10_10	-37.46	123.70	9.03	7.9%

3.1.3 1H-NMR

Proton NMR results are shown in **Figure 18**, where it is clear that the peroxide treatment has impacted the structure of the treated PBAT. Two new peaks developed in the samples that had undergone reactive batch mixing: one at 5.15 and the other at 1.45 ppm. The size of these peaks increased with H_2O_2 concentration suggesting the peroxide is at least partially responsible for the observed changes. The peak at 5.15 **(Figure 18c)**, may be caused by an increase in terephthalic acid generation. When PBAT undergoes hydrolysis, chain scission occurs at the ester linkages, producing 1,4-butanediol, adipic acid, and terephthalic acid.[180,181] The presence of additional terephthalic acid therefore suggests bond cleavage at the ester bonds with contributions from the peroxide as well as the water in the solution.

The other peak of interest at 1.45 ppm is likely attributed to an increase in butylene-based fragments and oligomers. The carbon of the methyl group near the C=O group is an ideal site for an attack by the free radical from the peroxide which can then develop into a radical that is capable of both chain scission and crosslinking. [182] From the rheology data, it was clear that in the studied system, chain scission is dominant, and the impact of crosslinking, if any, is limited. This aligns

with La Mantia et al. who established that chain scission dominates the free radical reaction with PBAT under wet conditions such as that present with aqueous H_2O_2.[182] When the radical reaction proceeds down the route of chain scission, butylene fragments are a byproduct therefore aligning with the new peak. Since this new peak is associated with free radical degradation, it is clear that the peroxide, and not simply the heat and water, is responsible for the observed degradation. This is also emphasized by the intensity of the peroxide induced peak, being much greater than that at 1.45 ppm. which was occurring due to moisture and peroxide jointly. All proposed reactions that are thought to occur during reactive batch mixing of PBAT with aqueous H_2O_2 are shown in **Figure 18d**. Overall, the proton NMR results align well with other evidence of degradation and support the proposed reaction mechanisms shown in **Figure 18 (a)**.

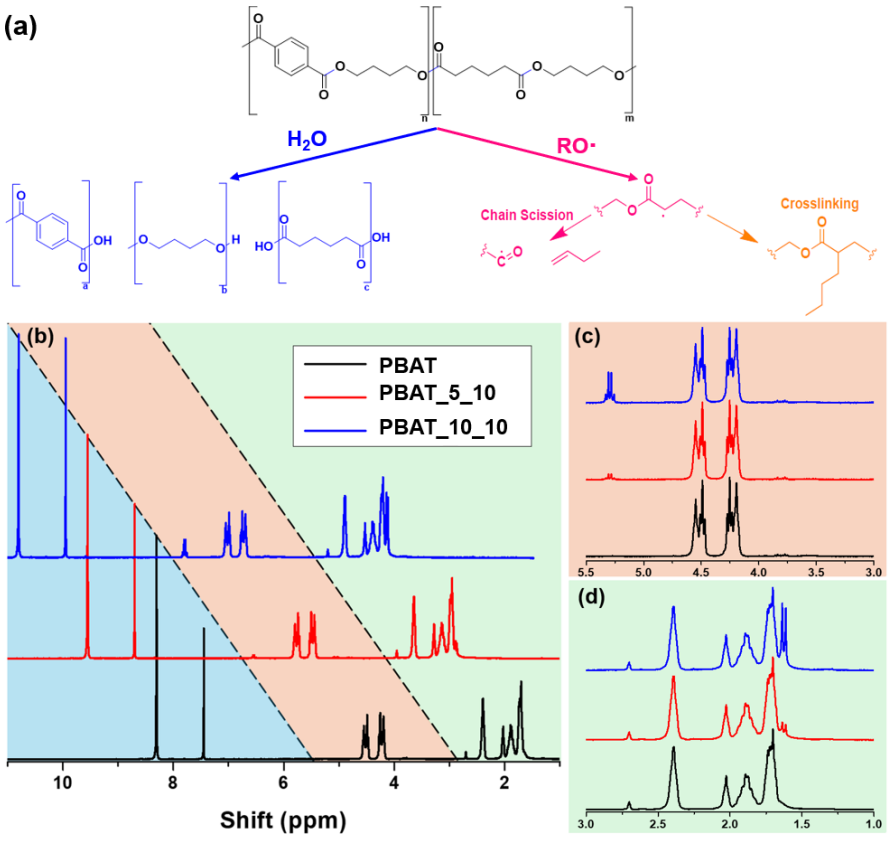


Figure 18: Proposed mechanism for reactions occuring during reactive batch mixing **(a)**; 1-H NMR spectrum **(b)** of treated PBAT samples with focus on the **(c)** terephphtalic acid region and **(d)** butylene region.

3.1.4 Melt-blown fibers

PBAT_10_5 was selected to proceed to melt blowing as the higher peroxide concentration had a much greater effect while further processing beyond 5 min had very little additional gain. Untreated PBAT was also melt-blown under the same conditions for comparison. SEM images and fiber distribution of both materials can be seen in **Figure 19**. The viscosity reduction associated with the peroxide treatment had a profound effect on both fiber diameter and distribution, reducing the average fiber diameter by 68% with the largest fibers of the treated sample being half the size of those of the untreated sample. Finer fibers are advantageous because they increase overall surface area therefore improving filtration and absorption efficiency in practical applications.[20] The improved fiber uniformity is also beneficial because it allows for more predictable and better controlled pore sizes as well as improved mechanical properties since forces are distributed more evenly across the individual strands of material.[22] Further indication that the degraded sample produces improved non-wovens is the presence of flies in the untreated PBAT sample. Flies, excessively thin frizzy fibers caused by fiber breakage, are commonly caused by an extreme difference between air and fiber flow speed.[21] Since the untreated PBAT is highly viscous, the air flow would be much faster in comparison, resulting in premature fiber breakage. The reduced viscosity of the treated sample, however, increases the speed of material flow and therefore prevents this from occurring. Overall, the peroxide treatment shows great promise in developing a controlled rheology grade of PBAT suitable for the melt-blowing process.

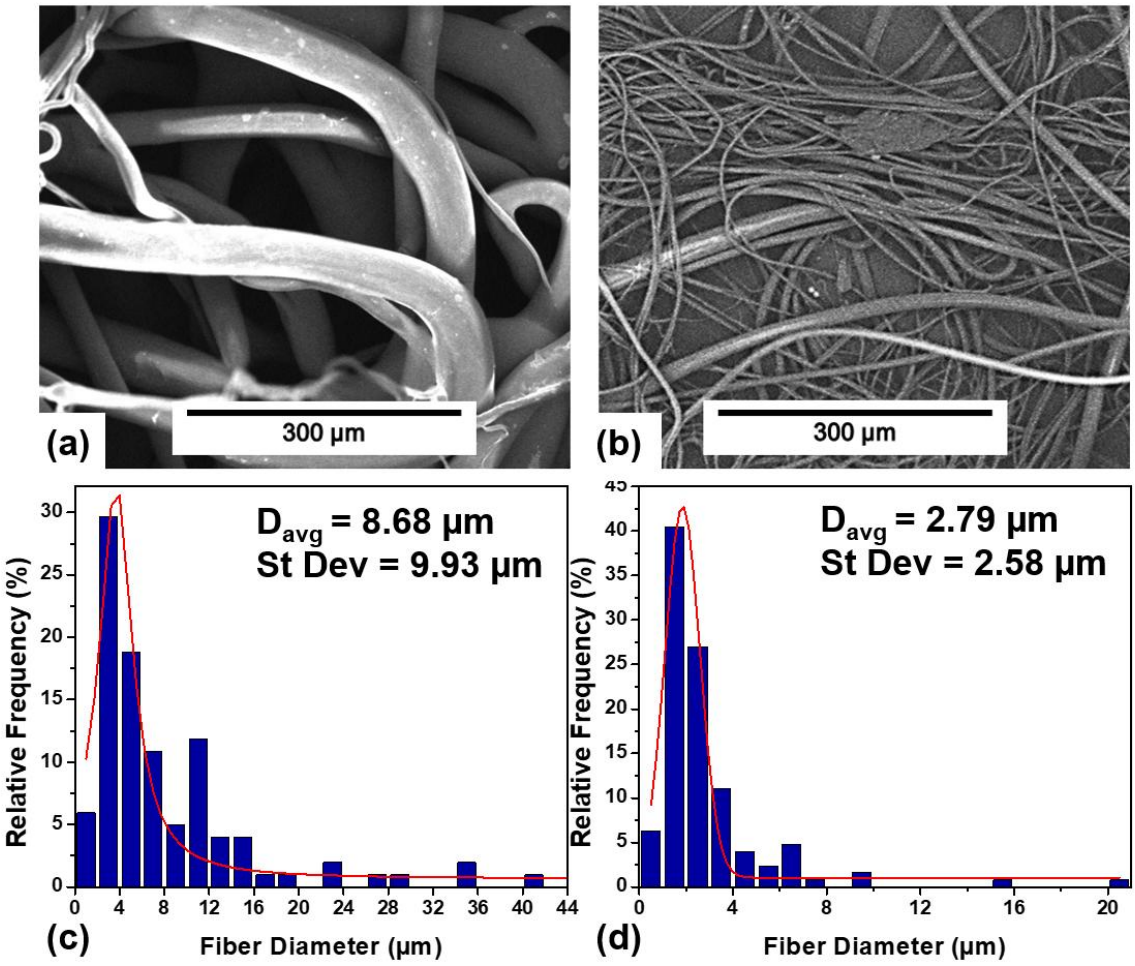


Figure 19: SEM images of melt-blown PBAT **(a)** and PBAT-10-5 **(b)** at 500X magnification. As well as fiber diameter distribution of PBAT **(c)** and PABT-10-5 **(d)**.

4.3.2 Blending with PLA

3.2.1 Atomic force microscopy

Atomic force microscopy (AFM) was used to gauge miscibility of the blends and identify phase separation through differences in the tapping hardness of the materials (**Figure 20**). AFM reveals a dark bumpy surface for PBAT and a smoother lighter surface for PLA. Therefore, the lighter spots and lines appearing in greater amounts with increasing PLA content are indicative of isolated PLA domains suggesting phase separation. **Figure 20 (b)** and **(c)** can be used to assess the effectiveness of maleation as a compatibilization strategy. Despite both samples being 50-50

blends of PBAT and PLA, the compatibilized sample shows little indication of phase separation while the untreated sample shows many distinct PLA fibers. This stark contrast emphasizes the value of a compatibilization agent in creating a homogenous mixture of PBAT and PLA. Overall, AFM reveals a clear distinction between blends and confirms the need for compatibilization.

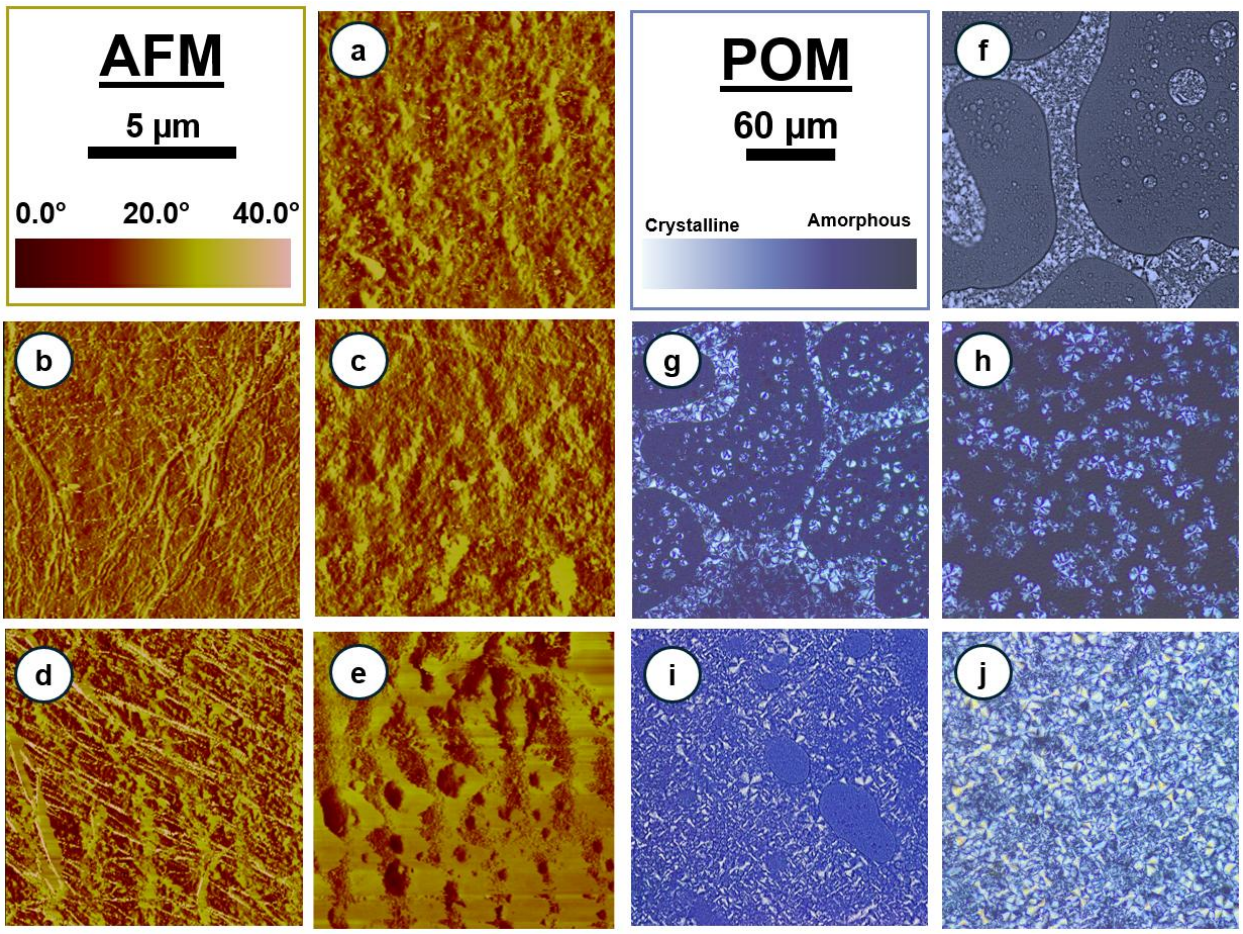


Figure 20: AFM images of 70_30 **(a)**, 50_50 **(b)**, 50_50_M **(c)**, 30_70 **(d)**, and PLA **(e);** POM images of the same blends in the same order (**f-j).**

3.2.2 POM

POM was also used to observe phase separation as well as investigate changes to the crystalline structure of the PBAT/PLA blends. PBAT is highly amorphous while PLA is highly crystalline, thus the two polymers look distinctly different when observed under a polarized microscope. When blended together with no assistance from a compatibilizer, it is clear that phase separation occurs

with the amorphous PBAT resting on top of the crystalline PLA (**Figure 20**). This aligns with the fact that PBAT is often slightly less dense than PLA, causing it to rise to the top while PLA sinks to the bottom.[183] Once a compatibilizer is added, however, only a single semi-crystalline phase is visible (**Figure 20 (h**)). While the blend more closely resembles PLA, it is clear that the sample selected is not solely PLA as the crystallinity is much lower than that of the pure PLA. Additionally, the blend appears more similar to PBAT in the AFM image. Together these two forms of microscopy confirm a successful compatibilized blend of the two and emphasize the impact of compatibilization in preventing phase separation.

3.2.3 DSC

DSC was performed to further analyze the thermal behavior and homogeneity of the blends (**Figure 21)**. The blends, with the exception of the compatibilized sample, show discrete thermal events associated with each individual polymer. PBAT is represented by the glass transition around -36 °C and the melting peak near 120 °C while PLA is responsible for the glass transition around 50 °C, the melting peak at about 170 °C, the cold crystallization peak around 90 °C, and finally the small exothermic shoulder present just before the melting peak. Assigning these events to their respective polymers allows for the calculation of crystallinity based on the composition. Key thermal events and overall crystallinity are shown in **Table 5**. The maleated sample, however, is less easily split into its individual components. While both glass transition temperatures can be seen, only one melting peak is present and the cold crystallization peak, while present, is nearly undetectable. The shoulder just before the melting peak has also vanished. As such, it can be stated that while there is still a small amount of separation detected, the majority of the specimen is a new material that behaves differently than either starting material. Both T_g values present in the compatibilized sample are reduced compared to their baseline. Since T_g is known to decrease with

molecular weight this is likely due to additional degradation caused by the peroxide present during the maleation process. The single melting peak is much higher in temperature than the melting peak of PBAT, but distinctly lower than that of PLA further indicating the improved interaction between the two materials. Finally, the near disappearance and reduced temperature of the cold crystallization peak provide additional evidence of compatibilization.[184]

The overall crystallinity of untreated samples as calculated from DSC also highlights the presence of phase separation. PBAT hinders the ability of PLA to crystallize, so even when PLA is in the majority (e.g. 30_70) the crystallinity is substantially reduced compared to pure PLA. Since PBAT has a lower melting point than PLA and the blend, PBAT remains in a molten state as the PLA begins to crystallize. Where this molten PBAT is present, the crystallization process may be impeded as it is more difficult for the crystals to align in an orderly fashion. Thus, the increase in the degree of crystallization of 50_50_M compared to 50_50 supports the claim of homogeneity since, by evenly dispersing the two materials within each other, nucleation sites may grow without interference from aggregated PBAT.[185] Overall, it is clear from DSC analysis, along with AFM and POM images, that maleation sufficiently mitigates phase separation within PBAT/PLA blends resulting in a compatibilized material with balanced thermal and crystalline properties. Since a small amount separation remains, further study of the amount and type of compatibilizer used would be required to optimize the process and improve crystal perfection.

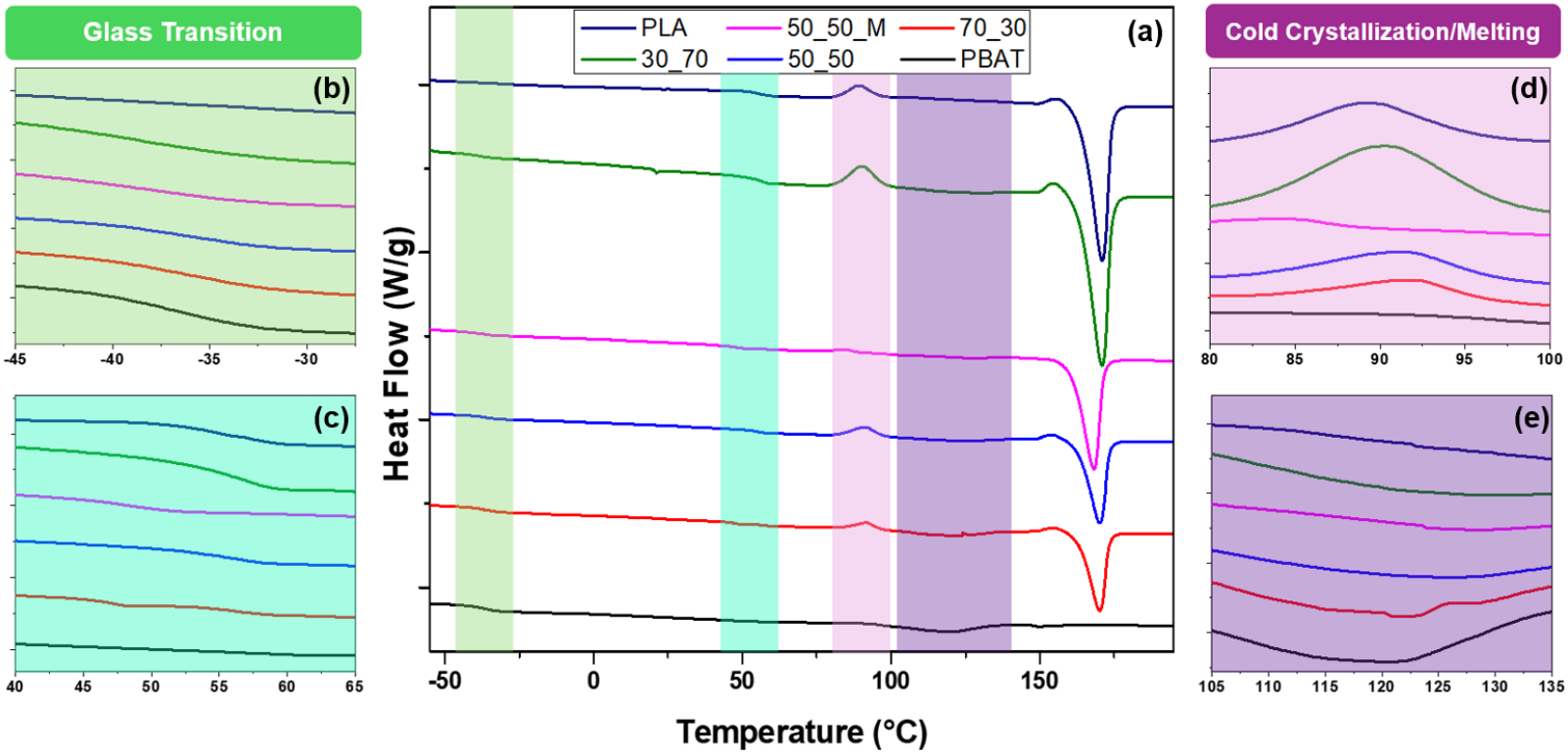


Figure 21: DSC thermogram of PBAT/PLA blends (a) with emphasis on the glass transition regions of PBAT (b) and PLA (c) as well as the cold crystallization region of PLA (d) and melting region of PBAT (e).

Table 5: Glass transition, melting, and cold crystallization temperatures of PBAT/PLA blends as well as their enthalpies of melting and cold crystallization with calculated crystallinity.

Sample ID	T_{g1} *(°C)*	T_{g2} *(°C)*	T_{m1} *(°C)*	T_{m2} *(°C)*	T_{cc} *(°C)*	ΔH_{m1} *(J/g)*	ΔH_{m2} *(J/g)*	ΔH_{cc} *(J/g)*	Crystallinity (%)
PBAT_10_5	-36.07	-	118.75	-	-	10.36	-	-	9%
70_30	-34.80	47.18	121.87	169.86	92.42	19.39	2.96	3.50	7%
50_50	-36.17	51.62	124.16	169.83	91.89	1.97	25.05	5.94	11%
50_50_M	-39.61	47.99	-	167.63	85.56	-	29.88	0.54	16%
30_70	-38.74	52.03	120.66	170.11	90.55	0.67	35.31	8.33	20%
PLA	-	54.96	-	170.28	89.40	-	46.25	6.66	42%

4.3.3 Melt blowing of PBAT/PLA Blends

3.2.1 Fibers

Melt-blown blends of the degraded PBAT sample and PLA were investigated using POM to identify any changes to the fiber diameter. As seen in **Table 6**, the average fiber diameter of all the blend ratios is nearly identical, with similar distribution as well. The blends, however, show a notable increase in diameter compared to the starting materials, with the average being 15 and 20 % greater than PBAT_10_5 and PLA, respectively. This increase in fiber size is likely due to the incompatibility of the materials causing phase separation and inconsistent flow as indicated by DSC and microscopic analysis.[22] Additional evidence of phase separation is the presence of droplets and shots (**Figure 22 (a)**). These malformations appear as larger blobs of material that are the result of surface tension instability.[22] While improving the flow of PBAT may improve its compatibility with PLA by bringing the viscosities closer together, it is insufficient for creating a completely homogenous blend. As such the resulting untreated blends are not quite as compatible with the melt-blowing process as the individual starting materials.

Table 6: Fiber distribution of PBAT/PLA blends

Sample ID	Average Fiber Diameter (µm)	Standard Deviation (µm)
PBAT_10_5	2.79	2.58
70-30	3.27	2.40
50-50	3.20	2.79
50_50_M	2.10	1.36
30-70	3.23	2.54
PLA	2.62	2.43

Since phase separation is observed among the untreated blends, compatibilization is recommended to improve the end product, the effect of which can be seen in **Figure 22.** A clear decrease in fiber diameter and distribution is seen with the compatibilized sample. Notably, the fibers produced in

this manner were even finer than either starting material alone. The finer fiber diameter is likely a result of both compatibilization, and the suspected additional degradation caused by the DCP reducing the melt viscosity. Further indication of compatibilization is the limited number of droplets and shots present in the maleated sample compared to pure blend. As previously discussed, these nonconformities likely occurred as a result of phase separation, thus their reduced quantity suggests a more homogenous blend. In addition to the minor degree of phase separation confirmed by DSC, the presence of the remaining small number of droplets may be due to operating conditions that can be optimized to prevent this from occurring. For example, beading may occur if operating temperature or air flow speed is too high.[22] Since the same processing conditions were applied to all samples, rather than optimized individually, it may be possible to further reduce these imperfections through changes to the operating parameters.

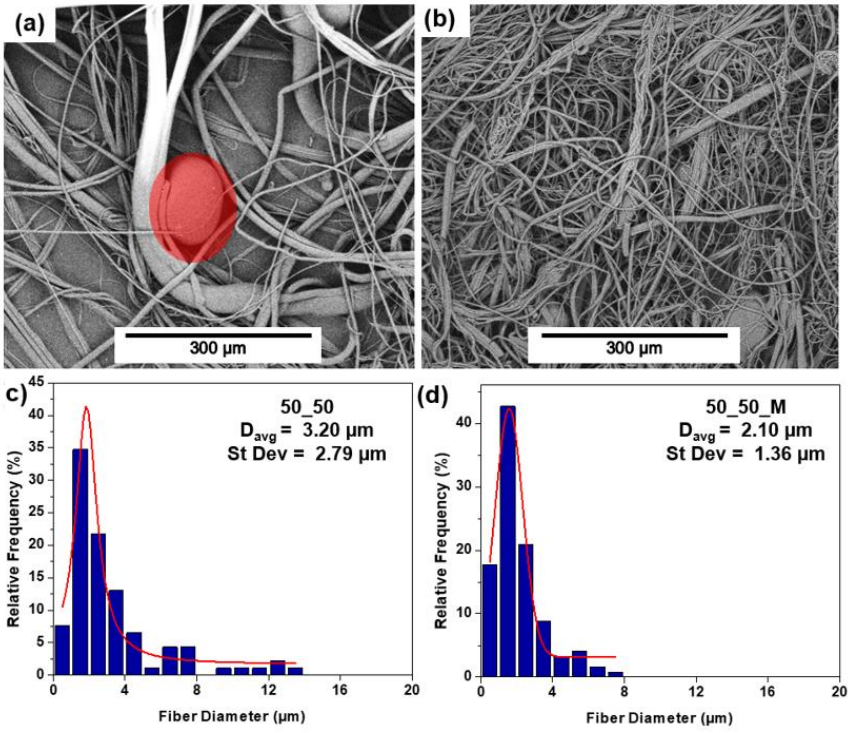


Figure 22: SEM image of 50-50 with beading (a) and 50-50-M (b) as well as their associated fiber diameter distributions (c and d).

3.2.2 Tensile

Tensile testing was performed on melt-blown samples of both the starting materials and blends. Testing procedure examined ultimate tensile strength, young's modulus, and elongation at break (**Figure 23 (b-d)**). As expected, PLA performed the best in ultimate tensile strength and young's modulus while PBAT_10_5 proved superior for elongation at break. Performance of the blends were indicative of the ratio of the species, with increasing PLA content increasing strength and decreasing elongation. Increased tensile strength benefits the material as it makes it more durable and resistant to tearing, while improved elongation allows for more flexibility preventing damage from repetitive deformation.

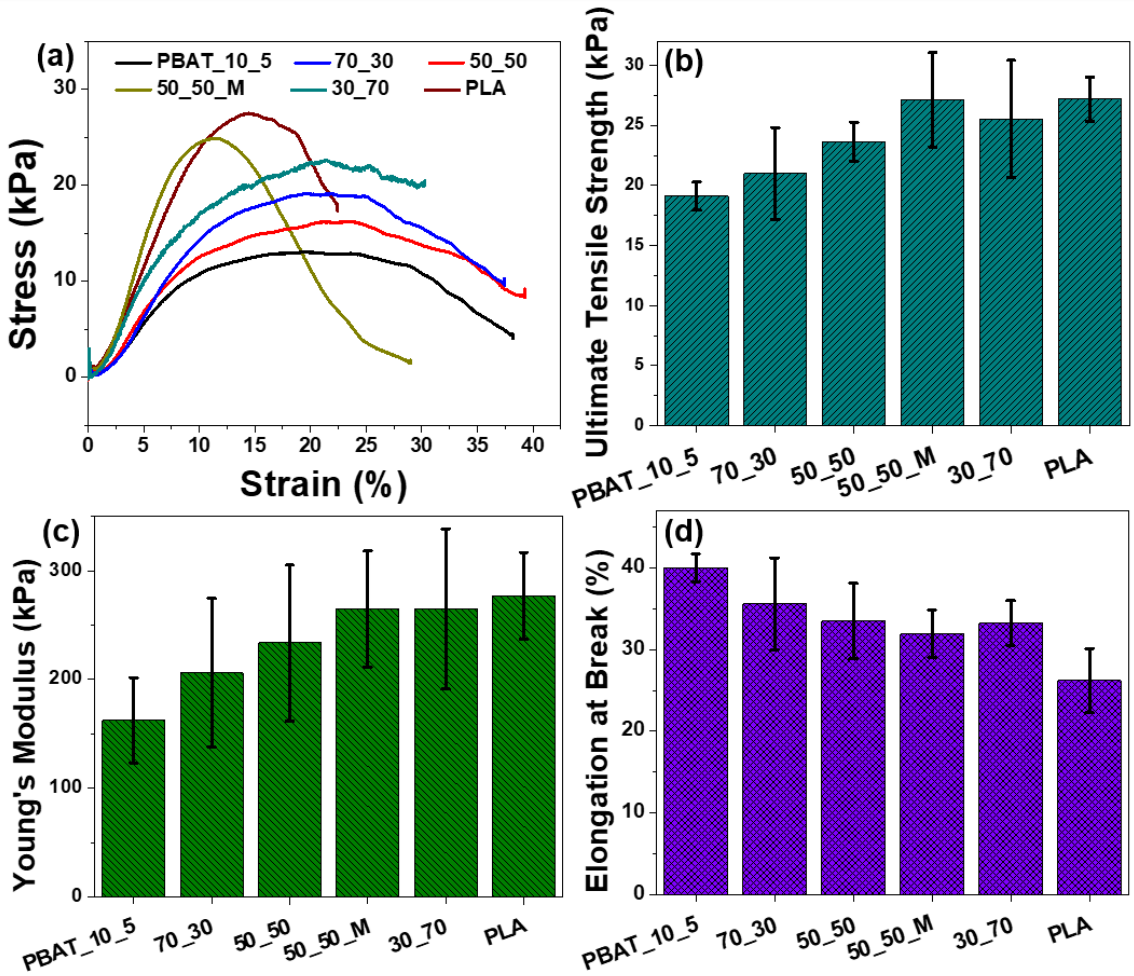


Figure 23: Tensile properties of PBAT/PLA nonwovens (**a-d**).

By blending PBAT and PLA, the combination gains the ability to be used in a wider range of applications where one or both of the individual materials would otherwise be incompatible. Considering the importance of both properties, a 50-50 blend appears to strike a good balance between strength and flexibility. The compatibilized blend of this ratio demonstrated a slight increase in ultimate tensile strength and young's modulus with negligible change to elongation at break when compared to the untreated 50-50 blend. This increase in overall strength of the material is likely because the fibers are more uniform. The increased uniformity causes stress to be applied more evenly across the fabric, therefore requiring the force to overtake all of the fibers at once rather than breaking at a weak point first. This suggests that the improved compatibility of the material also improves the tensile properties as well as the fiber morphology.

4.4 Conclusions

Reactive batch mixing with aqueous hydrogen peroxide has been demonstrated to be a prominent candidate for controlled degradation of PBAT. The degradation is thought to occur via free radical induced chain scission as well as hydrolysis of the ester bonds. This is supported by the clear reduction of viscosity (i.e. increase in MFI) as well as the reduction in storage and loss moduli at higher peroxide concentrations. Additional support for this degradation mechanism is given by 1H NMR detecting new peaks at 5.15 and 1.45 ppm for peroxide treated samples that suggest an increase in terephthalic acid and butylene fragments respectively. It is likely that crosslinking occurs as well, however chain scission is the dominant mechanism. Additionally, it was shown that the H_2O_2 treatment had little effect on the thermal and crystalline properties of the PBAT. The degraded PBAT was then melt-blown to produce fine uniform fibers. To reduce cost and improve the strength of the material, the degraded PBAT was blended with PLA, producing a material with a greater tensile strength than PBAT alone as well as a longer elongation at break than PLA. The

blends, however, showed evidence of immiscibility and phase separation: wide dispersity of fiber width, fiber imperfections, and inconsistent crystallization. This incompatibility was addressed using maleation, resulting in the finest fibers produced. While these fibers still exhibit small imperfections, the remaining defects can likely be eliminated through optimization of processing parameters and compatibilizer levels. Overall, this process presents an environmentally friendly method for producing high quality biodegradable nonwoven mats.

Chapter 5 – Conclusions and Future Work

5.1 Conclusions

With the right modifications, biodegradable polymers have the potential to greatly improve the sustainability of nonwoven fabrics. One of these modifications is to control molecular weight reduction and in turn increase MFI. To keep the process as sustainable as possible, this can be achieved through reactive batch mixing with H_2O_2. This method was explored for two different biodegradable polymers and shown to successfully reduce the molecular weight and improve the compatibility of the materials with the melt-blowing process for producing nonwovens.

The first material subjected to this treatment was PLA. PLA was shown to undergo random chain scission followed by crosslinking after a critical processing time dependent on H_2O_2. MFI was successfully increased up to 150x that of the untreated sample. This greatly improved the melt-blowing processability by reducing average fiber diameter by 87% at 180 °C. To achieve comparable, but still 33% larger fiber diameter, untreated PLA required the processing temperature to be increased to 200 °C. Between thinner, more uniform fibers and a reduced processing temperature, the treated PLA was determined to be a superior material.

The second material to undergo reactive batch mixing with H_2O_2 was PBAT. PBAT was also shown to experience random chain scission, the extent of which was linked primarily to H_2O_2 concentration with very little impact from processing time. Fiber diameter was reduced by 68% with minimal changes to thermal and crystalline properties. Since PBAT and PLA have complementary properties, the degraded PBAT was blended with PLA to reduce the cost and balance the properties. The blends, however, showed clear evidence of phase separation due to the immiscibility of the materials. This was easily overcome by introducing MA and DCP to the

system to serve as a compatibilization agent. The resulting compatibilized 50-50 blend demonstrated balanced tensile properties with increased ultimate tensile strength compared to PBAT and increased elongation at break compared to PLA.

Overall, the works presented demonstrate the potential to shift to biodegradable plastics for melt-blown nonwovens. Between PLA, PBAT, and blends of the two, nonwovens can be crafted to have the properties required for a wide variety of applications. While there is a long way to go to achieve industrial implementation, this research is an undeniable step towards a more sustainable future.

5.2 Future Work

There are three primary directions for future work beyond the studies presented: optimization of the current methods, expansion to additional biodegradable polymers, and functionalization of the produced fibers for further applications. When it comes to optimization, the first option is to optimize the melt-blowing conditions. While the PLA study modified processing temperature, there are various other critical parameters that were not modified including air temperature and velocity, extrusion speed, and distance between die and collector. These same parameters, as well as processing temperature, are also areas of improvement for PBAT and the PBAT/PLA blends. When it comes to optimizing the blends, compatibilization is a major area of interest. While maleation was shown to be effective, it was not perfect. Therefore, the process may be enhanced by adjusting MA and DCP concentrations or trying alternative compatibilization techniques such as chain extenders or surfactants. Finally, it would be of interest to determine if it is possible to combine the compatibilization and degradation into one reactive batch mixing step by allowing the reaction to proceed to crosslinking.

Expanding this procedure to additional biodegradable polymers would also be beneficial as PLA and PBAT require specific composting conditions to fully biodegrade. Poly(hydroxyalkanoates) (PHAs), for example, degrade readily in soil and home compost, however their extremely slow crystallization kinetics in addition to high melt viscosity limit their applications for many processes including melt-blowing. As such the described controlled degradation procedure paired with modification to improve crystallization kinetics such as the introduction of nucleating agents may make it possible to melt-blow PHA.

Finally, melt-blown nonwovens can be functionalized to expand their applications. For example, filter materials can be modified to capture chemicals in addition to particulate matter by using additives such as activated carbon. They can also be made to have antimicrobial with the addition of silver particles. Determining a method to apply these functional additives as coatings to the large surface area presented by melt-blown nonwovens without clogging the pores and sacrificing air flow could be a challenge worth taking on. Overall, biodegradable polymers show a promising future in sustainable melt-blown nonwovens.

References

(1) Martínez Silva, P.; Nanny, M. A. Impact of Microplastic Fibers from the Degradation of Nonwoven Synthetic Textiles to the Magdalena River Water Column and River Sediments by the City of Neiva, Huila (Colombia). *Water* **2020**, *12* (4), 1210. https://doi.org/10.3390/w12041210.

(2) Ajmeri, J. R.; Ajmeri, C. J. 5 - Nonwoven Personal Hygiene Materials and Products. In *Applications of Nonwovens in Technical Textiles*; Chapman, R. A., Ed.; Woodhead Publishing Series in Textiles; Woodhead Publishing, 2010; pp 85–102. https://doi.org/10.1533/9781845699741.2.85.

(3) Shambaugh, R. L. A Macroscopic View of the Melt-Blowing Process for Producing Microfibers. *Ind. Eng. Chem. Res.* **1988**, *27* (12), 2363–2372. https://doi.org/10.1021/ie00084a021.

(4) Hogt, A. H.; Meijer, J.; Jelenič, J. Modification of Polypropylene by Organic Peroxides. In *Reactive Modifiers for Polymers*; Al-Malaika, S., Ed.; Springer Netherlands: Dordrecht, 1997; pp 84–132. https://doi.org/10.1007/978-94-009-1449-0_2.

(5) Moad, G.; Dagley, I. J.; Habsuda, J.; Garvey, C. J.; Li, G.; Nichols, L.; Simon, G. P.; Nobile, M. R. Aqueous Hydrogen Peroxide-Induced Degradation of Polyolefins: A Greener Process for Controlled-Rheology Polypropylene. *Polymer Degradation and Stability* **2015**, *117*, 97–108. https://doi.org/10.1016/j.polymdegradstab.2015.04.001.

(6) Cruz, R. M. S.; Krauter, V.; Krauter, S.; Agriopoulou, S.; Weinrich, R.; Herbes, C.; Scholten, P. B. V.; Uysal-Unalan, I.; Sogut, E.; Kopacic, S.; Lahti, J.; Rutkaite, R.; Varzakas, T. Bioplastics for Food Packaging: Environmental Impact, Trends and Regulatory Aspects. *Foods* **2022**, *11* (19), 3087. https://doi.org/10.3390/foods11193087.

(7) Mohammadi, M.; Heuzey, M.-C.; Carreau, P. J.; Taguet, A. Morphological and Rheological Properties of PLA, PBAT, and PLA/PBAT Blend Nanocomposites Containing CNCs. *Nanomaterials* **2021**, *11* (4), 857. https://doi.org/10.3390/nano11040857.

(8) Gong, H.; Ozgen, B. 5 - Fabric Structures: Woven, Knitted, or Nonwoven. In *Engineering of High-Performance Textiles*; Miao, M., Xin, J. H., Eds.; The Textile Institute Book Series; Woodhead Publishing, 2018; pp 107–131. https://doi.org/10.1016/B978-0-08-101273-4.00007-X.

(9) Yilmaz, K. B.; Sabuncuoglu, B.; Yildirim, B.; Silberschmidt, V. V. A Brief Review on the Mechanical Behavior of Nonwoven Fabrics. *Journal of Engineered Fibers and Fabrics* **2020**, *15*, 1558925020970197. https://doi.org/10.1177/1558925020970197.

(10) Chen, J. Y. 10 - Nonwoven Textiles in Automotive Interiors. In *Applications of Nonwovens in Technical Textiles*; Chapman, R. A., Ed.; Woodhead Publishing Series in Textiles; Woodhead Publishing, 2010; pp 184–201. https://doi.org/10.1533/9781845699741.2.184.

(11) Midha, V. K.; Dakuri, A. Spun Bonding Technology and Fabric Properties: A Review. *JTEFT* **2017**, *1* (4). https://doi.org/10.15406/jteft.2017.01.00023.

(12) Li, K.-Y.; Tang, X.-W.; Zhao, W.-F.; Fei, M.-L.; Chen, X.-L.; Liang, J.-X. Microstructure Characteristics of Nonwoven Geotextiles Using SEM and CT Methods. *Geotextiles and Geomembranes* **2023**, *51* (2), 293–302. https://doi.org/10.1016/j.geotexmem.2022.11.003.

(13) Albrecht, W.; Fuchs, H.; Kittelmann, W. *Nonwoven Fabrics: Raw Materials, Manufacture, Applications, Characteristics, Testing Processes*; John Wiley & Sons, 2006.

(14) Das, A.; Kothari, V. K.; Mane, D. Frictional Characteristics of Woven and Nonwoven Wipes. *Fibers Polym* **2005**, *6* (4), 318–321. https://doi.org/10.1007/BF02875668.

(15) Hong, K. H.; Kim, S. C.; Kang, T. J.; Oh, K. W. Effect of Abrasion and Absorbed Water on the Handle of Nonwovens for Disposable Diapers. *Textile Research Journal* **2005**, *75* (7), 544–550. https://doi.org/10.1177/0040517505053856.

(16) Jha, D. K.; Dhekne, P. P.; Patwardhan, A. W. Characterization and Evaluation of Tea Bag Papers. *J Food Sci Technol* **2020**, *57* (8), 3060–3070. https://doi.org/10.1007/s13197-020-04339-z.

(17) Wilson, A. 1 - The Formation of Dry, Wet, Spunlaid and Other Types of Nonwovens. In *Applications of Nonwovens in Technical Textiles*; Chapman, R. A., Ed.; Woodhead Publishing Series in Textiles; Woodhead Publishing, 2010; pp 3–17. https://doi.org/10.1533/9781845699741.1.3.

(18) Borhade, M.; Ghatage, A.; Indi, Y.; Landage, S.; Kamat, S. A SHORT REVIEW ON SPUN BONDED TECHNOLOGY. **2021**, *7* (0932).
(19) Patnaik, P. K.; Swain, P. T. R.; Mishra, S. K.; Purohit, A.; Biswas, S. Recent Developments on Characterization of Needle-Punched Nonwoven Fabric Reinforced Polymer Composites – A Review. *Materials Today: Proceedings* **2020**, *26*, 466–470. https://doi.org/10.1016/j.matpr.2019.12.086.
(20) Drabek, J.; Zatloukal, M. Meltblown Technology for Production of Polymeric Microfibers/Nanofibers: A Review. *Physics of Fluids* **2019**, *31* (9), 091301. https://doi.org/10.1063/1.5116336.
(21) Dutton, K. C. Overview and Analysis of the Meltblown Process and Parameters. *Journal of Textile and Apparel, Technology and Management* **2009**, *6* (1).
(22) Ellison, C. J.; Phatak, A.; Giles, D. W.; Macosko, C. W.; Bates, F. S. Melt-blown Nanofibers: Fiber Diameter Distributions and Onset of Fiber Breakup. *Polymer* **2007**, *48* (11), 3306–3316. https://doi.org/10.1016/j.polymer.2007.04.005.
(23) Shenoy, A. V.; Chattopadhyay, S.; Nadkarni, V. M. From Melt Flow Index to Rheogram. *Rheologica Acta* **1983**, *22* (1).
(24) Doronin, F.; Rudakova, A.; Rytikov, G.; Nazarov, V. Simple Determination of the Melt Flow Index of Composite Polymer Filaments Used in Material Extrusion Additive Manufacturing. *Coatings* **2023**, *13* (9), 1592. https://doi.org/10.3390/coatings13091592.
(25) Seifali Abbas-Abadi, M.; Nekoomanesh Haghighi, M.; Yeganeh, H.; Bozorgi, B. The Effect of Melt Flow Index, Melt Flow Rate, and Particle Size on the Thermal Degradation of Commercial High Density Polyethylene Powder. *J Therm Anal Calorim* **2013**, *114* (3), 1333–1339. https://doi.org/10.1007/s10973-013-3133-0.
(26) Tayal, A.; Kelly, R. M.; Khan, S. A. Rheology and Molecular Weight Changes during Enzymatic Degradation of a Water-Soluble Polymer. *Macromolecules* **1999**, *32* (2), 294–300. https://doi.org/10.1021/ma980773w.
(27) Filippone, G.; Carroccio, S. C.; Mendichi, R.; Gioiella, L.; Dintcheva, N. T.; Gambarotti, C. Time-Resolved Rheology as a Tool to Monitor the Progress of Polymer Degradation in the Melt State – Part I: Thermal and Thermo-Oxidative Degradation of Polyamide 11. *Polymer* **2015**, *72*, 134–141. https://doi.org/10.1016/j.polymer.2015.06.059.
(28) Salehiyan, R.; Soleymani Eil Bakhtiari, S. A Review on Rheological Approaches as a Perfect Tool to Monitor Thermal Degradation of Biodegradable Polymers. *Korea-Aust. Rheol. J.* **2024**, *36* (4), 295–317. https://doi.org/10.1007/s13367-024-00111-3.
(29) Ghosal, A.; Chen, K.; Sinha-Ray, S.; Yarin, A. L.; Pourdeyhimi, B. Modeling Polymer Crystallization Kinetics in the Meltblowing Process. *Ind. Eng. Chem. Res.* **2020**, *59* (1), 399–412. https://doi.org/10.1021/acs.iecr.9b04840.
(30) Talbott, M. F.; Springer, G. S.; Berglund, L. A. The Effects of Crystallinity on the Mechanical Properties of PEEK Polymer and Graphite Fiber Reinforced PEEK. *Journal of Composite Materials* **1987**, *21* (11), 1056–1081. https://doi.org/10.1177/002199838702101104.
(31) Bossu, J.; Le Moigne, N.; Dieudonné-George, P.; Dumazert, L.; Guillard, V.; Angellier-Coussy, H. Impact of the Processing Temperature on the Crystallization Behavior and Mechanical Properties of Poly[R-3-Hydroxybutyrate-Co-(R-3-Hydroxyvalerate)]. *Polymer* **2021**, *229*, 123987. https://doi.org/10.1016/j.polymer.2021.123987.
(32) Martin, J. R.; Johnson, J. F.; Cooper, A. R. Mechanical Properties of Polymers: The Influence of Molecular Weight and Molecular Weight Distribution. *Journal of Macromolecular Science, Part C* **1972**, *8* (1), 57–199. https://doi.org/10.1080/15321797208068169.
(33) Zen, A.; Saphiannikova, M.; Neher, D.; Grenzer, J.; Grigorian, S.; Pietsch, U.; Asawapirom, U.; Janietz, S.; Scherf, U.; Lieberwirth, I.; Wegner, G. Effect of Molecular Weight on the Structure and Crystallinity of Poly(3-Hexylthiophene). *Macromolecules* **2006**, *39* (6), 2162–2171. https://doi.org/10.1021/ma0521349.
(34) Jiang, X. L.; Luo, S. J.; Sun, K.; Chen, X. D. Effect of Nucleating Agents on Crystallization Kinetics of PET. *Express Polym. Lett.* **2007**, *1* (4), 245–251. https://doi.org/10.3144/expresspolymlett.2007.37.

(35) De Yoreo, J. J.; Vekilov, P. G. Principles of Crystal Nucleation and Growth. *Reviews in Mineralogy and Geochemistry* **2003**, *54* (1), 57–93. https://doi.org/10.2113/0540057.
(36) Wypych, G. *Handbook of Plasticizers*; ChemTec Publishing, 2004.
(37) Ito, R.; Seshimo, F.; Haishima, Y.; Hasegawa, C.; Isama, K.; Yagami, T.; Nakahashi, K.; Yamazaki, H.; Inoue, K.; Yoshimura, Y.; Saito, K.; Tsuchiya, T.; Nakazawa, H. Reducing the Migration of Di-2-Ethylhexyl Phthalate from Polyvinyl Chloride Medical Devices. *International Journal of Pharmaceutics* **2005**, *303* (1), 104–112. https://doi.org/10.1016/j.ijpharm.2005.07.009.
(38) Jamarani, R.; Erythropel, H. C.; Nicell, J. A.; Leask, R. L.; Marić, M. How Green Is Your Plasticizer? *Polymers* **2018**, *10* (8), 834. https://doi.org/10.3390/polym10080834.
(39) Álvarez-Méndez, S. J.; Ramos-Suárez, J. L.; Ritter, A.; González, J. M.; Pérez, Á. C. Anaerobic Digestion of Commercial PLA and PBAT Biodegradable Plastic Bags: Potential Biogas Production and 1H NMR and ATR-FTIR Assessed Biodegradation. *Heliyon* **2023**, *9* (6). https://doi.org/10.1016/j.heliyon.2023.e16691.
(40) Aversa, C.; Barletta, M.; Cappiello, G.; Gisario, A. Compatibilization Strategies and Analysis of Morphological Features of Poly(Butylene Adipate-Co-Terephthalate) (PBAT)/Poly(Lactic Acid) PLA Blends: A State-of-Art Review. *European Polymer Journal* **2022**, *173*, 111304. https://doi.org/10.1016/j.eurpolymj.2022.111304.
(41) Thomsen, T. B.; Radmer, T. S.; Meyer, A. S. Enzymatic Degradation of Poly(Ethylene Terephthalate) (PET): Identifying the Cause of the Hypersensitive Enzyme Kinetic Response to Increased PET Crystallinity. *Enzyme and Microbial Technology* **2024**, *173*, 110353. https://doi.org/10.1016/j.enzmictec.2023.110353.
(42) Bher, A.; Mayekar, P. C.; Auras, R. A.; Schvezov, C. E. Biodegradation of Biodegradable Polymers in Mesophilic Aerobic Environments. *Int J Mol Sci* **2022**, *23* (20), 12165. https://doi.org/10.3390/ijms232012165.
(43) Pfohl, P.; Bahl, D.; Rückel, M.; Wagner, M.; Meyer, L.; Bolduan, P.; Battagliarin, G.; Hüffer, T.; Zumstein, M.; Hofmann, T.; Wohlleben, W. Effect of Polymer Properties on the Biodegradation of Polyurethane Microplastics. *Environ. Sci. Technol.* **2022**, *56* (23), 16873–16884. https://doi.org/10.1021/acs.est.2c05602.
(44) Amobonye, A.; Bhagwat, P.; Singh, S.; Pillai, S. Plastic Biodegradation: Frontline Microbes and Their Enzymes. *Science of The Total Environment* **2021**, *759*, 143536. https://doi.org/10.1016/j.scitotenv.2020.143536.
(45) Pathak, V. M.; Navneet. Review on the Current Status of Polymer Degradation: A Microbial Approach. *Bioresour. Bioprocess.* **2017**, *4* (1), 15. https://doi.org/10.1186/s40643-017-0145-9.
(46) Gowthami, A.; Syed Marjuk, M.; Santhanam, P.; Thirumurugan, R.; Muralisankar, T.; Perumal, P. Marine Microalgae – Mediated Biodegradation of Polystyrene Microplastics: Insights from Enzymatic and Molecular Docking Studies. *Chemosphere* **2025**, *370*, 144024. https://doi.org/10.1016/j.chemosphere.2024.144024.
(47) Hou, L.; Xi, J.; Liu, J.; Wang, P.; Xu, T.; Liu, T.; Qu, W.; Lin, Y. B. Biodegradability of Polyethylene Mulching Film by Two Pseudomonas Bacteria and Their Potential Degradation Mechanism. *Chemosphere* **2022**, *286*, 131758. https://doi.org/10.1016/j.chemosphere.2021.131758.
(48) Janczak, K.; Mazuryk, A.; Lisewska, D.; Puszczykowska, N.; Fiedurek, K. Comparative Studies on the Effectiveness of Proteases and Enzymes from Dietary Supplements in the Degradation of Polylactide (PLA). *International Biodeterioration & Biodegradation* **2025**, *196*, 105950. https://doi.org/10.1016/j.ibiod.2024.105950.
(49) Chen, S.; Su, L.; Chen, J.; Wu, J. Cutinase: Characteristics, Preparation, and Application. *Biotechnology Advances* **2013**, *31* (8), 1754–1767. https://doi.org/10.1016/j.biotechadv.2013.09.005.
(50) Álvarez-Barragán, J.; Domínguez-Malfavón, L.; Vargas-Suárez, M.; González-Hernández, R.; Aguilar-Osorio, G.; Loza-Tavera, H. Biodegradative Activities of Selected Environmental Fungi on a Polyester Polyurethane Varnish and Polyether Polyurethane Foams. *Applied and Environmental Microbiology* **2016**, *82* (17), 5225–5235. https://doi.org/10.1128/AEM.01344-16.

(51) Di Bisceglie, F.; Quartinello, F.; Vielnascher, R.; Guebitz, G. M.; Pellis, A. Cutinase-Catalyzed Polyester-Polyurethane Degradation: Elucidation of the Hydrolysis Mechanism. *Polymers* **2022**, *14* (3), 411. https://doi.org/10.3390/polym14030411.
(52) Alvarado, E.; Castro, R.; Castro-Rodríguez, J. A.; Navarro, A.; Farrés, A. Poly(Lactic Acid) Degradation by Recombinant Cutinases from Aspergillus Nidulans. *Polymers* **2024**, *16* (14), 1994. https://doi.org/10.3390/polym16141994.
(53) Lin, J.; Sun, K.; Ma, L.; Li, C.; Tong, H.; Wang, Z. Enzymatic Degradation of Polybutylene Succinate by Recombinant Cutinase Cloned from *Paraphoma Chrysanthemicola*. *Journal of Environmental Management* **2025**, *375*, 124288. https://doi.org/10.1016/j.jenvman.2025.124288.
(54) Han, Y.; Wang, R.; Wang, D.; Luan, Y. Enzymatic Degradation of Synthetic Plastics by Hydrolases/Oxidoreductases. *International Biodeterioration & Biodegradation* **2024**, *189*, 105746. https://doi.org/10.1016/j.ibiod.2024.105746.
(55) Chaudhary, A. K.; Vijayakumar, R. P. Studies on Biological Degradation of Polystyrene by Pure Fungal Cultures. *Environ Dev Sustain* **2020**, *22* (5), 4495–4508. https://doi.org/10.1007/s10668-019-00394-5.
(56) Zhang, J.; Gao, D.; Li, Q.; Zhao, Y.; Li, L.; Lin, H.; Bi, Q.; Zhao, Y. Biodegradation of Polyethylene Microplastic Particles by the Fungus *Aspergillus Flavus* from the Guts of Wax Moth *Galleria Mellonella*. *Science of The Total Environment* **2020**, *704*, 135931. https://doi.org/10.1016/j.scitotenv.2019.135931.
(57) Gómez-Méndez, L. D.; Moreno-Bayona, D. A.; Poutou-Piñales, R. A.; Salcedo-Reyes, J. C.; Pedroza-Rodríguez, A. M.; Vargas, A.; Bogoya, J. M. Biodeterioration of Plasma Pretreated LDPE Sheets by Pleurotus Ostreatus. *PLOS ONE* **2018**, *13* (9), e0203786. https://doi.org/10.1371/journal.pone.0203786.
(58) Bhat, M. K. Cellulases and Related Enzymes in Biotechnology. *Biotechnology Advances* **2000**, *18* (5), 355–383. https://doi.org/10.1016/S0734-9750(00)00041-0.
(59) Charnock, S. J.; Brown, I. E.; Turkenburg, J. P.; Black, G. W.; Davies, G. J. Convergent Evolution Sheds Light on the Anti-β-Elimination Mechanism Common to Family 1 and 10 Polysaccharide Lyases. *Proceedings of the National Academy of Sciences* **2002**, *99* (19), 12067–12072. https://doi.org/10.1073/pnas.182431199.
(60) Karimi-Avargani, M.; Bazooyar, F.; Biria, D.; Zamani, A.; Skrifvars, M. The Promiscuous Potential of Cellulase in Degradation of Polylactic Acid and Its Jute Composite. *Chemosphere* **2021**, *278*, 130443. https://doi.org/10.1016/j.chemosphere.2021.130443.
(61) Spiridonov, V.; Lukmanova, A.; Pozdyshev, D.; Antonova, Y.; Kusaja, V.; Muronetz, V.; Yaroslavov, A. Enzyme-Induced Degradation of Natural and Artificial Linear Polyanions. *Carbohydrate Research* **2024**, *546*, 109310. https://doi.org/10.1016/j.carres.2024.109310.
(62) Wang, Z.; Cui, F.; Sui, Y.; Yan, J. Radical Chemistry in Polymer Science: An Overview and Recent Advances. *Beilstein J Org Chem* **2023**, *19*, 1580–1603. https://doi.org/10.3762/bjoc.19.116.
(63) Sun, M.; Xu, Z.; Munyaneza, N. E.; Zhang, Y.; Posada, C.; Liu, G. Solvent-Induced Competing Processes in Polycarbonate Degradation: Depolymerization, Chain Scission, and Branching/Crosslinking. *Polym. Chem.* **2023**, *14* (16), 1915–1922. https://doi.org/10.1039/D2PY01572B.
(64) D. Gervasoni, B.; N. Khairallah, G.; J. O'Hair, R. A.; Wille, U. The Role of Peroxyl Radicals in Polyester Degradation – a Mass Spectrometric Product and Kinetic Study Using the Distonic Radical Ion Approach. *Physical Chemistry Chemical Physics* **2015**, *17* (14), 9212–9221. https://doi.org/10.1039/C4CP06056C.
(65) Huang, J.; and Turner, S. R. Hypercrosslinked Polymers: A Review. *Polymer Reviews* **2018**, *58* (1), 1–41. https://doi.org/10.1080/15583724.2017.1344703.
(66) von Sonntag, C. Free-Radical-Induced Chain Scission and Cross-Linking of Polymers in Aqueous Solution—an Overview. *Radiation Physics and Chemistry* **2003**, *67* (3), 353–359. https://doi.org/10.1016/S0969-806X(03)00066-5.

(67) Li, C.; Liu, Q.; Gong, W.; Zhou, Z.; Yao, Z.; Meng, X. Study on the Atomic Scale of Thermal and Thermo-Oxidative Degradation of Polylactic Acid via Reactive Molecular Dynamics Simulation. *Thermochimica Acta* **2022**, *709*, 179144. https://doi.org/10.1016/j.tca.2021.179144.
(68) Bahrololoumi, A.; Mohammadi, H.; Moravati, V.; Dargazany, R. A Physically-Based Model for Thermo-Oxidative and Hydrolytic Aging of Elastomers. *International Journal of Mechanical Sciences* **2021**, *194*, 106193. https://doi.org/10.1016/j.ijmecsci.2020.106193.
(69) Jewell, B.; Abadi, P. P.; Sain, T. Experimental Characterization and Constitutive Modeling of Bulk Epoxy under Thermo-Oxidative Aging. *Polymer Degradation and Stability* **2025**, *234*, 111215. https://doi.org/10.1016/j.polymdegradstab.2025.111215.
(70) Dintcheva, N. T.; Al-Malaika, S.; Morici, E.; Arrigo, R. Thermo-Oxidative Stabilization of Poly(Lactic Acid)-Based Nanocomposites through the Incorporation of Clay with in-Built Antioxidant Activity. *Journal of Applied Polymer Science* **2017**, *134* (24). https://doi.org/10.1002/app.44974.
(71) Antunes, M. C.; Agnelli, J. A. M.; Babetto, A. S.; Bonse, B. C.; Bettini, S. H. P. Correlating Different Techniques in the Thermooxidative Degradation Monitoring of High-Density Polyethylene Containing pro-Degradant and Antioxidants. *Polymer Testing* **2018**, *69*, 182–187. https://doi.org/10.1016/j.polymertesting.2018.05.008.
(72) Fan, W.; Li, J.-L.; Zheng, Y.; Guo, D. The Effect of Reinforced Structure on Thermo-Oxidative Stability of Polymer-Matrix Composites. *Journal of Industrial Textiles* **2016**, *46* (1), 237–255. https://doi.org/10.1177/1528083715580519.
(73) Karlsson, T. M.; Hassellöv, M.; Jakubowicz, I. Influence of Thermooxidative Degradation on the in Situ Fate of Polyethylene in Temperate Coastal Waters. *Marine Pollution Bulletin* **2018**, *135*, 187–194. https://doi.org/10.1016/j.marpolbul.2018.07.015.
(74) Dümichen, E.; Eisentraut, P.; Bannick, C. G.; Barthel, A.-K.; Senz, R.; Braun, U. Fast Identification of Microplastics in Complex Environmental Samples by a Thermal Degradation Method. *Chemosphere* **2017**, *174*, 572–584. https://doi.org/10.1016/j.chemosphere.2017.02.010.
(75) Zhou, J.; Hsu, T.-G.; Wang, J. Mechanochemical Degradation and Recycling of Synthetic Polymers. *Angewandte Chemie International Edition* **2023**, *62* (27), e202300768. https://doi.org/10.1002/anie.202300768.
(76) Liu, P.; Jimaja, S.; Immel, S.; Thomas, C.; Mayer, M.; Weder, C.; Bruns, N. Mechanically Triggered On-Demand Degradation of Polymers Synthesized by Radical Polymerizations. *Nat. Chem.* **2024**, *16* (7), 1184–1192. https://doi.org/10.1038/s41557-024-01508-x.
(77) Li, Z.; Zhang, X.; Zhao, Y.; Tang, S. Mechanochemical Backbone Editing for Controlled Degradation of Vinyl Polymers. *Angewandte Chemie* **2024**, *136* (33), e202408225. https://doi.org/10.1002/ange.202408225.
(78) Lin, Y.; Kouznetsova, T. B.; Chang, C.-C.; Craig, S. L. Enhanced Polymer Mechanical Degradation through Mechanochemically Unveiled Lactonization. *Nat Commun* **2020**, *11* (1), 4987. https://doi.org/10.1038/s41467-020-18809-7.
(79) Azizi, H.; Ghasemi, I.; Karrabi, M. Controlled-Peroxide Degradation of Polypropylene: Rheological Properties and Prediction of MWD from Rheological Data. *Polymer Testing* **2008**, *27* (5), 548–554. https://doi.org/10.1016/j.polymertesting.2008.02.004.
(80) Nguyen, T. A.; Lim, H. M.; Kinashi, K.; Sakai, W.; Tsutsumi, N.; Okubayashi, S.; Hosoda, S.; Sato, T. Spin Trapping Analysis of Radical Intermediates on the Thermo-Oxidative Degradation of Polypropylene. *Polymers* **2023**, *15* (1), 200. https://doi.org/10.3390/polym15010200.
(81) Parrondo, J.; Wang, Z.; Jung, M.-S. J.; Ramani, V. Reactive Oxygen Species Accelerate Degradation of Anion Exchange Membranes Based on Polyphenylene Oxide in Alkaline Environments. *Phys. Chem. Chem. Phys.* **2016**, *18* (29), 19705–19712. https://doi.org/10.1039/C6CP01978A.
(82) Ji, H. S.; Park, G.; Jung, H. W. Rheological Properties and Melt Spinning Application of Controlled-Rheology Polypropylenes via Pilot-Scale Reactive Extrusion. *Polymers* **2022**, *14* (15), 3226. https://doi.org/10.3390/polym14153226.

(83) Azizi, H.; Ghasemi, I. Reactive Extrusion of Polypropylene: Production of Controlled-Rheology Polypropylene (CRPP) by Peroxide-Promoted Degradation. *Polymer Testing* **2004**, *23* (2), 137–143. https://doi.org/10.1016/S0142-9418(03)00072-2.
(84) Xu, M.; Xia, X.; Luo, Z.; Liao, J.; He, R.; Yang, S.; Yang, L. Degradation Behaviors and Crystallization of Rapidly Degradable Polylactic Acid Prepared by Melting through Coordination Complexation Reaction. *Materials Today Communications* **2024**, *38*, 107789. https://doi.org/10.1016/j.mtcomm.2023.107789.
(85) Hofmann, M.; Alberti, C.; Scheliga, F.; Meißner, R. R. R.; Enthaler, S. Tin(II) 2-Ethylhexanoate Catalysed Methanolysis of End-of-Life Poly(Lactide). *Polym. Chem.* **2020**, *11* (15), 2625–2629. https://doi.org/10.1039/D0PY00292E.
(86) Song, X.; Bian, Z.; Hui, Y.; Wang, H.; Liu, F.; Yu, S. Zn-Acetate-Containing Ionic Liquid as Highly Active Catalyst for Fast and Mild Methanolysis of Poly(Lactic Acid). *Polymer Degradation and Stability* **2019**, *168*, 108937. https://doi.org/10.1016/j.polymdegradstab.2019.108937.
(87) Roy, P. K.; Surekha, P.; Rajagopal, C.; Raman, R.; Choudhary, V. Study on the Degradation of Low-Density Polyethylene in the Presence of Cobalt Stearate and Benzil. *Journal of Applied Polymer Science* **2006**, *99* (1), 236–243. https://doi.org/10.1002/app.22464.
(88) Egorova, K. S.; Ananikov, V. P. Toxicity of Metal Compounds: Knowledge and Myths. *Organometallics* **2017**, *36* (21), 4071–4090. https://doi.org/10.1021/acs.organomet.7b00605.
(89) Yan, C.; Wu, J.; Zhang, J.; He, J.; Zhang, J. Hydrolytic Degradation of Cellulose-*Graft*-Poly(l-Lactide) Copolymers. *Polymer Degradation and Stability* **2015**, *118*, 130–136. https://doi.org/10.1016/j.polymdegradstab.2015.04.019.
(90) Alberti, C.; Damps, N.; Meißner, R. R. R.; Enthaler, S. Depolymerization of End-of-Life Poly(Lactide) via 4-Dimethylaminopyridine-Catalyzed Methanolysis. *ChemistrySelect* **2019**, *4* (23), 6845–6848. https://doi.org/10.1002/slct.201901316.
(91) Lamberti, F. M.; Ingram, A.; Wood, J. Synergistic Dual Catalytic System and Kinetics for the Alcoholysis of Poly(Lactic Acid). *Processes* **2021**, *9* (6), 921. https://doi.org/10.3390/pr9060921.
(92) Wang, L.; Nelson, G. A.; Toland, J.; Holbrey, J. D. Glycolysis of PET Using 1,3-Dimethylimidazolium-2-Carboxylate as an Organocatalyst. *ACS Sustainable Chem. Eng.* **2020**, *8* (35), 13362–13368. https://doi.org/10.1021/acssuschemeng.0c04108.
(93) Gayathri, V.; Sheyara, R. T. B.; Devassy, N.; Samanta, D. Investigating the Degradation of PET Utilizing NHC-Based Catalysts and Effective Reuse of the Degradation Product as an Additive with Polyurethane Adhesive Material. *Journal of Applied Polymer Science* **2022**, *139* (27), e52474. https://doi.org/10.1002/app.52474.
(94) Nica, S.; Hanganu, A.; Tanase, A.; Duldner, M.; Iancu, S.; Draghici, C.; Filip, P. I.; Bartha, E. Glycolytic Depolymerization of Polyethylene Terephtalate (PET) Wastes. *REV. CHIM.* **2015**, No. 8.
(95) Jehanno, C.; Flores, I.; Dove, A. P.; Müller, A. J.; Ruipérez, F.; Sardon, H. Organocatalysed Depolymerisation of PET in a Fully Sustainable Cycle Using Thermally Stable Protic Ionic Salt. *Green Chem.* **2018**, *20* (6), 1205–1212. https://doi.org/10.1039/C7GC03396F.
(96) Yousif, E.; Haddad, R. Photodegradation and Photostabilization of Polymers, Especially Polystyrene: Review. *Springerplus* **2013**, *2*, 398. https://doi.org/10.1186/2193-1801-2-398.
(97) Jiang, S.; Chen, Y.; Huang, Y.; Hu, P. Photooxidation of Polystyrene into High-Value Chemicals. *European Journal of Organic Chemistry* **2025**, *28* (4), e202401109. https://doi.org/10.1002/ejoc.202401109.
(98) Nikitas, N. F.; Skolia, E.; Gkizis, P. L.; Triandafillidi, I.; Kokotos, C. G. Photochemical Aerobic Upcycling of Polystyrene Plastics to Commodity Chemicals Using Anthraquinone as the Photocatalyst. *Green Chem.* **2023**, *25* (12), 4750–4759. https://doi.org/10.1039/D3GC00986F.
(99) Oh, S.; Stache, E. E. Chemical Upcycling of Commercial Polystyrene via Catalyst-Controlled Photooxidation. *J. Am. Chem. Soc.* **2022**, *144* (13), 5745–5749. https://doi.org/10.1021/jacs.2c01411.
(100) Fa, W.; Wang, J.; Ge, S.; Chao, C. Performance of Photo-Degradation and Thermo-Degradation of Polyethylene with Photo-Catalysts and Thermo-Oxidant Additives. *Polym. Bull.* **2020**, *77* (3), 1417–1432. https://doi.org/10.1007/s00289-019-02813-z.

(101) Bäckström, E.; Odelius, K.; Hakkarainen, M. Trash to Treasure: Microwave-Assisted Conversion of Polyethylene to Functional Chemicals. *Ind. Eng. Chem. Res.* **2017**, *56* (50), 14814–14821. https://doi.org/10.1021/acs.iecr.7b04091.
(102) Khaleghi, A.; Sadrameli, S. M.; Manteghian, M. Thermodynamic and Kinetics Investigation of Homogeneous and Heterogeneous Nucleation. *Reviews in Inorganic Chemistry* **2020**, *40* (4), 167–192. https://doi.org/10.1515/revic-2020-0004.
(103) Zhou, Y.; He, L.; Gong, W. Effect of Organic Cage Nucleating Agent Structure on Nucleating Efficiency and the Structure-Property Relationship. *Polymers* **2020**, *12* (9), 1975. https://doi.org/10.3390/polym12091975.
(104) Lemanowicz, M.; Mielańczyk, A.; Walica, T.; Kotek, M.; Gierczycki, A. Application of Polymers as a Tool in Crystallization—A Review. *Polymers (Basel)* **2021**, *13* (16), 2695. https://doi.org/10.3390/polym13162695.
(105) Jin, Y.; Hiltner, A.; Baer, E. Effect of a Sorbitol Nucleating Agent on Fractionated Crystallization of Polypropylene Droplets. *Journal of Polymer Science Part B: Polymer Physics* **2007**, *45* (14), 1788–1797. https://doi.org/10.1002/polb.21195.
(106) Schawe, J. E.; Budde, F.; Alig, I. Non-Isothermal Crystallization of Polypropylene with Sorbitol-Type Nucleating Agents at Cooling Rates Used in Processing. *Polymer International* **2019**, *68* (2), 240–247. https://doi.org/10.1002/pi.5581.
(107) Iwasaki, S.; Inoue, M.; Takei, Y.; Nishikawa, R.; Yamaguchi, M. Modulus Enhancement of Polypropylene by Sorbitol Nucleating Agent in Flow Field. *POLYMER CRYSTALLIZATION* **2021**, *4* (2), e10170. https://doi.org/10.1002/pcr2.10170.
(108) Wang, W.; Zhou, S.; Xin, Z.; Shi, Y.; Zhao, S.; Meng, X. Preparation and Foaming Mechanism of Foamable Polypropylene Based on Self-Assembled Nanofibrils from Sorbitol Nucleating Agents. *J Mater Sci* **2016**, *51* (2), 788–796. https://doi.org/10.1007/s10853-015-9402-5.
(109) Zhang, X.; Yang, B.; Fan, B.; Sun, H.; Zhang, H. Enhanced Nonisothermal Crystallization and Heat Resistance of Poly(L -Lactic Acid) by D -Sorbitol as a Homogeneous Nucleating Agent. *ACS Macro Lett.* **2021**, *10* (1), 154–160. https://doi.org/10.1021/acsmacrolett.0c00830.
(110) Sebek, F. F. G.; Nguon, O. J.; Bartos, A.; Brinke, M. ten; van Drongelen, M.; Gojzewski, H.; Lefas, J.; Vancso, G. J. Crystallization of Poly(Lactic Acid) Nucleated with the Sorbitol TBPMN. *Polymer Testing* **2024**, *131*, 108322. https://doi.org/10.1016/j.polymertesting.2023.108322.
(111) Shi, K.; Liu, G.; Sun, H.; Yang, B.; Weng, Y. Effect of Biomass as Nucleating Agents on Crystallization Behavior of Polylactic Acid. *Polymers* **2022**, *14* (20), 4305. https://doi.org/10.3390/polym14204305.
(112) Shazleen, S. S.; Yasim-Anuar, T. A. T.; Ibrahim, N. A.; Hassan, M. A.; Ariffin, H. Functionality of Cellulose Nanofiber as Bio-Based Nucleating Agent and Nano-Reinforcement Material to Enhance Crystallization and Mechanical Properties of Polylactic Acid Nanocomposite. *Polymers* **2021**, *13* (3), 389. https://doi.org/10.3390/polym13030389.
(113) Banpean, A.; Hararak, B.; Winotapun, C.; Wijaranakul, P.; Kitchaicharoenporn, S.; Naimlang, S. Lignin Nanoparticles as Sustainable Biobased Nucleating Agents of Poly(L-Lactic Acid): Crystallization Behavior and Effect of Particle Sizes. *J Mater Sci* **2023**, *58* (15), 6823–6838. https://doi.org/10.1007/s10853-023-08418-2.
(114) Dartora, P. C.; da Rosa Loureiro, M.; de Camargo Forte, M. M. Crystallization Kinetics and Morphology of Poly(Lactic Acid) with Polysaccharide as Nucleating Agent. *J Therm Anal Calorim* **2018**, *134* (3), 1705–1713. https://doi.org/10.1007/s10973-018-7744-3.
(115) Chauvet, M.; Fages, J.; Sauceau, M.; Baillon, F. Use of Starch as Nucleating Agent for the Extrusion Foaming of Poly-(Lactic Acid); 2016.
(116) Xing, Q.; Zhang, X.; Dong, X.; Liu, G.; Wang, D. Low-Molecular Weight Aliphatic Amides as Nucleating Agents for Poly (L-Lactic Acid): Conformation Variation Induced Crystallization Enhancement. *Polymer* **2012**, *53* (11), 2306–2314. https://doi.org/10.1016/j.polymer.2012.03.034.
(117) Kong, W.; Zhu, B.; Su, F.; Wang, Z.; Shao, C.; Wang, Y.; Liu, C.; Shen, C. Melting Temperature, Concentration and Cooling Rate-Dependent Nucleating Ability of a Self-Assembly Aryl Amide

Nucleator on Poly(Lactic Acid) Crystallization. *Polymer* **2019**, *168*, 77–85. https://doi.org/10.1016/j.polymer.2019.02.019.
(118) Chen, X.; Yao, J.; Yu, J.; Mi, M.; Xu, Y.; Bai, H. Toward Heat-Resistant and Transparent Poly(l-Lactide) by Tailoring Crystallization with an Aliphatic Amide as a Nucleating Agent. *Ind. Eng. Chem. Res.* **2022**, *61* (37), 13921–13928. https://doi.org/10.1021/acs.iecr.2c02811.
(119) Leoné, N.; Roy, M.; Saidi, S.; de Kort, G.; Hermida-Merino, D.; Wilsens, C. H. R. M. Improving Processing, Crystallization, and Performance of Poly-l-Lactide with an Amide-Based Organic Compound as Both Plasticizer and Nucleating Agent. *ACS Omega* **2019**, *4* (6), 10376–10387. https://doi.org/10.1021/acsomega.9b00848.
(120) Tang, J.; Li, L.; Wang, X.; Yang, J.; Liang, X.; Li, Y.; Ma, H.; Zhou, S.; Wang, J. Tailored Crystallization Behavior, Thermal Stability, and Biodegradability of Poly(Ethylene Adipate): Effects of a Biocompatible Diamide Nucleating Agent. *Polymer Testing* **2020**, *81*, 106116. https://doi.org/10.1016/j.polymertesting.2019.106116.
(121) Legras, R.; Mercier, J. P.; Nield, E. Polymer Crystallization by Chemical Nucleation. *Nature* **1983**, *304* (5925), 432–434. https://doi.org/10.1038/304432a0.
(122) Wang, M.; Lin, F.; Zhao, T.; Dong, Y.; Hao, X.; Ning, D.; Zhang, Y.; Zhang, K.; Zhou, D.; Luo, J.; Li, X.; Wang, B. The Application of a Sodium Benzoate Salt-Nucleating Agent in Recycled Polyethylene Terephthalate: Crystallization Behavior and Mechanism. *Molecules* **2025**, *30* (1), 37. https://doi.org/10.3390/molecules30010037.
(123) Cao, J.; Zou, J.; Zheng, S.; Wen, N.; Xu, W.; Zheng, Y. Preparation of Clay-Supported Sodium Benzoate and Its Effect on the Rheology, Crystallization and Foaming of Long Chain Branched Polypropylene. *Journal of Cellular Plastics* **2023**, *59* (4), 313–334. https://doi.org/10.1177/0021955X231162187.
(124) Zhang, Y.-F.; Li, D.; Chen, Q.-J. Preparation and Nucleation Effects of Nucleating Agent Hexahydrophthalic Acid Metal Salts for Isotactic Polypropylene. *Colloid Polym Sci* **2017**, *295* (10), 1973–1982. https://doi.org/10.1007/s00396-017-4176-8.
(125) Yang, T.-C.; Hung, K.-C.; Wu, T.-L.; Wu, T.-M.; Wu, J.-H. A Comparison of Annealing Process and Nucleating Agent (Zinc Phenylphosphonate) on the Crystallization, Viscoelasticity, and Creep Behavior of Compression-Molded Poly(Lactic Acid) Blends. *Polymer Degradation and Stability* **2015**, *121*, 230–237. https://doi.org/10.1016/j.polymdegradstab.2015.09.012.
(126) Jongpanya-Ngam, P.; Khankrua ,Rattikarn; Seadan ,Manus; and Suttiruengwong, S. Effect of Synthesized Sulfonate Derivatives as Nucleating Agents on Crystallization Behavior of Poly(Lactic Acid). *Designed Monomers and Polymers* **2022**, *25* (1), 115–127. https://doi.org/10.1080/15685551.2022.2072697.
(127) Kale, G.; Kijchavengkul, T.; Auras, R.; Rubino, M.; Selke, S. E.; Singh, S. P. Compostability of Bioplastic Packaging Materials: An Overview. *Macromol Biosci* **2007**, *7* (3), 255–277. https://doi.org/10.1002/mabi.200600168.
(128) Balla, E.; Daniilidis, V.; Karlioti, G.; Kalamas, T.; Stefanidou, M.; Bikiaris, N. D.; Vlachopoulos, A.; Koumentakou, I.; Bikiaris, D. N. Poly(Lactic Acid): A Versatile Biobased Polymer for the Future with Multifunctional Properties—From Monomer Synthesis, Polymerization Techniques and Molecular Weight Increase to PLA Applications. *Polymers* **2021**, *13* (11), 1822. https://doi.org/10.3390/polym13111822.
(129) Zaaba, N. F.; Jaafar, M. A Review on Degradation Mechanisms of Polylactic Acid: Hydrolytic, Photodegradative, Microbial, and Enzymatic Degradation. *Polymer Engineering & Science* **2020**, *60* (9), 2061–2075. https://doi.org/10.1002/pen.25511.
(130) Hamad, K.; Kaseem, M.; Yang, H. W.; Deri, F.; Ko, Y. G. Properties and Medical Applications of Polylactic Acid: A Review. *Express Polym. Lett.* **2015**, *9* (5), 435–455. https://doi.org/10.3144/expresspolymlett.2015.42.
(131) Iñiguez-Franco, F.; Auras, R.; Dolan, K.; Selke, S.; Holmes, D.; Rubino, M.; Soto-Valdez, H. Chemical Recycling of Poly(Lactic Acid) by Water-Ethanol Solutions. *Polymer Degradation and Stability* **2018**, *149*, 28–38. https://doi.org/10.1016/j.polymdegradstab.2018.01.016.

(132) Iñiguez-Franco, F.; Auras, R.; Burgess, G.; Holmes, D.; Fang, X.; Rubino, M.; Soto-Valdez, H. Concurrent Solvent Induced Crystallization and Hydrolytic Degradation of PLA by Water-Ethanol Solutions. *Polymer* **2016**, *99*, 315–323. https://doi.org/10.1016/j.polymer.2016.07.018.
(133) Eul, W.; Moeller, A.; Steiner, N. Hydrogen Peroxide. In *Kirk-Othmer Encyclopedia of Chemical Technology*; Kirk-Othmer, Ed.; Wiley, 2001. https://doi.org/10.1002/0471238961.0825041808051919.a01.pub2.
(134) Södergård, A.; Näsman, J. H. Stabilization of Poly(l-Lactide) in the Melt. *Polymer Degradation and Stability* **1994**, *46* (1), 25–30. https://doi.org/10.1016/0141-3910(94)90104-X.
(135) Bednarek, M.; Borska, K.; Kubisa, P. New Polylactide-Based Materials by Chemical Crosslinking of PLA. *Polymer Reviews* **2021**, *61* (3), 493–519. https://doi.org/10.1080/15583724.2020.1855194.
(136) Rigolin, T. R.; Costa, L. C.; Venâncio, T.; Perlatti, B.; Bettini, S. H. P. The Effect of Different Peroxides on Physical and Chemical Properties of Poly(Lactic Acid) Modified with Maleic Anhydride. *Polymer* **2019**, *179*, 121669. https://doi.org/10.1016/j.polymer.2019.121669.
(137) Takamura, M.; Nakamura, T.; Kawaguchi, S.; Takahashi, T.; Koyama, K. Molecular Characterization and Crystallization Behavior of Peroxide-Induced Slightly Crosslinked Poly(L-Lactide) during Extrusion. *Polym J* **2010**, *42* (7), 600–608. https://doi.org/10.1038/pj.2010.42.
(138) Takamura, M.; Nakamura, T.; Takahashi, T.; Koyama, K. Effect of Type of Peroxide on Cross-Linking of Poly(l-Lactide). *Polymer Degradation and Stability* **2008**, *93* (10), 1909–1916. https://doi.org/10.1016/j.polymdegradstab.2008.07.001.
(139) Takamura, M.; Sugimoto, M.; Kawaguchi, S.; Takahashi, T.; Koyama, K. Influence of Extrusion Temperature on Molecular Architecture and Crystallization Behavior of Peroxide-Induced Slightly Crosslinked Poly(L-Lactide) by Reactive Extrusion. *Journal of Applied Polymer Science* **2012**, *123* (3), 1468–1478. https://doi.org/10.1002/app.34618.
(140) Måge, I.; Matić, J.; Dankel, K. R. SEC2MWD: A MATLAB Toolbox for Derivation of Molecular Weight Distributions from Size Exclusion Chromatography. *SoftwareX* **2024**, *25*, 101602. https://doi.org/10.1016/j.softx.2023.101602.
(141) Kara, Y.; Molnár, K. A Review of Processing Strategies to Generate Melt-Blown Nano/Microfiber Mats for High-Efficiency Filtration Applications. *Journal of Industrial Textiles* **2022**, *51* (1_suppl), 137S-180S. https://doi.org/10.1177/15280837211019488.
(142) *Melt-blown Dies: A Hot Innovation Spot*. https://doi.org/10.1177/1558925002OS-01100409.
(143) Lee, H.; Trinh, B. M.; Crawford, E. A.; Mekonnen, T. H. Thermoplastic Elastomer Melt-Blown Fiber Mats for Oil Spill Remediation: Fabrication, Oil Uptake, and Gel Formation Studies. *Separation and Purification Technology* **2023**, *326*, 124761. https://doi.org/10.1016/j.seppur.2023.124761.
(144) Crawford, E. A.; Gupta, S.; Trinh, B. M.; Mekonnen, T. H. Styrene-Ethylene-Butylene-Styrene (SEBS) Melt-Blown Fibers for Oil Spill Remediation and Oil Barrier Geotextiles. *Polymer* **2024**, *298*, 126942. https://doi.org/10.1016/j.polymer.2024.126942.
(145) Södergård, A.; Niemi, M.; Selin, J.-F.; Naesman, J. H. Changes in Peroxide Melt-Modified Poly(L-Lactide). *Ind. Eng. Chem. Res.* **1995**, *34* (4), 1203–1207. https://doi.org/10.1021/ie00043a024.
(146) Kervran, M.; Vagner, C.; Cochez, M.; Ponçot, M.; Saeb, M. R.; Vahabi, H. Thermal Degradation of Polylactic Acid (PLA)/Polyhydroxybutyrate (PHB) Blends: A Systematic Review. *Polymer Degradation and Stability* **2022**, *201*, 109995. https://doi.org/10.1016/j.polymdegradstab.2022.109995.
(147) Pérez, J. M.; Ruiz, C.; Fernández, I. Synthesis of a Biodegradable PLA: NMR Signal Deconvolution and End-Group Analysis. *J. Chem. Educ.* **2022**, *99* (2), 1000–1007. https://doi.org/10.1021/acs.jchemed.1c00824.
(148) Suganuma, K.; Horiuchi, K.; Matsuda, H.; Cheng, H. N.; Aoki, A.; Asakura, T. NMR Analysis and Chemical Shift Calculations of Poly(Lactic Acid) Dimer Model Compounds with Different Tacticities. *Polym J* **2012**, *44* (8), 838–844. https://doi.org/10.1038/pj.2012.106.
(149) Thakur, K. A. M.; Kean, R. T.; Hall, E. S.; Kolstad, J. J.; Lindgren, T. A.; Doscotch, M. A.; Siepmann, J. I.; Munson, E. J. High-Resolution 13C and 1H Solution NMR Study of Poly(Lactide). *Macromolecules* **1997**, *30* (8), 2422–2428. https://doi.org/10.1021/ma9615967.

(150) Suganuma, K.; Matsuda, H.; Cheng, H. N.; Iwai, M.; Nonokawa, R.; Asakura, T. NMR Analysis and Tacticity Determination of Poly(Lactic Acid) in C5D5N. *Polymer Testing* **2014**, *38*, 35–39. https://doi.org/10.1016/j.polymertesting.2014.05.018.
(151) Tuancharoensri, N.; Ross, G. M.; Kongprayoon, A.; Mahasaranon, S.; Pratumshat, S.; Viyoch, J.; Petrot, N.; Ruanthong, W.; Punyodom, W.; Topham, P. D.; Tighe, B. J.; Ross, S. In Situ Compatibilized Blends of PLA/PCL/CAB Melt-Blown Films with High Elongation: Investigation of Miscibility, Morphology, Crystallinity and Modelling. *Polymers (Basel)* **2023**, *15* (2), 303. https://doi.org/10.3390/polym15020303.
(152) Lamberti, F.; Román-Ramírez, L.; Mckeown, P.; Jones, M.; Wood, J. Kinetics of Alkyl Lactate Formation from the Alcoholysis of Poly(Lactic Acid). *Processes* **2020**, *8*, 738. https://doi.org/10.3390/pr8060738.
(153) Alex, A.; Ilango, N. K.; Ghosh, P. Comparative Role of Chain Scission and Solvation in the Biodegradation of Polylactic Acid (PLA). *J. Phys. Chem. B* **2018**, *122* (41), 9516–9526. https://doi.org/10.1021/acs.jpcb.8b07930.
(154) Ramli, H.; Zainal, N. F. A.; Hess, M.; Chan, C. H. Basic Principle and Good Practices of Rheology for Polymers for Teachers and Beginners. *Chemistry Teacher International* **2022**, *4* (4), 307–326. https://doi.org/10.1515/cti-2022-0010.
(155) Ming, Y.; Zhou, Z.; Hao, T.; Nie, Y. Molecular Simulation of Polymer Crystallization under Chain and Space Confinement. *Phys. Chem. Chem. Phys.* **2021**, *23* (32), 17382–17391. https://doi.org/10.1039/D1CP01799C.
(156) Cuadri, A. A.; Martín-Alfonso, J. E. Thermal, Thermo-Oxidative and Thermomechanical Degradation of PLA: A Comparative Study Based on Rheological, Chemical and Thermal Properties. *Polymer Degradation and Stability* **2018**, *150*, 37–45. https://doi.org/10.1016/j.polymdegradstab.2018.02.011.
(157) Rasselet, D.; Ruellan, A.; Guinault, A.; Miquelard-Garnier, G.; Sollogoub, C.; Fayolle, B. Oxidative Degradation of Polylactide (PLA) and Its Effects on Physical and Mechanical Properties. *European Polymer Journal* **2014**, *50*, 109–116. https://doi.org/10.1016/j.eurpolymj.2013.10.011.
(158) Ma, B.; Wang, X.; He, Y.; Dong, Z.; Zhang, X.; Chen, X.; Liu, T. Effect of Poly(Lactic Acid) Crystallization on Its Mechanical and Heat Resistance Performances. *Polymer* **2021**, *212*, 123280. https://doi.org/10.1016/j.polymer.2020.123280.
(159) Fang, Q.; Hanna, M. A. Rheological Properties of Amorphous and Semicrystalline Polylactic Acid Polymers. *Industrial Crops and Products* **1999**, *10* (1), 47–53. https://doi.org/10.1016/S0926-6690(99)00009-6.
(160) Fox, T. G.; Flory, P. J. The Glass Temperature and Related Properties of Polystyrene. Influence of Molecular Weight. *Journal of Polymer Science* **1954**, *14* (75), 315–319. https://doi.org/10.1002/pol.1954.120147514.
(161) Ekinci, A.; Gleadall, A.; Johnson, A. A.; Li, L.; Han, X. Mechanical and Hydrolytic Properties of Thin Polylactic Acid Films by Fused Filament Fabrication. *Journal of the Mechanical Behavior of Biomedical Materials* **2021**, *114*, 104217. https://doi.org/10.1016/j.jmbbm.2020.104217.
(162) Rasselet, D.; Ruellan, A.; Guinault, A.; Miquelard-Garnier, G.; Sollogoub, C.; Fayolle, B. Oxidative Degradation of Polylactide (PLA) and Its Effects on Physical and Mechanical Properties. *European Polymer Journal* **2014**, *50*, 109–116. https://doi.org/10.1016/j.eurpolymj.2013.10.011.
(163) Virág, Á. D.; Tóth, C.; Molnár, K. Photodegradation of Polylactic Acid: Characterisation of Glassy and Melt Behaviour as a Function of Molecular Weight. *International Journal of Biological Macromolecules* **2023**, *252*, 126336. https://doi.org/10.1016/j.ijbiomac.2023.126336.
(164) Sasaki, S.; Asakura, T. Helix Distortion and Crystal Structure of the α-Form of Poly(l-Lactide). *Macromolecules* **2003**, *36* (22), 8385–8390. https://doi.org/10.1021/ma0348674.
(165) Li, Y.; Tao, L.; Wang, Q.; Wang, F.; Li, G.; Song, M. Potential Health Impact of Microplastics: A Review of Environmental Distribution, Human Exposure, and Toxic Effects. *Environ. Health* **2023**, *1* (4), 249–257. https://doi.org/10.1021/envhealth.3c00052.

(166) Qin, C. Q.; Du, Y. M.; Xiao, L. Effect of Hydrogen Peroxide Treatment on the Molecular Weight and Structure of Chitosan. *Polymer Degradation and Stability* **2002**, *76* (2), 211–218. https://doi.org/10.1016/S0141-3910(02)00016-2.
(167) Binley, G.; Jubinville, D.; Prince, E.; Mekonnen, T. H. Hydrogen Peroxide-Induced Controlled Degradation of Poly(Lactic Acid) for Melt-Blown Nonwovens. *ACS Appl. Polym. Mater.* **2024**. https://doi.org/10.1021/acsapm.4c02897.
(168) Burford, T.; Rieg, W.; Madbouly, S. Biodegradable Poly(Butylene Adipate-Co-Terephthalate) (PBAT). *Physical Sciences Reviews* **2023**, *8* (8), 1127–1156. https://doi.org/10.1515/psr-2020-0078.
(169) Jafari, M.; Shim, E.; Joijode, A. Fabrication of Poly(Lactic Acid) Filter Media via the Meltblowing Process and Their Filtration Performances: A Comparative Study with Polypropylene Meltblown. *Separation and Purification Technology* **2021**, *260*, 118185. https://doi.org/10.1016/j.seppur.2020.118185.
(170) Dzierzkowska, E.; Scisłowska-Czarnecka, A.; Kudzin, M.; Boguń, M.; Szatkowski, P.; Gajek, M.; Kornaus, K.; Chadzinska, M.; Stodolak-Zych, E. Effects of Process Parameters on Structure and Properties of Melt-Blown Poly(Lactic Acid) Nonwovens for Skin Regeneration. *Journal of Functional Biomaterials* **2021**, *12* (1), 16. https://doi.org/10.3390/jfb12010016.
(171) Su, S.; Duhme, M.; Kopitzky, R. Uncompatibilized PBAT/PLA Blends: Manufacturability, Miscibility and Properties. *Materials (Basel)* **2020**, *13* (21), 4897. https://doi.org/10.3390/ma13214897.
(172) Nofar, M.; Maani, A.; Sojoudi, H.; Heuzey, M. C.; Carreau, P. J. Interfacial and Rheological Properties of PLA/PBAT and PLA/PBSA Blends and Their Morphological Stability under Shear Flow. *Journal of Rheology* **2015**, *59* (2), 317–333. https://doi.org/10.1122/1.4905714.
(173) Signori, F.; Coltelli, M.-B.; Bronco, S. Thermal Degradation of Poly(Lactic Acid) (PLA) and Poly(Butylene Adipate-*Co*-Terephthalate) (PBAT) and Their Blends upon Melt Processing. *Polymer Degradation and Stability* **2009**, *94* (1), 74–82. https://doi.org/10.1016/j.polymdegradstab.2008.10.004.
(174) Yu, J.; Zhao, T.; Li, C.; Pan, H.; Tan, Z.; Yang, H.; Zhang, H. Preparation and Characterization of Biodegradable Polylactic Acid/Poly (Butylene Adipate-Co-Terephthalate) Melt-Blown Nonwovens for Oil-Water Separation. *Colloid Polym Sci* **2024**, *302* (1), 43–56. https://doi.org/10.1007/s00396-023-05169-z.
(175) Scaffaro, R.; Maio, A.; Sutera, F.; Gulino, E. F.; Morreale, M. Degradation and Recycling of Films Based on Biodegradable Polymers: A Short Review. *Polymers* **2019**, *11* (4), 651. https://doi.org/10.3390/polym11040651.
(176) Mohanty, S.; Nayak, S. K. Biodegradable Nanocomposites of Poly(Butylene Adipate-Co-Terephthalate) (PBAT) and Organically Modified Layered Silicates. *J Polym Environ* **2012**, *20* (1), 195–207. https://doi.org/10.1007/s10924-011-0408-z.
(177) Hao, Y.; Chen, J.; Liu, Y.; Wang, F.; Chen, Q.; Zhang, W.; Zhang, S.; Chen, W.; Tian, H. Peroxide Cross-Linking and Its Role on the Rheological, Mechanical and Thermal Properties of Poly(Butylene Adipate-Co-Butylene Terephthalate). *Iran Polym J* **2023**, *32* (10), 1271–1280. https://doi.org/10.1007/s13726-023-01198-1.
(178) Ding, Y.; Yang, Q.; Wang, X.; Li, S. The Effect of Free Radical Initiators on Poly (Butylene Adipate-Co-Terephthalate) (PBAT) and Its Foaming Performance. *J Mater Sci* **2024**, *59* (44), 20854–20869. https://doi.org/10.1007/s10853-024-10415-y.
(179) Allen, N. S.; Edge, M.; Mohammadian, M.; Jones, K. Hydrolytic Degradation of Poly(Ethylene Terephthalate): Importance of Chain Scission versus Crystallinity. *European Polymer Journal* **1991**, *27* (12), 1373–1378. https://doi.org/10.1016/0014-3057(91)90237-I.
(180) WANG, Y.; CHEN, C.; LI, J.; HUANG, J.; XIONG, L. *Effect of Different Carbodiimide Additives on the Compatibility and Hydrolytic Behavior of PLA/PBAT Blends*; 2024. https://doi.org/10.21203/rs.3.rs-4384101/v1.
(181) Yang, Y.; Min, J.; Xue, T.; Jiang, P.; Liu, X.; Peng, R.; Huang, J.-W.; Qu, Y.; Li, X.; Ma, N.; Tsai, F.-C.; Dai, L.; Zhang, Q.; Liu, Y.; Chen, C.-C.; Guo, R.-T. Complete Bio-Degradation of Poly(Butylene

Adipate-Co-Terephthalate) via Engineered Cutinases. *Nat Commun* **2023**, *14* (1), 1645. https://doi.org/10.1038/s41467-023-37374-3.
(182) La Mantia, F. P.; Botta, L.; Mistretta, M. C.; Di Fiore, A.; Titone, V. Recycling of a Biodegradable Polymer Blend. *Polymers* **2020**, *12* (10), 2297. https://doi.org/10.3390/polym12102297.
(183) Mohd Sabee, M. M. S.; Tajuddin, N.; Ishak, K.; Rusli, A.; Shafiq, M.; Shuib, R.; Abdul Hamid, Z. Comparison of Physical and Mechanical Properties of Biodegradable Polybutylene Adipate Terephthalate, Polycaprolactone, and Poly(Lactic Acid) Fabricated via Fused Deposition Modeling and Conventional Molding. *Journal of Applied Polymer Science* **2022**, *139*, e52973. https://doi.org/10.1002/app.52973.
(184) Fernández-Tena, A.; Otaegi, I.; Irusta, L.; Sebastián, V.; Guerrica-Echevarria, G.; Müller, A. J.; Aranburu, N. High-Impact PLA in Compatibilized PLA/PCL Blends: Optimization of Blend Composition and Type and Content of Compatibilizer. *Macro Materials & Eng* **2023**, *308* (12), 2300213. https://doi.org/10.1002/mame.202300213.
(185) Zainal, N. F. A.; Chan, C. H. Crystallization and Melting Behavior of Compatibilized Polymer Blends. In *Compatibilization of Polymer Blends*; Elsevier, 2020; pp 391–433. https://doi.org/10.1016/B978-0-12-816006-0.00014-1.

Appendix A – Supporting Information from Chapter 3

Table A1: Molar mass distribution details from SEC analysis

Sample ID	*Retention Volume*	M_W *(kDa)*	M_n *(kDa)*	*Đ*
Raw PLA	9.45	112.2	71.2	1.58
Ctrl 1	9.63	84.6	49.0	1.73
Ctrl 2	9.87	51.7	27.1	1.92
PLA-5-5	9.87	49.0	31.5	1.56
PLA-7.5-7.5	9.95	43.6	23.1	1.89
PLA-5-10	10.10	34.0	17.7	1.92
PLA-10-5	9.99	48.3	24.1	2.01
PLA-10-10	9.84	57.4	24.7	2.35

Table A2: Carreau model fitting of PLA samples at 200 °C.

Sample ID	*Zero-shear viscosity value (Carreau model)*	R^2
Raw PLA	1.5×10^8	1.00
Ctrl 1	1.5×10^8	1.00
Ctrl 2	6.9×10^7	1.00
PLA-5-5	5.7×10^7	1.00
PLA-5-10	1.8×10^7	1.00
PLA-7.5-7.5	1.9×10^7	1.00
PLA-10-5	2.7×10^7	1.00
PLA-10-10	5.4×10^7	1.00

Table A3: Glass transition, melting, and cold crystallization temperatures as well as enthalpies of melting and cold crystallization from DSC analysis.

Sample ID	*T_G (°C)*	*T_M (°C)*	*Tcc (°C)*	*ΔHm (J/g)*	*ΔHcc (J/g)*
Raw PLA	59.57	173.57	101.75/157.85	55.28	29.23/5.12
Ctrl 1	59.40	172.55	101.07/157.45	45.82	29.69/4.12
Ctrl 2	56.61	170.51	98.43/157.86	45.57	27.66/2.47
PLA-5-5	57.13	167.98	98.28/156.09	41.91	26.26/1.48
PLA-5-10	53.12	164.57	101.79/156.55	46.05	36.37/0.39
PLA-7.5-7.5	57.25	167.18	104.61	40.93	33.79
PLA-10-5	55.94	166 .79/169.0	98.82/157.53	45.08	27.78/0.76
PLA-10-10	55.84	166.08	101.99	48.49	30.79